

**Exploring the Importance of Sediment Disconnectivity and Connectivity in Glacierized
Catchments, Tahoma Creek, WA**

by

Michael Turley

B.Sc., Utah State University, 2018

A THESIS SUBMITTED IN PARTIAL FULFILLMENT OF
THE REQUIREMENTS FOR THE DEGREE OF

MASTER OF SCIENCE

in

THE FACULTY OF GRADUATE AND POSTDOCTORAL STUDIES

(Geography)

THE UNIVERSITY OF BRITISH COLUMBIA

(Vancouver)

August 2020

© Michael Turley, 2020

The following individuals certify that they have read, and recommend to the Faculty of Graduate and Postdoctoral Studies for acceptance, the thesis entitled:

“Exploring the Importance of Sediment Disconnectivity and Connectivity in Glacierized Catchments, Tahoma Creek, WA”

submitted by Michael Turley in partial fulfillment of the requirements for

the degree of Master of Science

in Geography

Examining Committee:

Marwan Hassan, Geography
Supervisor

Olav Slaymaker, Geography (Professor Emeritus)
Supervisory Committee Member

Michele Koppes, Geography, Canada Research Chair in Landscapes of Climate Change
Additional Examiner

Abstract

In recent decades, connectivity has emerged as a prominent topic of discussion within the geomorphology community but lacks consensus around a general definition. On the other hand, disconnectivity is often an afterthought even though it is prevalent at most spatiotemporal scales. In response, we suggest defining disconnectivity as the dominant but inefficient state of the system in transferring matter and energy within and between system components at all spatial and temporal scales. Connectivity is then a special case within disconnectivity in which the efficient transfer of matter and energy occurs within the spatiotemporal scale of interest. In this study, we explore whether disconnectivity controls the spatial patterns of sediment dynamics, and how well current methods of quantifying connectivity captures these spatial patterns.

We conducted a case study within the Tahoma Creek Watershed of Mount Rainier National Park, WA, in which we present fieldwork and historical data in the form of a geomorphic map and conceptual sediment budget and map all sources of disconnectivity. These analyses are compared to methods of measuring the influence of landscape history and hillslope-channel coupling, followed by several semi-quantitative connectivity indices.

Slope-Area plots clearly show the topographic signature of Pleistocene glaciations within the confines of relict cirques, while the mainstem channel appears fully adjusted to contemporary fluvial processes. Hillslope-channel coupling estimates based on the method proposed by Whiting and Bradley (1993) generally match fieldwork evidence, where the uppermost 6 km of the channel are coupled to the hillslopes, and the lowermost 7 km are decoupled.

We found that the spatial distribution of sources of disconnectivity and their upslope affected areas explains the spatial patterns of sediment transfers and assumed transfer efficiencies within the watershed. Even locations with intense morphodynamics, such as Mount Rainier, are predominantly disconnected over human-timescales. The methods of quantifying sediment connectivity all performed rather well within their stated limitations and inherent resolution, although discrepancies exist. The primary sources of error result from inaccurately modelling

runoff pathways and overlooking the effects of vegetation. We suggest explicitly integrating sources of disconnectivity within disconnectivity indices for improved performance and physical grounding.

Lay Summary

The landscape can be viewed as a complex system with many parts, some of which are linked together by sediment transport processes such as rivers or landslides. In this context, most landscapes are fragmented, and very few locations contribute sediment to the system as a whole. The degree of linkages between the different parts of the landscape determines how efficiently signals are transferred and is termed sediment connectivity. In this study, we map landforms and other landscape characteristics that decrease the functioning/efficiency of these linkages (disconnectivity), and test methods that estimate the patterns of linkages. By understanding how fragmented natural systems are, we can better understand how efficiently/quickly they will respond to changing conditions such as climate change or human influences.

Preface

This thesis was designed and completed by the author, M. Turley, under the supervision of Dr. Marwan Hassan (supervisor) and Dr. Olav Slaymaker (committee member). The fieldwork and mapping was completed by M. Turley in 2019 with the guidance of Taylor Kenyon, Robert Jost, and Scott Beason of the Imminent Threats Team at Mount Rainier National Park.

Table of Contents

Abstract.....	iii
Lay Summary.....	v
Preface.....	vi
Table of Contents	vii
List of Tables	xiv
List of Figures.....	xv
List of Supplementary Materials.....	xvii
List of Abbreviations	xviii
Glossary	xix
Acknowledgements	xxi
Chapter 1: Introduction	1
1.1 Background.....	1
1.1.1 Previous Definitions.....	1
1.1.2 Unequal Discussion of Connectivity	2
1.1.3 Disconnectivity	3
1.1.3.1 Our Definition.....	3
1.1.3.2 Framework.....	4
1.1.3.3 Temporal Scale	6
1.1.3.4 Spatial Scale	7
1.1.3.5 Grain Size	8
1.1.4 Connectivity.....	9

1.1.4.1	Our Definition.....	9
1.1.4.2	Framework.....	9
1.1.4.3	Temporal Scale	10
1.1.4.4	Spatial Scale	10
1.2	Glacial and Proglacial Specific Considerations	11
1.3	Study Area	12
1.3.1	Geologic History.....	14
1.3.1.1	Mount Rainier Volcanics.....	14
1.3.1.2	Glacial History.....	14
1.3.1.3	Mass Wasting	15
1.3.2	Anthropogenic Influence	16
1.4	Research Design.....	16
Chapter 2: The Relative Importance of Connectivity vs. Disconnectivity: A Case Study		
from Mount Rainier, WA.....		18
2.1	Geomorphic Map	18
2.2	Connectivity Within a Sediment Budget Framework.....	18
2.2.1	Calculating Components of the Budget	20
2.2.2	Sources	22
2.2.2.1	Primary Sources.....	22
2.2.2.2	Secondary Sources.....	23
2.2.3	Sinks/ Sediment Storage	24
2.2.4	Production and Transport Processes	24
2.2.4.1	Weathering.....	25

2.2.4.2	Soil Creep/Tree Throw	25
2.2.4.3	Rockslide, Avalanche, Debris Slide	25
2.2.4.4	Rockfall, Frost Shattering.....	26
2.2.4.5	Bank Erosion	26
2.2.4.6	Debris Flows.....	27
2.2.4.7	Lahars	29
2.2.4.8	Glaciation.....	30
2.2.4.9	Fluvial Transport	30
2.2.5	The Unbalanced Sediment Budget.....	31
2.2.5.1	Sediment Delivery Ratios	32
2.2.5.2	Sources of Uncertainty	32
2.3	Sources of Disconnectivity	34
2.3.1	Buffers.....	34
2.3.1.1	Lateral Moraines.....	34
2.3.1.2	Debris Flow Levees	36
2.3.1.3	Low-Gradient Areas	36
2.3.1.4	Lakes.....	39
2.3.1.5	Vegetation.....	39
2.3.1.6	Terraces, Floodplains.....	39
2.3.1.7	Fans, Cones.....	40
2.3.1.8	Roads, Culverts.....	40
2.3.2	Barriers.....	41
2.3.2.1	Culverts, Bridges	41

2.3.2.2	Grain Size / Competence	41
2.3.2.3	In-Stream LWD / Dams	41
2.3.2.4	Valley Constrictions	42
2.3.2.5	Sediment Bulges, Pulses, or Slugs.....	42
2.3.3	Blankets.....	43
2.3.3.1	Sediment Bulges / Slugs	43
2.3.4	Effective Timescales	43
Chapter 3: Quantitative Estimations of Connectivity		45
3.1	The Influence of Landscape History.....	45
3.1.1	Process-Domain Delineation	45
3.1.1.1	Slope-Area Plots	45
3.1.2	Long-Profile Analysis.....	46
3.1.2.1	Stream Gradient Index.....	46
3.1.2.2	Valley Cross-Sections.....	47
3.1.3	Whiting-Bradley Classification	47
3.2	Measures of Sediment Connectivity	48
3.2.1	Effective Catchment Area.....	48
3.2.2	Network Structural Connectivity	49
3.2.3	Index of Connectivity	50
3.2.4	Spatially Distributed Sediment Delivery Ratio.....	52
Chapter 4: Results.....		54
4.1	The Influence of Landscape History.....	54
4.1.1	Process-Domain Delineation	55

4.1.2	Long-Profile Analysis	55
4.1.2.1	Stream Gradient Index	58
4.1.2.2	Valley Cross-Sections	58
4.1.3	Whiting-Bradley Classification	59
4.2	Measures of Sediment Connectivity	61
4.2.1	Effective Catchment Area	61
4.2.2	Network Structural Connectivity	62
4.2.2.1	Contemporary Network	62
4.2.2.2	Near Complete Connectivity	65
4.2.3	Index of Connectivity	67
4.2.3.1	Standard Index of Connectivity	67
4.2.3.2	Joint Index of Connectivity	69
4.2.3.3	Weight Factor Values	69
4.2.4	Spatially Distributed Sediment Delivery Ratio	71
4.2.4.1	AOIs 1 and 2 (2002 – 2008)	71
4.2.4.2	AOIs 1 and 2 (2008 – 2012)	73
4.2.4.3	AOI 3 (2002 – 2008)	74
4.2.4.4	Areas Removed	75
Chapter 5: Discussion		76
5.1	Qualitative Assessment	76
5.1.1	Field Observations: Patterns and Degree of Connectivity	76
5.1.1.1	Hillslope-Channel Coupling	76
5.1.1.2	Effective Catchment Area	76

5.1.1.3	Efficient Sediment Pathways.....	77
5.1.1.4	Event Magnitude Controls Connectivity.....	78
5.1.2	Field Observations: Patterns and Degree of Disconnectivity.....	79
5.1.2.1	Buffers.....	79
5.1.2.2	Barriers.....	79
5.1.2.3	Blankets.....	80
5.1.2.4	Inefficient Sediment Pathways.....	80
5.1.2.5	Spatial Patterns.....	81
5.1.2.6	Effective Timescales.....	83
5.2	Quantitative Connectivity Assessment.....	84
5.2.1	Landscape History and Hillslope-Channel Coupling.....	84
5.2.1.1	Landscape History.....	85
5.2.1.2	Hillslope - Channel Coupling.....	86
5.2.2	Measures of Sediment Connectivity.....	86
5.2.2.1	ECA.....	86
5.2.2.2	NSC and RF Indices.....	89
5.2.2.3	IC and IC _j	90
5.2.2.4	SD SDR.....	91
	Chapter 6: Conclusions.....	93
6.1	Main Conclusions.....	94
6.2	General Conclusions.....	94
	References.....	97
	Appendices.....	106

Appendix 1: DEM Co-referencing and Uncertainty	106
A.1: Co-referencing	106
A.2: Uncertainty Estimates	107
Appendix 2: Quantitative Methods	110
A.3: Slope-Area Plots	110
A.4: SDR – Area Plot.....	112

List of Tables

Table 1. Effective timescales of barrier, buffer, and blanket features within the Tahoma Creek watershed.	44
Table 2. Percent of area removed when calculating the SD SDR.	75
Table 3. Estimated spatial coverage values of selected sources of disconnectivity and their upstream affected areas.	83

List of Figures

Figure 1: Conceptual diagram of disconnectivity and connectivity within an open systems framework.	5
Figure 2: Location map of the Tahoma Creek watershed.	13
Figure 3. Geomorphic map of the Tahoma Creek watershed, Mount Rainier, WA.	19
Figure 4. Conceptual sediment budget of the Tahoma Creek watershed.	21
Figure 5. Sediment budget for the Tahoma Creek watershed during the (a) 2002 to 2008 period, and the (b) 2008 to 2012 period.	33
Figure 6. Selected photographs of sources of Disconnectivity within the Tahoma Creek watershed. All photos were taken during the 2019 field season.	35
Figure 7. Sources of disconnectivity landform map of Tahoma Creek.	37
Figure 8. Remote sensing map of sources of disconnectivity within the Tahoma Creek watershed.	38
Figure 9. Methodological example of calculating the stream gradient index.	46
Figure 10. Slope-Area plot of Tahoma Creek.	55
Figure 11. Longitudinal profiles and profiles of difference along Tahoma Creek.	56
Figure 12. Tahoma Creek long profile and cross-sections.	57
Figure 13. Stream gradient index for Tahoma Creek calculated following methods proposed by Hack (1973).	58
Figure 14. Degree of hillslope-channel coupling along Tahoma Creek.	59
Figure 15. Effective catchment area calculated using a variety of DEM resolutions and slope thresholds.	61
Figure 16. Accessibility, potential flow, NSC, and RF indices of the contemporary network at Tahoma Creek.	63
Figure 17. Residual flow regression plot of the contemporary network.	64
Figure 18. NSC and RF indices of Tahoma Creek assuming near complete connectivity.	65
Figure 19. Residual flow regression plot of the nearly completely connected network.	66
Figure 20. Index of connectivity (IC) map of Tahoma Creek with the river as the target.	68
Figure 21. Joint Index of Connectivity (IC _j) map of Tahoma Creek with the river as the target.	70

Figure 22. Distribution of weight factor values considering the two different scenarios.....	71
Figure 23. DoD and SDR maps of AOIs 1 and 2 for the period 2008 – 2002.....	72
Figure 24. DoD and SDR maps of AOIs 1 and 2 for the period 2012 – 2008.....	73
Figure 25. DoD and SDR maps of AOI 3 for the period 2008 – 2002.	74
Figure 26. Map of disconnectivity elements and their upstream affected areas based on flow routing.	82
Figure 27. Overlay map of connectivity indices.....	88
Figure 28. Graph of apparent change by aspect when performing a terrain-matching technique.	107
Figure 29. Long profiles and histograms of apparent change along the Westside Road.....	109
Figure 30. Slope – Area plots of selected tributary channels in the Tahoma Creek Watershed.	111
Figure 31. SDR – Area plots based on the SD SDR method.....	113

List of Supplementary Materials

Geomorphic map of the Tahoma Creek watershed, Mount Rainier, WA.

List of Abbreviations

accDoD.....	Accumulated DEMs of Difference (along flow pathways)
accErosion.....	Accumulated Erosion (along flow pathways)
AOI.....	Area of Interest
CIS.....	Cordilleran Ice Sheet
DEM.....	Digital Elevation Model
DoD.....	DEM of Difference
ECA.....	Effective Catchment Area
Fi.....	Potential Flow (of sediment through a node, NSC method)
GOF.....	Glacial Outburst Flood
IC.....	Index of Connectivity (method)
IC _j	Joint Index of Connectivity (method)
LIA.....	Little Ice Age
LiDAR.....	Light Detection And Ranging
LGM.....	Last Glacial Maximum
MFD.....	Multiple Flow Direction (Algorithm)
NPS.....	National Park Service (U.S.)
NSC.....	Network Structural Connectivity (method)
RF.....	Residual Flow (method)
RKM.....	River Kilometer (beginning at Tahoma Creek Bridge)
SDR.....	Sediment Delivery Ratio
SD SDR.....	Spatially Distributed Sediment Delivery Ratio (method)
Shi.....	Shimbel's Index (NSC method)
SSY.....	Specific Sediment Yield

Glossary

Alluvial Fan: Fluvial deposits in the shape of a low broad fan.

Barrier: Landform or feature that causes longitudinal disconnectivity within the fluvial process domain.

Blanket: Landform or feature that causes lateral disconnectivity between hillslopes and the active channel.

Buffer: Landform or sediment accumulation that causes vertical disconnectivity by smothering other sediments.

Connectivity: The spatially and temporally limited efficient state of a system in transferring matter and energy within and between system components.

Coupling: A physical linkage between two landscape compartments and subsequent exchange of mass and/or energy.

Debris Cone: Debris deposited in a conical shape with a surface slope greater than 10 degrees.

Debris Fan: A wedge-shaped deposit of loose rock, debris, and vegetation. Surfaces are steeper than alluvial fans, but less steep than debris cones.

Debris Flow: Fast moving flows of saturated mud, rock, and debris influenced by both solid and fluid forces.

Debris Torrent: A channelized debris flow.

Decoupling: The lack of a physical linkage between two landscape compartments resulting in no exchange of mass or energy.

Digraph: A graph made up of vertices connected by unidirectional edges. Often called a directed graph.

Disconnectivity: The dominant but inefficient state of a system in transferring matter and energy within and between system components at all spatial and temporal scales.

Effective Timescale: The timescale over which something operates or is functional.

Flowslide: Shallow failure of granular soil due to saturation.

Functional Connectivity: The component of connectivity controlled by how the active processes interact with the structural connectivity of the system resulting in the transfer of matter and energy.

Glaciofluvial: Sediment deposited and reworked by glacial meltwater streams in an ice-contact or proglacial setting.

Graph Theory: The mathematical theory of the properties and applications of graphs.

Hyper-concentrated Flow: A two-phase flow intermediate to “normal” stream flows and debris flows in both sediment concentration and behavior. May transition into or from a non-cohesive debris flow.

Index: A representation of a phenomenon based on conceptual understanding and/or statistical relationships.

Lahar: A mass wasting runout event or deposit directly or indirectly related to volcanic activity.

Paraglacial: Non-glacial processes or deposits that are directly conditioned by glaciation and deglaciation.

Parkland: Gently sloping bedrock surface composed of ancient lava flows scoured by glacial erosion.

Process Domain: Delineated zones within the landscape in which a suite of processes plays a significant role in the detachment, transport and deposition of sediment.

Proglacial: The area located close to the ice front of a glacier, ice cap, or ice sheet.

Sediment Delivery Ratio: The ratio between sediment yield and gross erosion, often expressed as a percentage.

Sediment Yield: The amount of sediment reaching or passing a specified point in a given period of time.

Structural Connectivity: The component of connectivity controlled by the structural configuration and topographic characteristics of the system.

Tarn: Small mountain lake occupying a depression in glacially carved bedrock.

Valley Train: A long narrow body of glaciofluvial sediment along the floor of a valley.

Acknowledgements

I would first like to thank my partner McKelle. She has always been incredibly supportive of my personal and career goals. She is the only reason I have any semblance of work-life balance and is always planning wonderful adventures that are a welcome distraction.

Marwan, thank you for allowing me to develop my ideas under watchful care. I have learned a lot from you concerning geomorphology and exceptional leadership. I look forward to working with you throughout my Ph.D. Olav, I greatly appreciate the fruitful discussions we had, and your kind words throughout the research process. Your past and current work continually inspire me.

I want to thank the Geology and Imminent Threats Team at Mount Rainier National Park for their immense help throughout the fieldwork process. Taylor Kenyon, Robert Jost, and Scott Beason were always willing to help with the logistics of field research and answer any questions about Rainier. Paul Kennard provided an expert introduction to the geomorphology and previous research at Mount Rainier. Scott Anderson was always willing to discuss the Tahoma Creek watershed and kindly shared data from his work. His research provided a strong foundation for my thesis, to which I am grateful.

To the entire Hassan research group, thank you for bringing clarity to diverse research topics and guiding my research through conversations and feedback. I would also like to thank the UBC Geography Department staff for their logistical and technical support.

Chapter 1: Introduction

1.1 Background

Connectivity has emerged as a prominent topic of discussion (Slaymaker and Embleton-Hamann, 2018), but is still a source of confusion within geomorphology (Wohl et al., 2018).

Disconnectivity, on the other hand, remains largely unexplored with very few studies focusing on its importance (Fryirs et al., 2007a and 2007b; Fryirs, 2013; Hoffmann, 2015; Grant et al., 2017). Neither term has been defined and placed within a framework in a satisfactory way.

Some authors are beginning to hypothesize that both connectivity and disconnectivity play a role in landscape evolution and system dynamics with neither holding sway over the other and both needed to see the landscape as it is (Grant et al., 2017), while most authors still focus entirely on the connectivity of systems.

This thesis focuses on both disconnectivity and connectivity within glaciated landscapes, to better understand the relative importance and applicability of each term, and to assess a variety of methods that quantify connectivity. In addressing the above issues, chapter 1 will; (i) clearly define disconnectivity and connectivity and discuss where they fit within a conceptual framework, (ii) discuss glacial- and proglacial- specific considerations of the study, (iii) introduce the study area while placing it within a geological context, and (iv) layout the research design.

1.1.1 Previous Definitions

Connectivity is a term that was used in many fields, such as ecology (Bennett, 2004), before being introduced into geomorphology where it has emerged as a prominent topic of discussion (Harvey, 2001; Hooke, 2003; Brierly et al., 2006; Fryirs, 2013; Bracken et al., 2015; Cossart et al., 2017; Slaymaker and Embleton-Hamann, 2018). Despite, or possibly because of, the increased attention that the term connectivity has received in the last two decades, it carries many different definitions and meanings (Harvey, 2002; Hooke, 2003; Bracken and Croke, 2007; Fryirs et al., 2007; Bracken et al., 2013; Cavalli et al., 2013; Fryirs, 2013; Bracken et al., 2015; Czuba and Foufoula-Georgiou, 2015; Carrivick et al., 2017) and is not clearly defined within the

geomorphology community (Wohl et al., 2018). For example, Fryirs (2013) defines sediment disconnectivity as “*the water-mediated transfer of sediment between two different compartments of the catchment sediment cascade,*” while Cavalli et al. (2013) define it as “*the degree of linkage that controls sediment fluxes throughout landscapes and in particular between sediment sources and downstream areas.*” Without establishing a broad, all-encompassing definition, many descriptors have been attached to the term including hydrologic, sediment, structural, static, functional, dynamic, process, geomorphic, and landscape, each ascribing a different meaning. As a result of the loosely related nature of the many terms, it is difficult to compare across studies, and there is a lack of standardization of what is conceptually a simple parameter describing a system. It is also important to note that while the term became prevalent only recently, the concept has been inferred for a long time when calculating sediment budgets (Dietrich et al., 1982).

The disconnected nature of landscapes is noted in studies of geomorphic thresholds (Schumm, 1979), where landscapes can be considered in a state of disconnectivity until necessary thresholds are surpassed, and efficient transfer occurs (briefly). Disconnectivity is generally seen as the antithesis or inverse of connectivity such as, “*the degree to which any limiting factor constrains the efficiency of sediment transfer relationships*” (Fryirs et al., 2007). Framing disconnectivity in terms of connectivity suggests that systems are generally in a state of efficiency/connectivity. However, disconnectivity dominates most geomorphic systems at nearly all spatiotemporal scales. In response, we suggest new general definitions of disconnectivity and connectivity, emphasizing disconnectivity.

1.1.2 Unequal Discussion of Connectivity

One might wonder why connectivity has been so preferentially discussed within the literature if disconnectivity is the more common state of the system. One potential explanation lies in the changing intellectual climate of geomorphology. From the birth of “modern geomorphology” up until the mid-20th century, geomorphologists were primarily concerned with historical interpretations and descriptions of the Earth’s surface and landforms (Church, 2010).

Beginning around the second half of the 20th century, technological advances and the development of absolute dating methods (Walker, 2005) aided the transition from historical to process geomorphology (Church, 2010). Several seminal papers are notable in encouraging this transition (Horton, 1945; Strahler, 1950 and 1952; Wolman and Miller, 1960). Process geomorphology was and is still concerned with quantitatively understanding the processes that shape Earth's surface applying math- and physics-based arguments. Process geomorphology extends to predictions of future events and public safety issues, calling for indices and models to aid in this prediction.

In recent decades, connectivity indices evolved alongside process geomorphology to aid in the quantification and prediction of system functioning. Today numerous connectivity indices exist (Heckmann et al., 2018). It seems reasonable that the shift in focus from historical to process geomorphology had a ripple effect on subdisciplines within the field, leading to the pronounced emphasis on connectivity rather than disconnectivity. Disconnectivity is firmly grounded on the principles of historical geomorphology, helping to understand sedimentary archives and modern landscape morphology, fields of research that have not so intently called for indices.

1.1.3 Disconnectivity

1.1.3.1 Our Definition

Because we judge that disconnectivity is the more common characteristic of geomorphic systems, we suggest defining disconnectivity as the dominant but inefficient state of a system in transferring matter and energy between system components at all spatial and temporal scales. By defining disconnectivity as the dominant state, the emphasis is placed on the infrequent and spatially limited nature of mass and energy transfer within systems.

This new definition will not come as a surprise to those who are familiar with the literature, as it modifies previous definitions (Wohl et al., 2018; Chorley and Kennedy, 1971), with additional emphasis on the fragmented and inefficient nature of most landscapes. In response to the recognized benefit of generalizing the term (Wohl et al., 2018), this definition is meant to be general enough to apply to and facilitate comparisons between all fields within the earth

sciences. The word “inefficient” within the definition implies viewing disconnectivity as a parameter describing a system and can, therefore, be quantified and measured. The inclusion of the word energy also seems to be necessary. It acknowledges that signals are often transferred (or not) through a system as changes in energy in addition to the transfer of mass. For example, stream systems respond to base-level changes by propagating energy signals upward through the system. We are careful to note that disconnectivity should be held independent of volumetric transfers; low transfer rates/volumes do not always indicate disconnectivity but may be a function of sediment availability.

In its most general form, disconnectivity can be a measure of the inefficiency of a system in transferring energy, water, dissolved solids, suspended load, coarse load, etc. Throughout this thesis, we are specifically referring to coarse sediment disconnectivity (bedload) unless otherwise specified. Throughout the following sections, we will discuss the application and implications of the term sediment disconnectivity within a framework and in relation to different spatiotemporal scales, and grain sizes.

1.1.3.2 Framework

We suggest that the term disconnectivity should be considered as a parameter describing the inefficiency of a system’s response to changing conditions within an open systems framework, and not in and of itself a conceptual framework (Figure 1). An open system framework allows energy and mass to both enter and leave the system, which is often a general requirement of geomorphic systems. For example, at the catchment scale, climatic events add mass to the system through rainfall, while water and sediment exit the system through a variety of erosion and transfer processes.

In considering coarse sediment disconnectivity, process domains are particularly useful spatial units of measure. Process domains are delineated zones within the landscape in which a suite of processes plays a significant role in the detachment, transport and deposition of sediment (Brardinoni and Hassan, 2007). Within a given process domain, the form of the landscape (as

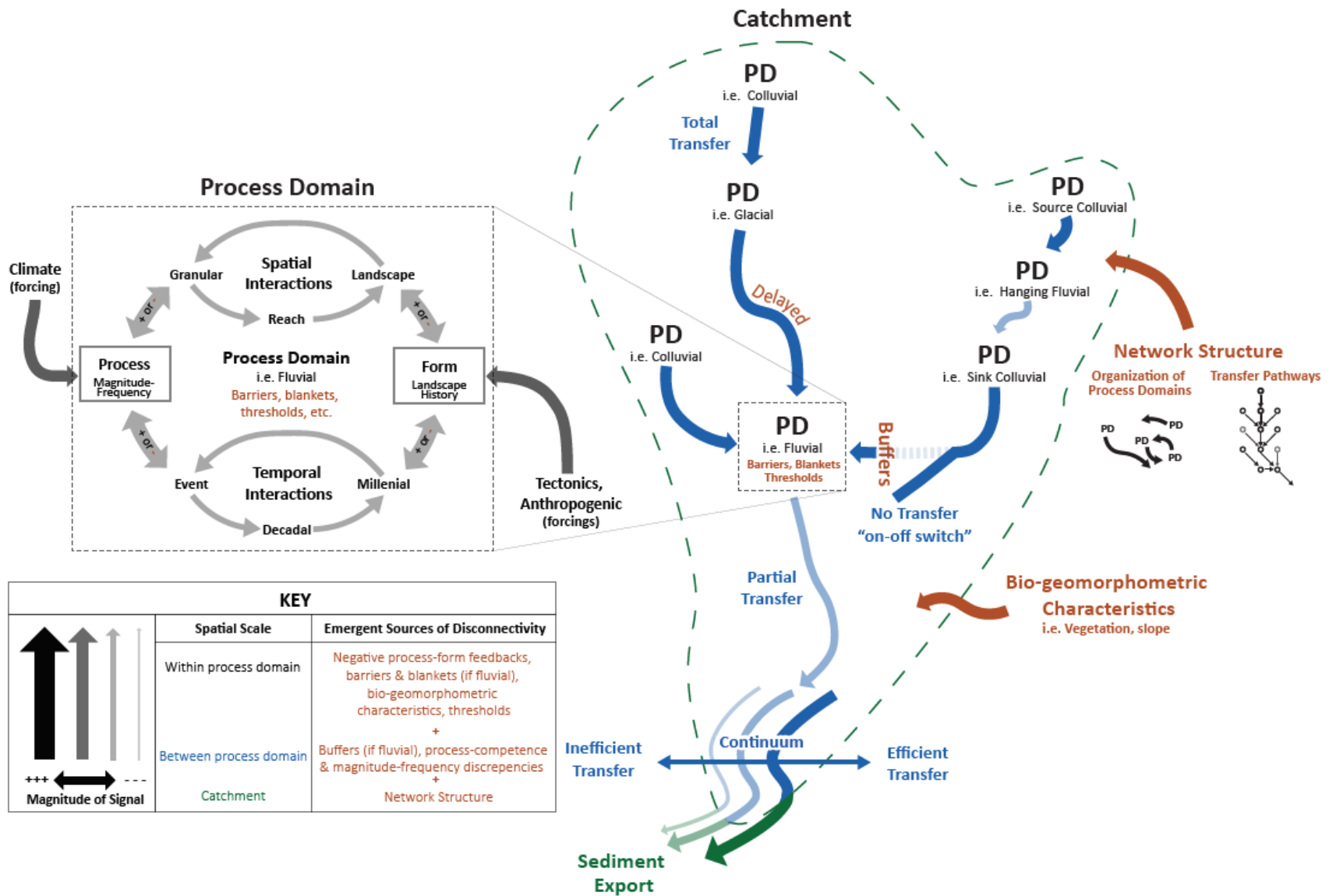


Figure 1: Conceptual diagram of disconnection and connectivity within an open systems framework.

determined by the landscape history), alongside the climate, sets the boundary conditions for and controls the types and magnitudes of active processes (Figure 1). The processes, in turn, reshape the landscape altering the form, etc. Within process domains, there exist negative feedbacks, and sources of disconnectivity that result in inefficient signal transfer. For example, within fluvial process domains, barriers and blankets are common, and thresholds exist that limit significant sediment transport to higher discharges. The application of critical shear stress in most sediment transport equations highlights the importance of thresholds in relation to grain size. As the grain size of interest increases, so does the measured disconnectivity of the system.

At the catchment scale, sediment disconnectivity is generally influenced by the spatial arrangement and presence of disconnecting landforms, bio-geomorphometric characteristics, thresholds, negative feedbacks, network structure, and the magnitude-frequency distributions of the dominant processes of sediment detachment, transport and deposition (Figure 1).

Disconnectivity arises at all spatial scales, as is noted in Figure 1 as emergent sources of disconnectivity. Sources of disconnectivity act to delay, disperse or disrupt the signal transfer (as represented as arrows of reduced size and opacity in Figure 1). Thresholds may also fully prevent transfer until an energy level is surpassed (shown as the “on-off switch”, Figure 1).

Disconnectivity is essential in understanding how and why landscapes retain matter and energy and remain in a state of transience or disequilibrium. The degree of disconnectivity is also determined by the spatial and temporal scale of interest.

1.1.3.3 Temporal Scale

When assessing the degree of disconnectivity, one must first define the temporal scale of interest (i.e. event, annual, decadal, etc.), because scale determines whether a given variable is dependent or independent (Schumm and Lichty, 1965). In general, a system’s degree of disconnectivity decreases with increasing temporal scale. Additionally, a landscape that is connected according to long-term processes but disconnected in terms of short-term processes would be considered less sensitive to landscape change (resilient), requiring longer temporal scales for change to occur (Harvey, 2001). The complex interactions between the dominant processes of sediment detachment, transport and deposition directly influence the temporal patterns of disconnectivity.

For example, landscapes dominated by infrequent high-magnitude landslides will be more temporally disconnected than a landscape dominated by frequent gully erosion events, even though both landscapes may have similar denudation rates.

Fryirs et al. (2007a and 2007b) noted many different sources of disconnectivity as well as their postulated effective timescales, which range from years to thousands of years. One reason to treat disconnectivity as separate from connectivity is that the effective timescales of landforms and characteristics causing disconnectivity don't always match the timescales over which connectivity operates.

1.1.3.4 Spatial Scale

Disconnectivity studies have three main spatial scale components, (i) the area of interest, (ii) the division of the area of interest (as a system) into component parts, and (iii) the spatial resolution of the data used to measure disconnectivity. Process domains and catchments are common areas of interest in geomorphology, but disconnectivity can be measured at all spatial scales. In general, as the area of interest increases, so does the disconnectivity of a system. For example, even if connectivity is high within individual process domains, the landscape may be in a state of disconnectivity. Boundaries between process domains are often locations of sediment disconnectivity, at least in part due to the different thresholds, magnitude-frequency relationships, and the complex ways in which adjacent domains do or do not interact (Harvey, 2002; Croke et al., 2013). Additionally, at small spatial scales, most parameters can be held constant (i.e. climate, land use, etc.), but as the reference area increases, many parameters must instead vary in space.

Studies concerned with disconnectivity and connectivity then subdivide the area of interest into component parts such as raster cells (Cavalli et al., 2013; Heckmann and Vericat, 2018), nodes and edges (Cossart and Fressard, 2017; Fressard and Cossart, 2019), geomorphic cells (Poepl and Parsons, 2018), river reaches (Wohl, 2017), etc. The component parts are chosen to match the area of interest and are inherently smaller in scale. For example, if the area of interest is the fluvial process domain, then individual river reaches are an obvious component part.

Finally, the spatial resolution of the data used to measure disconnectivity must be carefully selected. For example, if a raster dataset is used, the spatial resolution of the raster must be chosen to be representative of the system and its component parts. One study found that the measured/calculated disconnectivity systematically increases with higher DEM resolution (Cantreul et al., 2018). Measured disconnectivity from raster datasets will contain both “real” sources of disconnectivity and artifacts from the DEMs. DEM resolution will be discussed in more detail in chapters 3 and 4.

1.1.3.5 Grain Size

When referring to the inefficiency of mass transfer within a system, the differentiation between dissolved solids, suspended load, and coarse load material is necessary. These three-grain size distributions each have different characteristics and will subsequently have different patterns of disconnectivity.

At the catchment scale, grain size distributions will not be constant in space but follow general trends. For example, the dissolved solids and much if not all of the suspended load reach the catchment outlet while the bed load is often limited to the upper portion of the catchment, depending on the scale. This is a result of stream power and selective transport. As a result, the efficiency of transfer decreases as the grain size in question increases.

Additionally, disconnecting landforms differentially affect sediment of varying size. Landforms such as proglacial lakes effectively disconnect the upslope contributing area with respect to the coarse load and suspended load (Geilhausen et al., 2013), while channel bed armouring may only partially disconnect the coarse load without affecting either the suspended load or dissolved solids. The spatial arrangement and presence of landforms that cause disconnectivity, therefore, create increased spatial heterogeneity and moderate sediment fluxes within the landscape.

1.1.4 Connectivity

1.1.4.1 Our Definition

We suggest defining connectivity as the spatially and temporally limited efficient state of a system in transferring matter and energy between system components. In other words, connectivity is a special case of disconnectivity in which efficient transfer occurs within the spatiotemporal scale of interest.

Within the literature, the distinction between connectivity and disconnectivity is not a clearly defined value. Instead, it is often a subjective distinction made by the authors of individual studies based on their definitions and framework. For example, Hooke (2003) created a classification with five categories of connectivity/disconnectivity, noting the specific criteria for each category. Connectivity indices often provide relative rather than absolute values facilitating comparisons between the component parts of the system. Once general definitions are agreed upon, it would be greatly beneficial to identify the boundary between or categories of connectivity and disconnectivity, an avenue for future work.

1.1.4.2 Framework

When focusing on sediment transfer within a river catchment, sediment connectivity is the spatially and temporally limited efficient state of the landscape in transferring sediment within and between process domains. Connectivity is dependent on the internal functioning of the process-form relationship in response to changing external forcings, with all the associated positive and negative spatiotemporal feedbacks and thresholds (Figure 1). A catchment in a state of connectivity would be represented by the efficient transfer of sediment and energy, as shown by larger and uninterrupted arrows and would have little or no time-lag in transferring the signal (Figure 1). Such a system would have few or no negative feedbacks that delay, disperse, or disrupt the signal transfer. Additionally, positive feedbacks (represented by the addition sign in the spatial and temporal interactions within process domains) may amplify the signal.

1.1.4.3 Temporal Scale

In general, a system's connectivity increases with increasing temporal scale. Additionally, increasing overall catchment connectivity results in a greater sensitivity to changing conditions (i.e. climate change, tectonics, anthropogenic disturbances, etc.).

Within the literature, there are numerous methods of quantifying sediment connectivity (Heckmann et al., 2018), many of which are static (Fryirs et al., 2007b; Cavalli et al., 2013; Heckmann et al., 2013; Cossart et al., 2017) rather than representative of changes that occur over time (Lane et al., 2017; Heckamann et al., 2018). These snapshot measurements of connectivity are applicable at the temporal scale at which process-form feedbacks occur. In other words, as geomorphic processes alter existing landforms or produce new landforms, the connectivity of the system may change in response, rendering previous assessments no longer valid.

1.1.4.4 Spatial Scale

A detailed discussion of the spatial components of connectivity will not be repeated here; instead, spatial characteristics that are unique to connectivity will be addressed. In general, system connectivity negatively correlates to the spatial scale of interest. It is important to note that the connectivity of a large area is not merely the sum of the connectivity of its components but must also consider emergent properties (Heckmann et al., 2018). For example, catchment-scale connectivity is not the sum of the connectivity within the individual process domains but must also consider the organization and degree of coupling between them (Brardinoni and Hassan, 2006; Figure 1). To capture the emergent properties of scale, the area of reference should be sufficiently larger than the landforms or process domains over which you want to measure connectivity. One study found that previously glaciated catchments display variable hillslope-channel coupling as a result of the reorganization of process domains and therefore have a unique signature of catchment connectivity (Hassan et al., 2018). In this case, a connectivity assessment at the individual process-domain scale would be ignorant of this reorganization. This thesis approaches the quantification of connectivity at the catchment scale to capture the effects of the spatial organization of landforms and process domains within the catchment.

We are also mindful of the effects of spatial data resolution on results. A recent study comparing the effects of DEM resolution on the index of connectivity (Cavalli et al., 2013) suggests that 1-meter DEMs may be ideal for catchment-scale assessments of connectivity, offering a compromise between computing efficiency and level of detail (Cantreul et al., 2018). Other studies modelling the effective catchment area suggest that low-resolution DEMs (25 meter) better model tributary sediment connectivity as opposed to 1- or 5-meter DEMs (Lisenby and Fryirs, 2017).

1.2 Glacial and Proglacial Specific Considerations

The history of the landscape influences the spatial arrangement and morphology of landscape features, which in turn directly affects the spatial heterogeneity of sediment disconnectivity and connectivity (Slaymaker et al., 2017). Landscape history can also impose controls on the current processes to a large degree. For example, the landscapes of British Columbia have still not fully recovered from past glaciations 14 ka since the last ice retreat. As a result, the glacially inherited topography drives the active processes of sediment transport (Brardinoni et al., 2006).

Pleistocene glaciations in British Columbia were also found to control the channel gradient and subsequently the transport of coarse sediment and channel morphology within previously glaciated mountain streams (Cowie et al., 2014; Dell’Agnese et al., 2015).

Within previously glaciated basins, the specific sediment yield may increase as the area drained becomes larger due to the reworking of fine material in the stream banks and adjacent slopes (Church and Slaymaker, 1989). The specific sediment yield in non-glaciated basins, however, consistently declines as the drainage area increases. Glacially carved valleys, which are generally U-shaped and have wide valley bottoms, often have hillslopes that are decoupled from the stream channel (Hassan et al., 2018).

Proglacial systems are transitional landscapes between glacial and nonglacial conditions, and as such, are among some of the most dynamic and rapidly changing places on earth. Some studies indicate that the rate of change is fastest in the area closest to the glacier front and declines with

increasing distance (Staines et al., 2015; Delaney et al., 2018). This finding complements the paraglacial sedimentation curve proposed by Church and Ryder (1972), which shows maximum sediment movement occurring during and immediately following deglaciation, with rates rapidly declining thereafter. The rapid rates of geomorphic change in proglacial systems, (Church and Ryder, 1972; Carrivick and Heckmann, 2017) shortens the period required to measure significant change and subsequent transfer efficiencies, making them great places to study connectivity. Proglacial systems are also great locations to explore disconnectivity due to the introduction of disconnecting landforms from glacial processes.

Several studies on connectivity were designed for and applied to glaciated or recently deglaciated landscapes (Cossart, 2008; Cavalli et al., 2013; Cossart and Fressard, 2017; Heckmann and Vericat, 2018). Additionally, many studies address proglacial morphodynamics, such as those from the PROSA (High-resolution measurements of morphodynamics in rapidly changing PROglacial Systems of the Alps) project in Tyrol, Austria (Morche et al., 2015; Heckmann et al., 2016; Hilger et al., 2017). Considerations of landscape history, relative rates of geomorphic change, and applicability of published methods factored into the selection of our study site, the Tahoma Creek watershed at Mount Rainier, WA.

1.3 Study Area

The Tahoma Creek watershed drains the southwest flank of Mount Rainier, an active stratovolcano within the Cascade Range of Washington (Figure 2). The watershed covers approximately 40 km² and contains two glaciers, the South Tahoma Glacier and a small fork of the much larger Tahoma Glacier. Throughout this thesis, locations along the valley floor will be noted in kilometers upstream from the Tahoma Creek bridge along the Paradise Road (Figure 2). The main branch of Tahoma Creek originates at the base of the South Tahoma Glacier at about river kilometer (RKM) 13. From its headwaters, Tahoma Creek cascades over bedrock ribs and patches of Neoglacial sediments for one kilometer before flowing through a deeply incised narrow canyon of unconsolidated Neoglacial drift.

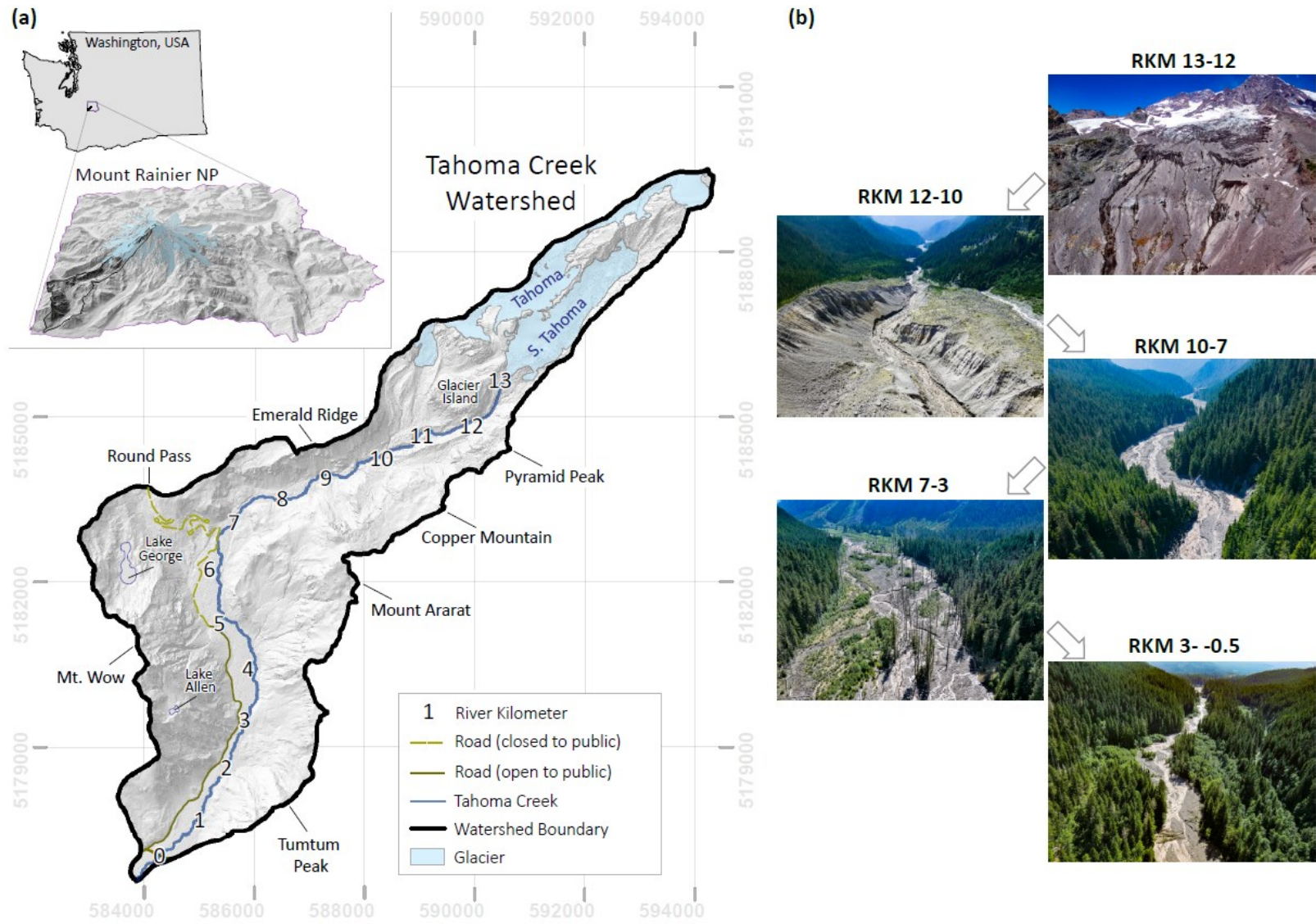


Figure 2: Location map of the Tahoma Creek watershed. (a) Location map with selected place names from the text. (b) Photos chosen to represent the defined reaches of river. River kilometers are measured as upstream distances from the Tahoma Creek bridge.

By RKM 10, Tahoma Creek joins a tributary draining a fork of the Tahoma Glacier and continues to flow through a narrow canyon for another half of a kilometer. From here, RKM 9.5, the river exits the proglacial zone and flows through a moderately narrow confined reach for two more kilometers before spilling out into an expansive unconfined valley. The valley remains unconfined and is characterized by mixed terrace, floodplain, and active channel components with numerous dead tree-stands between RKM's 7.5 – 3.5. Downstream of this point, the active channel narrows once again and is flanked by forested paired terraces for three kilometers before the valley opens to a broad debris fan, and Tahoma Creek joins the Nisqually river.

1.3.1 Geologic History

1.3.1.1 Mount Rainier Volcanics

The first andesite lavas flows that built Mount Rainier's volcanic edifice surged down canyons carved into a mountainous pre-Rainier landscape during the early Pleistocene (Fiske et al., 1963). Over time, episodic lava flows built the volcanic cone to a height of 1000 feet higher than its present form. Glaciers and mass wasting processes that once failed to keep pace with these voluminous lava flow events have, since the local LGM, reduced the overall height of the volcano and have once again carved deep canyons into the volcanic cone. Today, many of the oldest intra-canyon lava flows now form ridge crests hundreds of meters above the modern valley floors recording the dynamic history of Mount Rainier's landscape.

1.3.1.2 Glacial History

Throughout the Pleistocene and Holocene, glacier extents at Mount Rainier fluctuated dramatically. During the early to mid-Pleistocene, much of Mount Rainier was covered in a thick ice cap, and glacier tongues may have extended past the volcano's flanks to coalesce with the Puget lobe of the Cordilleran Ice Sheet (CIS) (Crandell and Miller, 1974). During the late Pleistocene (~80-40 ka) and corresponding to the Salmon Springs Glaciation, the ice cap over Rainier extended as far west as Mount Wow overtopping Mount Ararat and leaving Tumtum peak as a nunatak (Crandell and Miller, 1974).

Later, during the LGM (locally termed the Fraser Glaciation, 17-18 ka) the South Tahoma Glacier was likely confined to the valley floor, but still extended beyond the modern watershed boundary to join the Nisqually Glacier. This period of glaciation is evidenced by Evans Creek Drift exposed here and there along lower hillslopes as far as the catchment outlet (Crandell and Miller, 1974). Locally, the Pleistocene-Holocene transition corresponded to a cold and dry climate without glacier advances, in contrast to many other areas globally (Heine, 1998). More recently, Neoglacial advances during the 16th and 19th centuries (1550 AD, 1840 AD) within the Tahoma Creek watershed are recorded in terminal moraines 3.5 kilometers below the modern-day glacier termini (Sigafos and Hendricks, 1972). During this time, Garda drift was deposited, and impressive lateral moraines were formed.

Today, Mount Rainier's summit is covered in over 91 km² of snow and ice, including 25 glaciers, making it the largest single-peak glacial system in the U.S. (Graham, 2005). Many of the glaciers are only divided by sharp bedrock ridges and extend several kilometers down valley. As the glaciers continue to retreat up the flanks of the volcano, a newly uncovered thick blanket of unconsolidated glacial till (~3.5 km²) is subject to fluvial and mass wasting processes. We refer to this zone within the confines of the Neoglacial (LIA) moraines as the proglacial zone (Carrivick and Heckmann, 2017).

1.3.1.3 Mass Wasting

Many mass wasting processes occur at Mount Rainier including, rockfall events, lahars, debris avalanches and debris flows. While exact definitions of many mass wasting processes vary, this thesis will adopt terminology from previous work done at Mount Rainier (Scott et al., 1995). The term lahar will be used exclusively for events and deposits directly or indirectly related to volcanic activity (i.e. melting of snow/ice by volcanic heat, large flank collapse due to hydrothermal alteration), mudflows are the fine-grained counterparts (>50 % sand-size or smaller) of debris flows, and debris flows are divided into cohesive and non-cohesive categories.

Cohesive debris flows are those that have a high (>3%) clay content. The clay particles add cohesion and strength to the flow as well as reduce the grain interaction, the differential

movement and settling of particles, and the miscibility of the flow with streamflow (Scott et al., 1995). Non-cohesive debris flows have a low (<3%) clay content and are characterized by grain-to-grain interaction, cataclasis, high rate of flow attenuation, and flow transitioning. Non-cohesive debris flows often begin as streamflow surges or floods, transition to hyper-concentrated flows and then debris flows through bulking, followed by inverse transitioning downstream as the coarse sediment is deposited. Here, the term debris flow corresponds to small, non-cohesive debris flows that occur regularly within Tahoma Creek unless otherwise specified. Chapter 2 discusses mass wasting process in greater detail.

1.3.2 Anthropogenic Influence

Mount Rainier is the focal point of Mount Rainier National Park, which was established in 1899 as the fifth national park in the United States. Mount Rainier is located 95 kilometers (straight-line-distance) to the southeast of Seattle, Washington. The National Park Service (NPS) is mandated to ‘preserve unimpaired the natural and cultural resources of the National Park System for the enjoyment, education, and inspiration of this and future generations’ (Thomas and Kennard, 2015). This is not an easy task with increased visitation, climate change and natural hazards. In recent years, debris flows and floods within the watershed have caused the closure of the Tahoma Creek Campground (1967), the Westside Road past Dry Creek (1993), and the Tahoma Creek Trail (2019) (Thomas and Kennard, 2015). This thesis aims to provide additional insight into sediment source areas, transfer pathways, and transfer efficiencies within this dynamic watershed to better inform management decisions.

1.4 Research Design

This thesis addresses two primary objectives formed as research questions. First, does disconnectivity or connectivity explain the spatial variability of sediment transfers? We address this question in chapter 2 by first presenting a geomorphic landform map created in the field while also noting the connectivity within a sediment budget framework. We then identify sources of disconnectivity and map their spatial configurations.

Second, how well do current methods of quantifying sediment connectivity describe the observed spatial patterns of sediment transfers? This question is addressed in chapters 3 (methods) and 4 (results), by first gaining an understanding of the topographic signature of process domains and paraglacial adjustment, followed by applying a wide variety of connectivity indices. The indices of connectivity that will be applied include the Effective Catchment Area (Fryirs et al., 2007a and 2007b; Lisenby and Fryirs, 2017), the Network Structural Connectivity and Residual Flow (Cossart and Fressard, 2017; Fressard and Cossart, 2019), the Index of Connectivity (Cavalli et al., 2013), and the Spatially Distributed Sediment Delivery Ratio (Heckmann and Vericat, 2018). These methods are compared against fieldwork and historical data based on the previously defined definitions and framework. Chapters 5 and 6 are dedicated to the interpretation/discussion of the results and the conclusion, respectively.

Chapter 2: The Relative Importance of Connectivity vs. Disconnectivity: A Case Study from Mount Rainier, WA

The Tahoma Creek watershed lies within Mount Rainier National Park, and as a result, there is a rich history of monitoring and research efforts regarding sediment transfers and geomorphic processes. This chapter synthesizes park records of significant events within the watershed and includes many qualitative descriptions that should be taken as such. Following the distinction between connectivity and disconnectivity offered in Chapter one, the first half of this chapter seeks to synthesize descriptions of connectivity through a sediment budget framework after introducing a geomorphic map created by the author during the 2019 field season. The second half of the chapter synthesizes the sources of disconnectivity, their spatial distributions, and their estimated effective timescales using the same geomorphic map and field descriptions.

2.1 Geomorphic Map

During the 2019 field season a geomorphic landform map of the Tahoma Creek watershed was created at a scale of 1:8,000 (Figure 3). This map builds on work from others, especially a 1:24,000 scale landform map by Riedel and Dorsch (2016). Exposed bedrock was delineated while in the field and then specific rock Formations were labeled based on previous work by Fiske et al. (1963). Moraine ages are based on work by Sigafoos and Hendricks (1972). Additionally, notes were taken while in the field concerning locations of hillslope-channel coupling, sediment transfer pathways, sediment transfer processes and their relative importance, and sources of disconnectivity. The resulting geomorphic map and subsequent sediment budget best represent the lens through which we discuss sediment disconnectivity and connectivity within the watershed, while providing a comparison for the indices of connectivity in the following chapters.

2.2 Connectivity Within a Sediment Budget Framework

“A sediment budget for a drainage basin is a quantitative statement of the rates of production, transport, and discharge of detritus” with the incorporation of changes in storage and

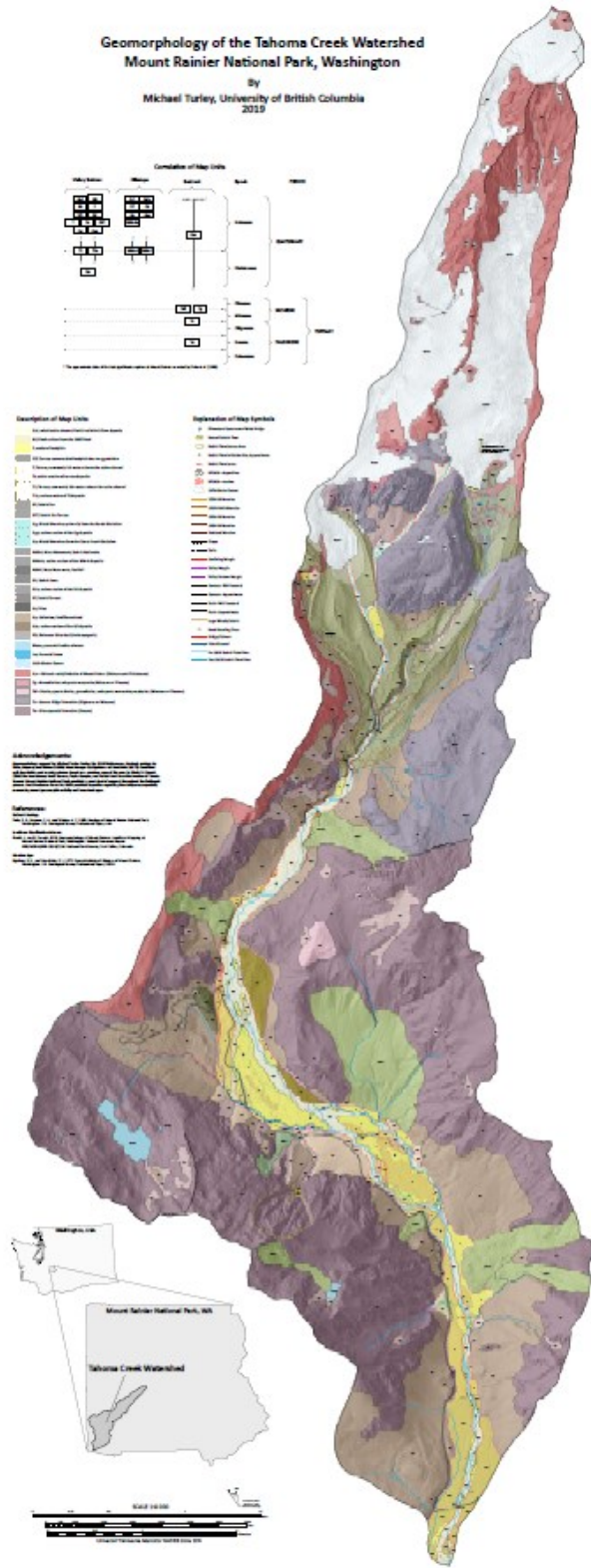


Figure 3. Geomorphic map of the Tahoma Creek watershed, Mount Rainier, WA. See supplementary materials for full-sized image.

specification of the contribution of different processes (Dietrich et al., 1982). The sediment budget framework is a rich management tool (Slaymaker, 2003; Walling and Collins, 2008) and is often applied at the catchment-scale (Walling and Collins, 2008). In conceptualizing the system as a sediment cascade through temporary sediment stores, sediment budgets are products of functional connectivity and sediment availability/production. While acknowledging that as a mass balance approach, sediment budgets should include an accounting of water, sediment, solute, and nutrient fluxes, and that anything less may seriously limit its quality (Slaymaker, 2004) this thesis is restricted to a description of the coarse fraction of sediment. Here we are primarily concerned with land-forming materials (coarse sediment), which have been the main focus of past literature at Mount Rainier.

In this section, we present a coarse sediment budget over human-timescales (~100 years) for the Tahoma Creek watershed based on a compilation of historical records, published literature, and original contributions from this thesis. This synthesis relies heavily on a previous coarse sediment budget of the area (Anderson and Pitlick, 2014; Anderson, 2013), and park records. Sediment sources, sinks, and pathways were noted in the field during the 2019 field season. The sources were then categorized as either primary or secondary in nature. The secondary sources category refers to hillslope or valley storage components that periodically act as sediment sources, while primary sources are the original stores. Significant sources, sinks, and pathways will be discussed in the following paragraphs, while a more complete accounting is conceptualized in Figure 4.

2.2.1 Calculating Components of the Budget

Several components of the sediment budget were calculated by performing net change analysis using LiDAR from 2002, 2008, and 2012. The 2008 and 2012 LiDAR data cover virtually the entire watershed, while the 2002 LiDAR covers the active channel and adjacent hillslopes from the glacier front to RKM 1.25. For a more complete description of the datasets see Anderson and Pitlick (2014). The LiDAR datasets were co-referenced using a terrain-matching technique (Anderson and Pitlick, 2014), and the uncertainty was calculated using the Westside road as registration points (see appendix A.2: on uncertainty). We restricted our analysis to the valley

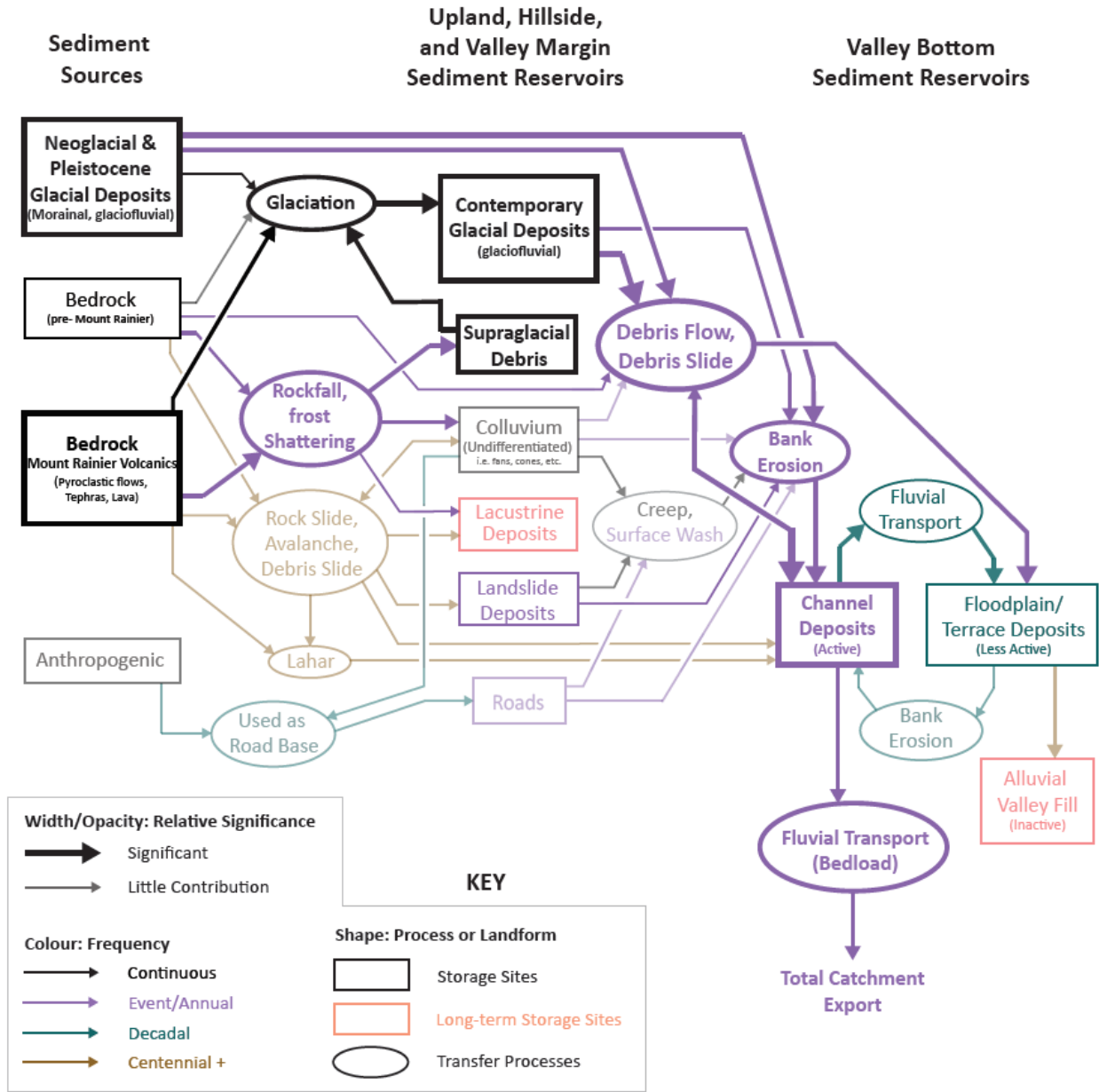


Figure 4. Conceptual coarse sediment budget of the Tahoma Creek watershed. Figure modified from Jordan and Slaymaker (1991).

floor and adjacent active hillslopes to avoid unnecessarily including large areas with insignificant change and increased uncertainties (vertical datum uncertainty scales linearly with area).

2.2.2 Sources

2.2.2.1 Primary Sources

The primary sources of sediment within the Tahoma Creek watershed include bedrock (both pre-Mt. Rainier and Mt. Rainier volcanics), glaciogenic sediment, and sediment synthetically added to the system by humans. Bedrock outcrops in the headwall of the South Tahoma Glacier, along the bedrock ridges dividing the Tahoma, South Tahoma, and Pyramid glaciers, and along many of the ridges forming the watershed divide. Pre-Mount Rainier bedrock, including the Ohanapecosh and Stevens Ridge Formations as well as intrusive granodiorites and quartz monzonites, dominate the watershed below the glacier termini. Above the glacier termini, andesite of the Mount Rainier volcanics dominates and subsequently is the main source of supraglacial, englacial, and subglacial debris. The bedrock forming the volcanic cone, composed mainly of andesite, is susceptible to hydrothermal alteration into clay which can cause large flank collapses (Fiske et al., 1963). Frost wedging/shattering occurs throughout much of the year and leads to high rates of rockfall especially within the South Tahoma Glacier headwall. The unique nature of volcanoes in adding new volumes of rock and ash should be noted but does not occur at the timescale of this study. The last known significant eruption of Mount Rainier occurred 550 to 600 years ago, blanketing the mountain in a thin layer of ash (Fiske et al., 1963). Primary glaciogenic sediment is derived directly from glacial processes.

Unsurprisingly, basal and ablation till as well as glaciofluvial sediment makes up most of the sediment in the proglacial zone. These primary glacial deposits are easily delineated by the prominent LIA lateral and end moraines. Glaciogenic sediment is the most significant and active source within the watershed at the human-timescale. During periods of moderate and low magnitude floods, sediment is mainly sourced from the proximal slope of the lateral moraine through periodic gullying at or near the moraine crest and is then temporarily stored along the base in cones or sheets. Shallow translational slides originating near the moraine crest are also likely common (Curry et al., 2009). During larger magnitude floods and debris flows, the sediment accumulations at the base of the moraines are eroded and contribute to bulking of debris flows.

Situated within a national park, humans have minimal direct influence within the watershed. The Westside road lies at the hillslope valley transition for several kilometers before dropping down into the valley bottom between RKM's 5.5 and 7 (Figure 2). Debris flows routinely course down the valley and destroy this section of road (Walder and Driedger, 1994ab). Following these events, the damaged section of road is often repaired using sediment from Dry Creek debris flows, collected near RKM 5 (NPS Staff, personal communication, 2019). Sediment sourced from the damaged roadway contributes relatively little and is not estimated in this thesis.

2.2.2.2 Secondary Sources

Secondary sources of sediment within the watershed are abundant owing to paraglacial (and proglacial) sedimentation occurring within the valley train and on the adjacent hillslopes. The secondary sources can be further divided into two broad categories in terms of the primary source they are generally derived from and their valley position.

The first grouping of secondary sources, those that are primarily derived from bedrock, includes mass movement – debris avalanche deposits, mass movement – rock fall deposits, talus, debris cones, and undifferentiated colluvium. These sources generally lie along the lower flanks of the hillslopes and at the hillslope-valley bottom transition. Eight mass movement deposits were mapped within the watershed, five of which are periodically eroded as the river shifts course and undercuts the landforms causing slumping. Undifferentiated colluvium consisting of weathered rock, debris, soil, and vegetation is sourced in the same way. Debris cones lie at the hillslope-valley bottom transition and are sourced through lateral incision at the toe or longitudinal incision by the tributary stream. Talus generally lies higher on the hillslopes directly below rocky cliffs, and seldomly reaches the valley floor. Talus becomes a source of sediment in locations where bedrock outcrops proximal to the valley floor such as at RKM 5.5 in Figure 3.

The second grouping of secondary sources, derived primarily from glaciogenic sediment within the proglacial zone, includes the active channel, floodplain, terrace, alluvial fan, and debris fan deposits. Debris flow levees would also fit into this category but are relatively less voluminous.

Situated on the valley floor, sediment is exchanged between these secondary sources on a regular basis as the river shifts course.

2.2.3 Sinks/ Sediment Storage

Sediment sinks either partially or completely prevent the transfer of sediment through the system. Different storage landforms also operate over varying effective timescales. Within the watershed, lakes are highly effective sediment sinks and operate over millennial timescales. Glacial ice is a much slower transport medium than rivers and can provide a buffering effect or long-term storage of debris. Glaciers mediate the transfer of rockfall from cirque headwalls to the terminus through slow, continuous transport. Other sediment stores include, colluvium (undifferentiated), landslide deposits, talus, debris cones and fans, alluvial fans, terraces, floodplains, and the active channel.

Walder and Driedger (1994b) estimate that debris flow/flood deposition between 1967-1991 amounted to approximately $0.5 - 1 \times 10^6 \text{ m}^3$ between RKM 8.5 and 4.5, or 2 meters of uniform valley aggradation. No other storage volume estimates exist for this period, or for other locations within the basin. Between 2002 and 2008 approximately $1.66 \times 10^6 \text{ m}^3$ and $81 \times 10^3 \text{ m}^3$ of sediment was re-stored within the active channel and within the contributing banks, respectively. The majority of this deposition occurred between RKM 8.5 and 4.5, a common zone of debris flow deposition. Between 2008 and 2012 approximately $5 \times 10^5 \text{ m}^3$ of sediment was deposited within the active channel while $1.9 \times 10^5 \text{ m}^3$ of sediment was restored along the base of the lateral moraine within the proglacial zone.

2.2.4 Production and Transport Processes

Through careful fieldwork and mapping, source to sink/outlet sediment pathways were delineated (Figure 4). Numerous processes of sediment transport are significant at the human-timescale (Figure 4). Perhaps the most dramatic if not dominant process within the Tahoma Creek watershed are the debris flows that course through the proglacial zone, bulking along the way, before causing valley-wide aggradation. Other active processes include, rockfall, bank erosion, soil creep/surface wash, glacial transport, and fluvial transport. Many other processes

become significant only at much longer timescales including, debris avalanches, lahars, and mudflows.

2.2.4.1 Weathering

Weathering is a primary source of sediment production, causing the breakdown of bedrock into detritus/soil. Weathering is often a precursor to and catalyst for sediment transfer on hillslopes. The hydrothermal alteration of andesite bedrock results in debris avalanches at Mount Rainier. Weathering facilitates the production of dissolved solids and fine sediment that is more easily transported and eventually exported from the system.

2.2.4.2 Soil Creep/Tree Throw

Soil creep and tree throw act over a large area, but at slow rates. These factors make it difficult to directly measure rates in the field, and as such, none were attempted. Jordan and Slaymaker (1991) note a combined average soil creep/tree throw rate of 2-5 mm y⁻¹ for shallow (0.5 - 1m), forested soils in mountainous settings. The drainage density of the Tahoma Creek watershed is approximately 2.8 km per km², while field estimates suggest that less than 5.5 km² of soil-mantled slopes are coupled to the valley floor. Based on the above values, soil creep volumetric estimates range between 15 m³ y⁻¹ to 80 m³ y⁻¹ (~1500 m³ to 8000 m³ in the last 100 years). As will be shown in the following paragraphs, soil creep estimates are within the uncertainty bounds of more significant processes (i.e. fluvial erosion, debris flows) within the watershed.

2.2.4.3 Rockslide, Avalanche, Debris Slide

Eight mass movement deposits were mapped within the Tahoma Creek watershed (Figure 3), seven of which are classified as debris avalanche and one rockfall. The debris avalanche deposits contain a mixture of rock, soil, and plant material, while the rockfall contains mostly large blocky rock fragments. Five of the debris avalanches reached the valley floor and bank erosion commonly occurs at their toes. These events likely did not transition to lahars. Debris avalanches that did directly mobilize into lahars are discussed in the section on lahars below. The mass movement rockfall deposit also reached the valley floor and was last active in 2014 when

approximately 240 m³ of rock slid off the East face of Mount Wow and deposited boulders in the parking area, totaling at least one car on the West Side road (Beason, 2020). Approximately half of the mobilized rock and debris reached the valley floor, while the other half was stored on the hillslope. This location was also thought to be active on April 13, 1949 as a result of the Olympia earthquake (Scott et al., 1995). An additional mass movement is noted having occurred above Lake George (Scott et al., 1995), but was not mapped due to unclear dimensions. Scott et al. (1995) note that debris avalanches of this magnitude have a recurrence interval of less than 100 years within the park, but many of the events that created these landforms may have occurred as much as 17,000 (Fraser Glaciation) years ago, following the local LGM, in response to the debuttressing of the valley walls.

2.2.4.4 Rockfall, Frost Shattering

Bedrock cliffs crop out within the South Tahoma Glacier cirque, Pyramid Peak, along Emerald Ridge, and Mount Wow (Figure 2 and Figure 3). Rockfall and frost shattering rates are especially high within the South Tahoma Glacier cirque. During a hot August day in 2019, rockfall could be heard from the cirque every few minutes. Rockfall-derived supraglacial debris is more or less continuously transported to the proglacial front where it can be eroded by the meltwater channels. In the other locations of active rockfall within the catchment, much of the debris is stored in talus slopes for centuries and contribute relatively little to the total export. No rockfall rates were estimated in this study due to a lack of resources.

2.2.4.5 Bank Erosion

Bank erosion results in hillslope-channel coupling and therefore facilitates the movement of sediment down the sediment cascade. Net change analysis was used to estimate the volume of sediment entering the channel through bank erosion between 2002 and 2012. It is difficult to disentangle what proportion of bank erosion is the result of gully/slumping, fluvial undercutting at the toe, or debris flow initiation/bulking, and as such undifferentiated volumes are presented here. Additionally, erosion at the proglacial front that results from the lateral migration of the many proglacial channels is included in these estimates.

Between 2002 and 2008 approximately $1.8 \times 10^6 \text{ m}^3$ ($3 \times 10^5 \text{ m}^3 \text{ y}^{-1}$) of sediment entered the channel from bank erosion along the mainstem within the proglacial area. Downstream of the LIA moraines only about $1.2 \times 10^5 \text{ m}^3$ ($2 \times 10^4 \text{ m}^3 \text{ y}^{-1}$) of sediment entered the channel from bank erosion. This erosion was concentrated at the base of the landslide deposits.

Between 2008 and 2012 much less bank erosion occurred. An estimated $3.7 \times 10^5 \text{ m}^3$ ($9.25 \times 10^4 \text{ m}^3 \text{ y}^{-1}$) of material was eroded from the adjacent hillslopes and banks within the proglacial zone mainly at the base of the glacier and along the lateral moraine. Below RKM 10 bank erosion was negligible for the 2008 to 2012 period. During the 2019 field season bank erosion was observed resulting from the reorganization of the channel following the August 5th debris flow event. Bank erosion was mainly observed between RKMs 8 and 6, but volumes were not estimated due to a lack of resources. Significant bank erosion below the LIA extent likely only occurs during floods and debris flows which overcome adjacent floodplains and cause the reorganization of the channel and subsequent undercutting of hillslopes.

2.2.4.6 Debris Flows

Fieldwork evidence suggests that the most significant transfer processes connecting contemporary glacial and Neoglacial sediments within the proglacial zone to the active channel deposits are debris flows and flooding. Debris flows, which initiate near the glacier termini, deposit their coarse fraction between RKMs 7.5-3.5, where it remains in storage until remobilized by fluvial processes.

More than 37 debris flow events have been recorded within the Tahoma Creek watershed since 1967, with each event commonly containing multiple debris flow pulses. The debris flows often originate as glacial outburst floods (GOFs) or failure of proglacial gully walls (Walder and Driedger, 1995; Legg et al., 2014). Thirty-three of these recorded events originated within the proglacial zone and directly entered the mainstem fluvial system, while 4 events coursed down Dry Creek before depositing on the valley floor near RKM 5. Walder and Driedger (1994a, 1994b, 1995) contributed the most detailed record of debris flows within the watershed to date, including 15 separate events between the period 1986-1992 and general descriptions of

subsequent geomorphic change. Outside of this detailed period, only sporadic records exist (Richardson, 1968; Crandell, 1971; Copeland, 2009; Beason et al., 2019). Very few estimated erosional/depositional volumes exist but are on the order of 10^5 m^3 for individual events (Walder and Driedger, 1994a). Walder and Driedger (1994a) estimated the volumetric change within the lower stagnant ice area between 1967-1991 as 10^7 m^3 ($4 \times 10^5 \text{ m}^3 \text{ y}^{-1}$) and assumed that 50% or less comprised glacier ice.

As previously mentioned, debris flows are one of the major processes responsible for the erosion and subsequent export of sediment from the proglacial zone. We estimate that a significant proportion of the material accounted for in the bank erosion component above was transported by debris flows. On August 5, 2019 4 debris flow pulses rushed down the valley resulting in several avulsions and depositing a significant but unknown volume of sediment between RKMs 7.5 and 6.5. An additional debris flow event occurred on September 26, 2019 after the field season and mapping efforts ended.

Debris flows have a recurrence interval of approximately 1.4 years within the last half of a century (37 events in 52 years). If the estimated average debris flow volume of $1 \times 10^5 \text{ m}^3$ is applied to the 33 events that occurred within the proglacial zone, an approximate $3.3 \times 10^6 \text{ m}^3$ of sediment has been mobilized by debris flows in the last half century. This value is meant as a first order estimate only and many assumptions limit the confidence of this value, including changes in the frequency and magnitude of debris flow events.

Using dendrochronology and growth disturbances from damaged/killed trees, Scott Anderson reconstructed a number of debris flow, flood, landslide, and lahar events dating back to 1508 (Anderson, 2013). In total, 17 debris flow and 18 flood events were identified in this record, likely recording only the largest and most impactful of a much larger total number. The timing of these events roughly correlates to periods of glacier retreat with a clustering around the end of the LIA. There is evidence that glacier retreat exerts a first order control on debris flow frequency within the watershed, which would explain the clustering of events around the end of the LIA and the high number of events in the last half century (Anderson, 2013).

2.2.4.7 Lahars

Scott et al. (1995) note that large flank collapses (debris avalanches) at Mount Rainier, which result from the hydrothermal alteration of the volcanic cone, rapidly mobilize into lahars and pose the largest threat to downstream communities. These events rapidly transport large volumes of debris downslope, and often export this material out of the watershed. Crandell (1971) noted four lahars within the Tahoma Creek watershed, each originating as flank collapses from Sunset Amphitheater (within the South Puyallup watershed). These lahars added large volumes of sediment from sources outside of the watershed boundary making a long term (500+ year) catchment-scale sediment budget nearly impossible.

The Round Pass mudflow (2610-2790 AD) is an example of a high-magnitude event which transported large volumes of cohesive, clay-rich debris across watershed boundaries (in the west near the Tahoma Glacier as well as at Round Pass, and to the east near Indian Henry's Hunting Grounds) before attenuating in the lower reaches of the watershed. This flow was approximately 300 meters thick in the upper watershed. Events of this size only occur approximately every 500-1000 years but play a substantial role in sculpting the landscape (Scott et al., 1995). A representative volume for events of this frequency is $2.3 \times 10^8 \text{ m}^3$ while the "maximum lahar", or 10,000-year event, might be larger than $3 \times 10^9 \text{ m}^3$.

On the other end of the spectrum, the Tahoma Lahar, tentatively dated to 1508 AD (Anderson, 2013), was much smaller in magnitude. The Tahoma Lahar is more than 20-meters thick where it is interbedded with glaciogenic sediment within the proglacial zone. Events of similar size have a recurrence interval of less than 100 years. The Tahoma Lahar underlies many of the terraces along the valley bottom margin. All recurrence intervals (RIs) noted in the above paragraph are based on events from all watersheds of Mount Rainier and not Tahoma Creek alone. Therefore, similar magnitude events in Tahoma Creek likely have longer RIs than noted.

2.2.4.8 Glaciation

Approximately 4.48 km² (~11%) of the watershed is currently occupied by glaciers, while up to 8 km² (20%) of the watershed was glaciated during the LIA. Glaciation is a key component in the sediment cascade within the catchment. As previously mentioned, rockfall is active within the South Tahoma Cirque contributing to a significant amount of supraglacial debris.

Approximately 0.56 km² of the South Tahoma Glacier's surface was covered in debris in 2015 (Beason, 2017). Much of the Tahoma Glacier snout that enters the watershed is also covered in debris. The glaciers then act as conveyor belts, transporting debris to their termini and linking directly to meltwater channels.

Glaciers also contribute substantial volumes of dissolved and suspended sediment as a result of abrasion and geochemical weathering. Unfortunately, no measurements of dissolved or suspended load exist for the watershed, and no estimations of the relative contribution from glaciation. Glacier retreat has exposed ~3 km² of unconsolidated glaciogenic sediment since the LIA that is readily reworked by debris flows and floods.

2.2.4.9 Fluvial Transport

Fluvial transport is a particularly important component of the overall sediment budget because it is virtually the only process responsible for the export of coarse sediment out of the watershed. One major exception to this rule, is coarse sediment evacuated during the hyper-concentrated flow phase of debris flows. Although this process likely only contributes to the export of coarse sand and finer sediment. While direct bedload measurements do not exist within the watershed due to the difficulty of sampling cobble-boulder sized sediment in braided channels, net change analysis and predicted bedload transport volumes exist.

During the 2002 to 2008 period, an estimated $1.5 \times 10^6 \text{ m}^3$ ($250 \times 10^3 \text{ m}^3 \text{ y}^{-1}$) of sediment was exported from the watershed, while only $1.4 \times 10^5 \text{ m}^3$ ($36 \times 10^3 \text{ m}^3 \text{ y}^{-1}$) of sediment was exported between 2008 and 2012. The large 2006 flood is likely responsible for the order of magnitude difference in sediment transfer volumes. Differences between the exported volumes of sediment we estimated and those that were estimated by Anderson and Pitlick (2014) are likely the result

of accounting for bank erosion and redeposition in our analysis, as well as slightly different delineated areas. However, this study is focused on relative rather than absolute volumes and so differences in the delineation method is of minor importance.

In 2014, Anderson and Pitlick estimated continuous bed material transport, for the period 1956-2011, for the Tahoma Creek watershed by constructing a synthetic daily hydrograph and two-parameter sediment rating curve for the basin (Anderson and Pitlick, 2014). DoD measurements provide the volumetric bed material transport, and a critical discharge of $5.5 \text{ m}^3 \text{ s}^{-1}$ was applied.

The rating curve predicts the transport of $40 \times 10^3 \pm 12 \times 10^3 \text{ m}^3 \text{ y}^{-1}$ for the 1956 to 1985 period, and a rate of $87 \times 10^3 \pm 14 \times 10^3 \text{ m}^3 \text{ y}^{-1}$ for the 1985 to 2011 period. This corresponds to an average rate of $62 \times 10^3 \pm 13 \times 10^3 \text{ m}^3 \text{ y}^{-1}$ or roughly a total of $3.4 \times 10^6 \text{ m}^3$ for the 1956 to 2011 period. The authors then compared these bed material transport estimates to deltaic depositional measurements (Alder Reservoir) for the same time periods. Assuming that the deltaic deposits are composed of roughly 30% bed material, the estimates of coarse sediment exported from the Tahoma Creek watershed represent 35% of the total coarse sediment deposition within the delta. These values are reasonable given the watersheds relative size and abundant glacial sediments compared to the other contributing basins. It is worth noting that an estimated 80% of the total bedload transport for the 2002-2012 period was accomplished during the 3-day flood in 2006. This event also accounts for an estimated 50% - 60% of the total transport during the 1956 to 2011 period.

2.2.5 The Unbalanced Sediment Budget

In constructing a sediment budget for the Tahoma Creek watershed, we attempt to assess the relative importance of various processes of sediment transfer and the causes of disconnectivity within the watershed. As such, no attempt is made to balance the budget and little weight should be placed on absolute values presented herein. Figure 5 illustrates the estimated coarse sediment budget between 2002 and 2012 based on the DoD analysis. In the following paragraphs we discuss the estimated delivery ratios and the possible sources of uncertainty presented within the budget.

2.2.5.1 Sediment Delivery Ratios

The sediment delivery ratio (SDR) was calculated every 3-4 kilometers for both periods based on the net export of sediment past a point divided by the gross erosion upstream of that point (Figure 5). The gross erosion volumes are minimum estimates only and therefore the delivery ratios are maximum estimates. The SDR from the proglacial zone (RKMs 13-10) is 94% for the period 2002-2008, and 61% between 2008 and 2012. The lower delivery ratio in the latter period is a reflection of sediment re-stored at the base of the lateral moraines. The SDR past RKM 7 drops to 71% and 43% for the periods 2002-2008 and 2008-2012, respectively. The SDR past RKM 3 drops to 48% and 22% for the 2002-2008 and 2008-2012 periods, respectively. This amounts to approximately a 40% decrease in the SDR between RKMs 10-3 for both periods, reflecting the largely depositional nature of this area. Downstream of RKM 3 the SDR changes relatively little with erosion approximately balancing out deposition. For the period 2002-2008 the SDR dropped a mere 2% to 46% at RKM 1.25 where the DoD coverage ends. For the 2008-2012 period the SDR is reduced by 1% and then an additional 4% (down to 17%) between RKMs 3 to 1.25 and 1.25 to -0.5, respectively. The resulting ~ 30% difference in SDR between the two periods is largely a result of the temporary storage of eroded sediment at the base of the lateral moraine within the proglacial zone. All other erosion/deposition patterns within each zone remained similar between the two periods.

2.2.5.2 Sources of Uncertainty

DEM-based uncertainty presented within Figure 5 was calculated following Anderson and Pitlick (2014) (see appendix A.2: Uncertainty Estimates). The absence of the geochemical mass is likely the largest single source of uncertainty in the budget. This might be roughly estimated based on Alder Reservoir delta accumulation rates, the estimated percent contribution from Tahoma Creek, and the estimated proportions of coarse to fine sediment within the delta.

An unknown volume of coarse sediment enters the system at the glacier front but is assumed to be much less than other proglacial sources. A large proportion of the sediment directly entering the proglacial channels is likely suspended and dissolved load that is readily exported from the basin causing minimal morphological change. Nevertheless, fine sediment accumulations in

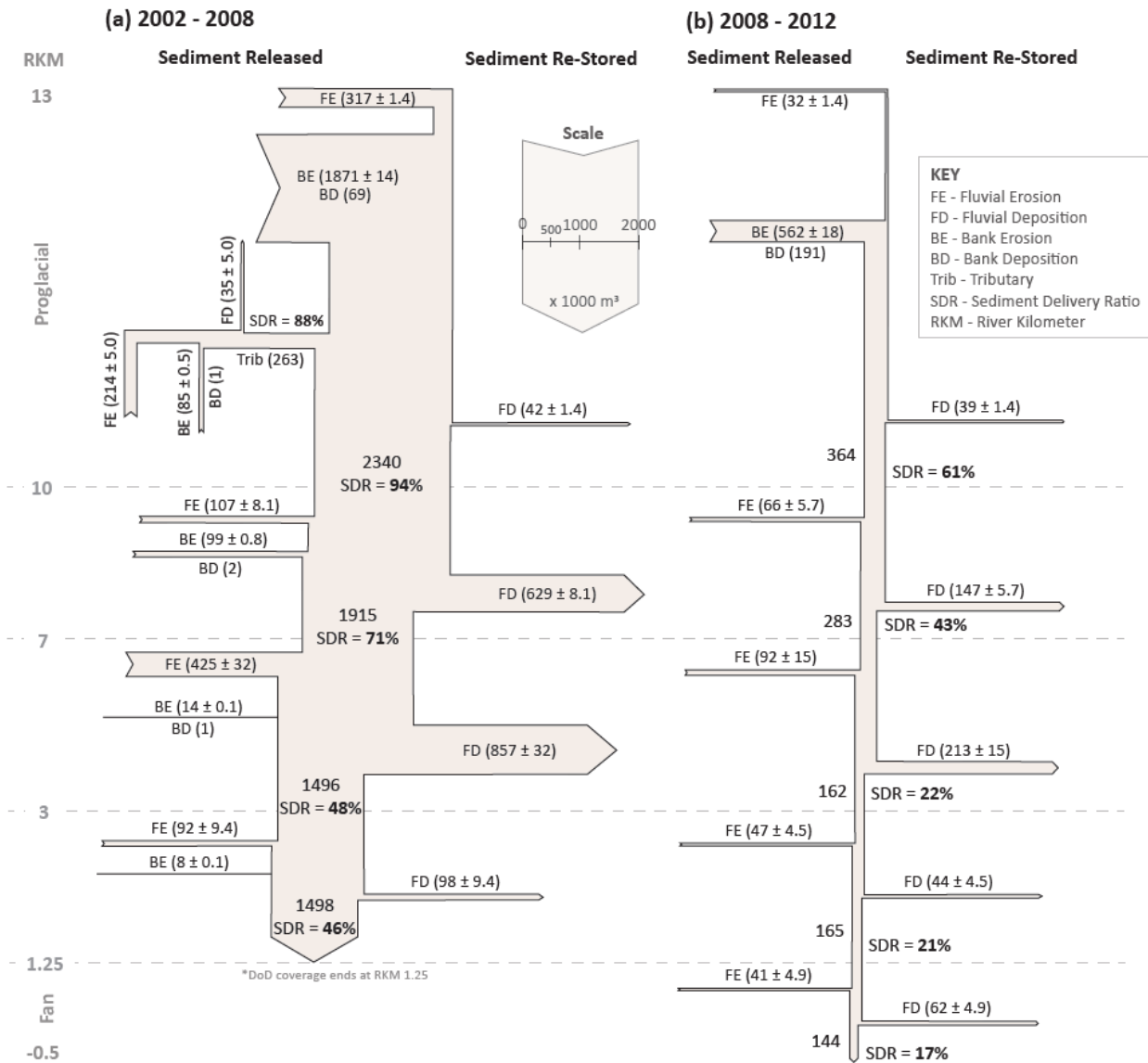


Figure 5. Sediment budget for the Tahoma Creek watershed during the (a) 2002 to 2008 period, and the (b) 2008 to 2012 period. Sediment volumes measured from consecutive 1-meter LiDAR datasets cropped to the active channel and contributing hillslopes.

backwater areas or floodplains are not uncommon and complicate the assumption that all morphological changes can be attributed to coarse sediment.

Stagnant ice within the proglacial zone (no longer fed by the glacier and immobile) also contributes to a significant amount of uncertainty. As previously mentioned, Walder and Driedger (1994a) associated up to 50% of the volumetric change between 1967-1991 within the

proglacial area to stagnant ice. The melting/erosion of stagnant ice comprised an unknown volume of apparent sediment erosion between the 2002-2012 period but is likely less than 20%. To avoid unnecessarily including changing ice volumes a small area at the glacier termini was excluded from the DoD analysis. Anderson and Pitlick (2014) note that the LiDAR data and field observations (i.e. no mass movement or deltas at tributary junctions) suggest that little sediment entered the channel from the forested hillslopes. Density differences between eroded sediment and re-stored sediment contributes to additional uncertainty, although is likely less important than those previously mentioned.

2.3 Sources of Disconnectivity

As previously discussed, disconnectivity is the dominant but inefficient state of a system in transferring matter and/or energy between system components. Sources of sediment disconnectivity are therefore characteristics of the system (i.e. vegetation, slope, network structure) or landforms that reduce the efficiency of sediment transfer. Sources of disconnectivity are abundant within the Tahoma Creek watershed. The following discussion of sources of disconnectivity builds on Fryirs et al.'s seminal work (Fryirs et al., 2007a and 2007b). Sources of disconnectivity are classified as buffers, barriers or blankets based on whether they prevent sediment from entering the channel, disrupt sediment moving along the channel, or prevent vertical reworking of sediment through smothering, respectively (Fryirs et al., 2007a).

2.3.1 Buffers

2.3.1.1 Lateral Moraines

Within the Tahoma Creek watershed, Neoglacial advances (1550 AD, 1835-1860 AD), of nearly equal extent, are recorded in terminal moraines 3.5 kilometers below the modern-day glacier termini (Sigafos and Hendricks, 1972). Additionally, a sequence of prominent lateral moraines (1835 AD and younger) delineate the proglacial zone. As seen in Figure 6a the lateral moraines disrupt the sediment cascade by causing localized deposition of hillslope sediment on the distal slope of the moraines. In effect, the area upslope of the lateral and end moraines has been disconnected with respect to coarse sediment from the sediment cascade since the LIA and will

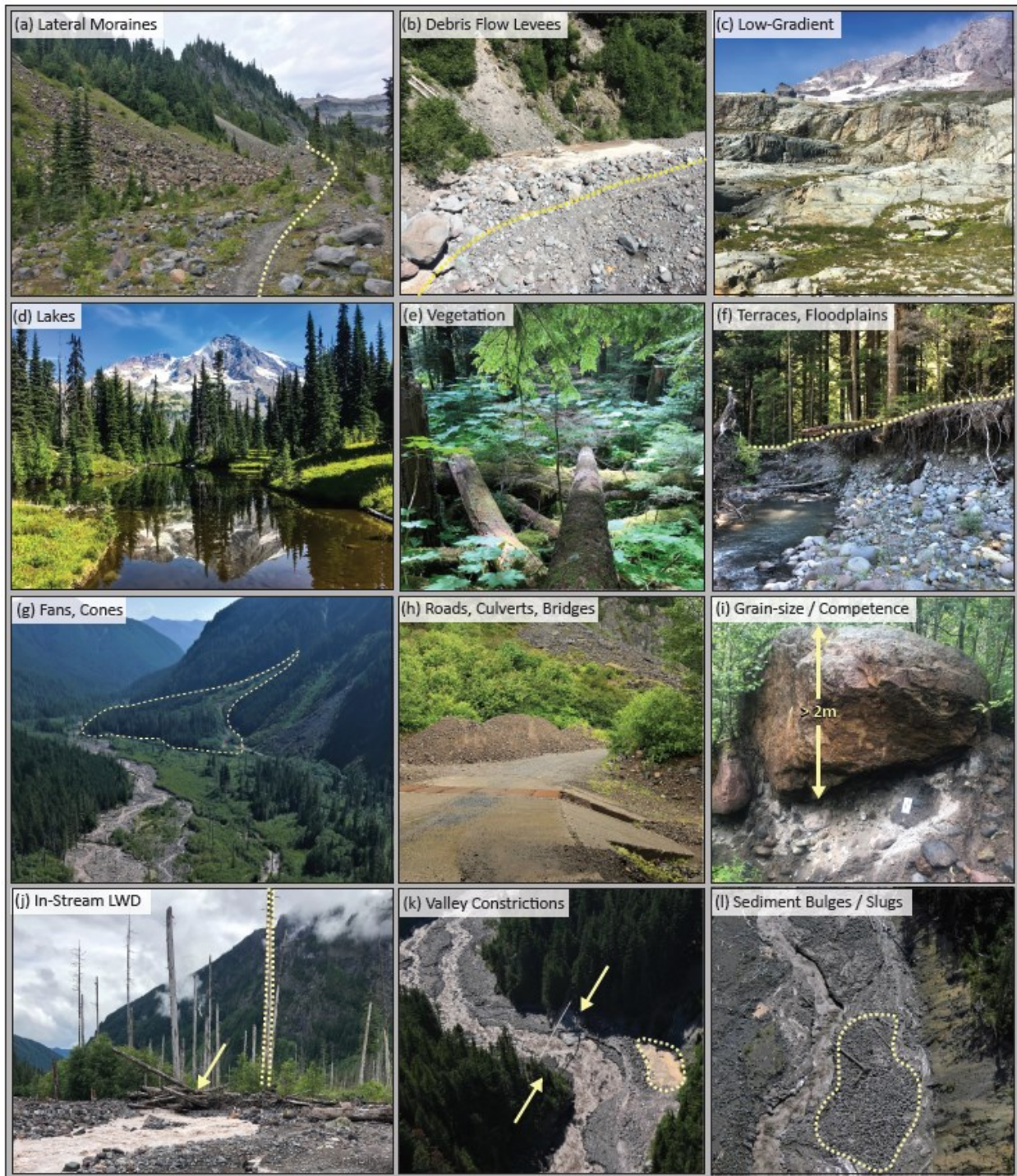


Figure 6. Selected photographs of sources of Disconnectivity within the Tahoma Creek watershed. All photos were taken during the 2019 field season. Photos (g, k, and l) courtesy of Taylor Kenyon, NPS.

likely remain so for centuries. The exact locations of each of the lateral and end moraines can be seen in Figure 7.

2.3.1.2 Debris Flow Levees

Debris flow levees are shear-related boundary features resulting from non-cohesive debris flows (Scott et al., 1995) and are common between RKM 9.5 and 4 (Figure 7). Levees inhibit the lateral migration of the river, and if located near the valley margin, may prevent hillslope sediment from entering the channel (Figure 6b).

2.3.1.3 Low-Gradient Areas

Low gradient areas within the watershed include, parkland, cirque floors, locations of divide breaches during past glaciations, and the valley bottom (Figure 6cf). This section focuses on low-gradient hillslope landforms, while valley bottom landforms will be discussed in the sections below. Interestingly, all the low-gradient landforms within the hillslopes are glacial in origin.

Parkland, which are low-gradient surfaces composed of ancient lava flows scoured by glacial erosion (Riedel and Dorsch, 2016), occurs at the base of Copper Mountain and Pyramid Peak (Figure 7). There are glacial cirques in the eastern portion of the catchment containing Lake George and Lake Allen. Additionally, low-gradient upland areas are often the result of breached divides. These occur mainly in the northern half of the watershed, north of Round Pass in the east, and north of Mount Ararat in the west. The divides were likely last breached in the late Pleistocene during the Salmon Springs Glaciation (Crandell and Miller, 1974).

Low-gradient areas result in reduced gravitational potential energy available for sediment transport processes and favor deposition over transport when slope thresholds are not surpassed. As a result, these areas have reduced system efficiency (connectivity). Low-gradient landforms therefore increase lateral and/or longitudinal disconnectivity. Methods of delineating the effective catchment area (the area that potentially contributes sediment to the outlet) utilize slope

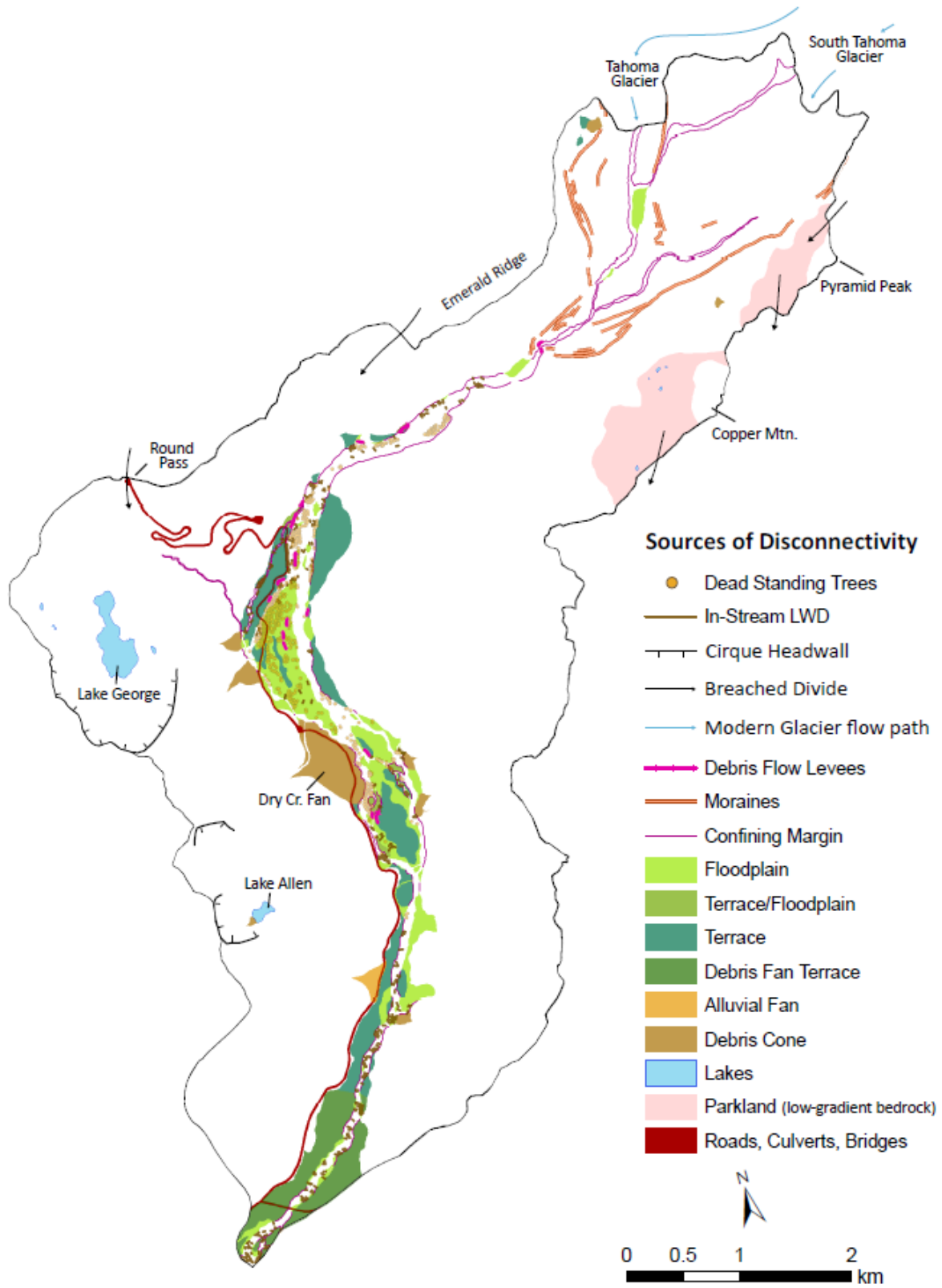


Figure 7. Sources of disconnectivity landform map of Tahoma Creek.

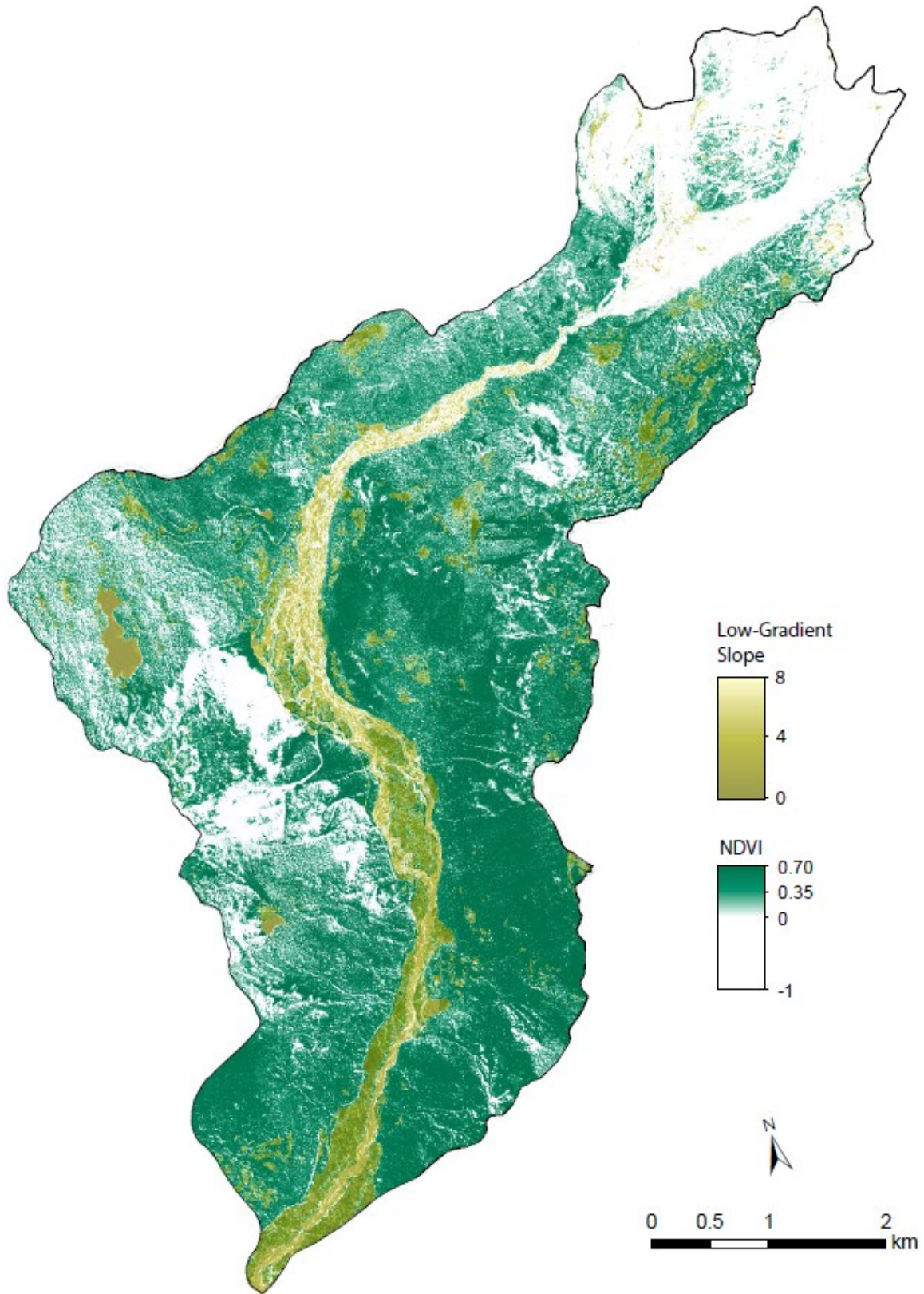


Figure 8. Remote sensing map of bio-geomorphic sources of disconnectivity within the Tahoma Creek watershed.

thresholds as will be seen in Chapters 3 and 4. Figure 8 shows areas where the local slope (based on 5-meter raster cells) is less than or equal to 8 degrees (Nicoll and Brierley, 2016).

2.3.1.4 Lakes

Lakes are scattered throughout much of the low-gradient areas mentioned above. Notably, Lake George and Lake Allen are large glacial tarns that effectively disconnect all upstream areas with respect to coarse (and likely suspended) sediment. Additionally, Mirror Lakes (Figure 6d), situated within the parkland at the base of Copper Mountain (Figure 7), are a collection of small lakes and ponds connected by streams and marshes overlying the glacially scoured bedrock. Much less extensive marshes exist below Round Pass at the headwaters of Fish Creek

2.3.1.5 Vegetation

Much of the hillslopes and valley bottom terraces are densely forested with Western Hemlock, Western Red Cedar, and Douglas Fir trees (Figure 8). Up to 1-meter of litterfall (Figure 6e) blankets the forest floor protecting the underlying sediment from erosion and transport from surface processes. Areas of recent mass wasting are marked by the lack of conifers and presence of shrubs. The floodplains are dominated by Red Alder, a common pioneer species in the Pacific Northwest. Red Alder generally establishes within a year or two of major disturbances followed by inactivity (Anderson, 2013). As Alder forests mature during periods of inactivity, shade-tolerant conifers dominate the understory and eventually form the canopy as the Alder trees die off. Because of the fast rate of recolonization and known forest succession cycles, the presence and type of vegetation is a useful proxy for geomorphic activity in the watershed. Vegetation increases surface roughness and infiltration, stabilizes sediment, and generates disconnections within the sediment cascade (Ortiz-Rodriguez et al., 2017). These disconnections decrease the efficiency of the system in transferring sediment from source to sink.

2.3.1.6 Terraces, Floodplains

Beginning at RKM 6.5, the valley bottom widens, and continuous floodplains and terraces become prominent (Figure 6f and Figure 7). Upstream of this point, discontinuous floodplains

exist only in discrete locations as a result of the narrow/confined nature of the valley floor. These landforms are both low-gradient and vegetated and are therefore effective at causing disconnectivity. Terraces and floodplains act as buffers for hillslope-derived sediment, causing localized deposition at the hillslope-valley bottom transition. Tree core data from within the watershed suggests that many of the terraces have been stable for several centuries (Anderson, 2013). While recent valley wide deposition (Walder and Driedger, 1994a, 1994b) has reactivated many terrace features between RKMs 7 and 3 as denoted by the Terrace/Floodplain and Dead Standing Trees units in Figure 7.

2.3.1.7 Fans, Cones

Fans and cones mark the hillslope-valley floor transition between RKMs 6 and 2 (Figure 7). The Dry Creek fan is perhaps the most notable of these features (Figure 6g). The fans and cones range in size from a few tens of square meters to nearly a square kilometer. Tahoma Creek also forms a broad debris fan where it meets the Nisqually River. Fans and cones function as buffers in the sediment cascade, reducing the degree of connectivity between hillslopes and the mainstem channel. A recent article on tributary-junction fans identified both upstream and downstream controls on fan evolution and buffering effectiveness (Leenman and Tunncliffe, 2020). Key upstream controls are sediment supply and stream power, and key downstream controls are mainstem aggradation and distal confinement. The fans and cones in the Tahoma Creek watershed are fed by ephemeral streams, and therefore downstream (mainstem) controls are likely more important. Valley wide aggradation and subsequent increased lateral mobility of the mainstem may decrease the buffering effectiveness of these features by causing fan head entrenchment and incision at the toe. Nevertheless, they will remain long-term buffers within the sediment cascade.

2.3.1.8 Roads, Culverts

The Westside Road follows the hillslope-valley floor transition between RKMs 0 and 5 before dropping down into the contemporary floodplain between RKMs 5 and 6.5 (Figure 7). The road then winds its way up the eastern hillslope all the way to Round Pass where it exits the watershed. To reduce erosion along the roadway, a system of culverts was put in place to route

runoff underneath the roadway (Figure 6h). The roadway and culvert system reduces the transference of sediment from the hillslopes to the valley floor as seen by localized deposition upstream of the culverts and alongside the roadway.

2.3.2 Barriers

2.3.2.1 Culverts, Bridges

The Paradise Road passes through the southern tip of the Tahoma Creek watershed and includes a bridge over Tahoma Creek (Figure 7). Past versions of the bridge have been washed out, including during the 2006 flood event, resulting in the temporary closure of the park. The bridge limits the lateral mobility of the river and creates backwater areas and zones of deposition upstream during large flood events. This reduces the longitudinal connectivity of the river by causing localized deposition within the active channel.

2.3.2.2 Grain Size / Competence

Much of the debris flow generated sediment that accumulates between RKMs 7 and 3.5 is coarser than fluviably transported sediment. Boulders the size of cars, as seen in Figure 6i, are not uncommon in this area. These coarse deposits limit downstream sediment transport as a result of a difference in process competence and support persistent aggradation, subsequently increasing longitudinal disconnectivity.

2.3.2.3 In-Stream LWD / Dams

In-stream large woody debris (LWD) is common within the Tahoma Creek watershed (Figure 6j). Channel-spanning log jams create areas of backwater and accumulation of sediment wedges. In August 2019 a debris flow caused the formation of the log jam in Figure 6j resulting in the channel shifting course. Woody debris often accumulates at the bouldery and debris filled snout of debris flows and aids their deposition through increased flow resistance. Additionally, dead standing trees (Figure 6j), which were killed following rapid aggradation due to debris flow deposition (1967-present) increase flow resistance in the active channel between RKMs 7 and 3.5 (Figure 7).

2.3.2.4 Valley Constrictions

Figure 7 shows the confining margin, which is where the active channel is directly confined by the valley wall, terraces, or fans. The river is confined between RKMs 12 and 7 as a result of incision through the proglacial sediments. This constriction prevents the river from migrating laterally and can cause backwater areas and aggradation upstream as a result of the bottleneck effect. Perhaps this is best seen in Figure 6k. Here bedrock protrudes into the active channel causing it to narrow and sediment to aggrade upstream. Additionally, deep-seated landslides, debris fans, and debris cones that enter/prograde into the channel similarly cause narrowing.

2.3.2.5 Sediment Bulges, Pulses, or Slugs

Sediment slugs are large fluxes of sediment that can act as plugs within the active channel during low to moderate flows, and thereby limit downstream sediment transport (Nicholas et al., 1995; Fryirs et al., 2007a). For a more complete discussion of sediment slugs, the reader is referred to Nicholas et al., 1995. The formation of these features can be the result of single events (i.e. landsliding, debris flows, etc.), or long-term incremental input at a range of spatial scales. Sediment pulse evolution is in part controlled by network structure (Benda et al., 2004), which can enhance or disperse the pulse as a result of synchronization and translation or desynchronization and storage, respectively (Gran and Czuba, 2017). Researchers at Mount Rainier have identified sediment slugs (often termed sediment bulges at Mount Rainier) that form as the result of debris flows (Paul Kennard, personal communication, 2019). Figure 6L shows a sediment bulge that formed during the August 2019 debris flow event. The August 2019 debris flow depositional zones can also be seen in Figure 3. Sediment bulge evolution is then subdivided into three phases or orders. First order bulges are the original debris flow deposits. Second order bulges are accumulations of reworked debris flow sediment during headward incision into the first order deposit. And third order bulges are wood-supported sediment accumulations that result from the reworking of second order bulges and subsequent wood recruitment from the banks. Additionally, valley-wide aggradation between RKMs 6.5 and 3 can be seen as a sediment pulse, even if at a much larger spatiotemporal scale.

2.3.3 Blankets

2.3.3.1 Sediment Bulges / Slugs

Sediment bulges as discussed above can also limit the vertical reworking of sediment by effectively smothering other landforms. The degree of vertical linkages is also controlled by the relation between grain size and river competence. For example, mass wasting processes often introduce boulder-sized sediment that cannot be reworked by fluvial processes except during the most extreme floods (Figure 6i).

2.3.4 Effective Timescales

Fryirs et al. (2007a) noted the timescales at which features causing disconnectivity operate. Effective timescales of disconnectivity features in the Tahoma Creek watershed range between the individual event and thousands of years. Many of the same features noted by Fryirs et al. (2007a) are present in the study area, but additional glacier and debris flow features are noted. Table 1 lists the buffers, barriers, and blankets within the watershed as well as their postulated effective timescales. In general, within the watershed, blankets operate at shorter timescales than do barriers, and barriers operate at a shorter timescale than buffers. This is likely the result of buffers relating to basin-scale macroforms, both glacial and tectonic in origin, while barriers and blankets are often related more to process competence and biological/anthropogenic structures.

Classification	Feature	Nature	Postulated Effective Timescale
Buffers	Debris Fans/Cones	Debris Flow	Hundreds to thousands of years
	Debris Flow Levees	Debris Flow	Tens to hundreds of years
	Alluvial Fans	Fluvial	hundreds to thousands of years
	Terraces	Fluvial	Thousands of years
	Floodplain	Fluvial	Hundreds to thousands of years
	Hillslope Vegetation	Biological / Climatic	Dependent on climate and mass wasting activity
	Wide / Flat, U-Shaped Valleys	Glacial	Permanent over thousands of years
	Lateral Moraines	Glacial	Hundreds to thousands of years
	Tarns / Lakes	Glacial	Permanent until filled
	Cirques / Hanging Valleys	Glacial	Permanent over thousands of years
	Parkland	Glacial	Permanent over thousands of years
	Roads	Anthropogenic	Tens to hundreds of years
Barriers	*Sediment Bulges / Slugs	Debris Flow	Years to tens of years
	Grain Size / Competence (high width/depth ratio channels + Large Grains)	Debris Flow	Tens to hundreds of years
	Valley Constrictions (natural)	Tectonic / Glacial / Fluvial	Permanent over thousands of years
	In-Stream Dead Standing Trees	Biological / Climatic / Debris Flow	Tens to hundreds of years
	In-Stream LWD / Dams	Biological / Climatic	Tens to hundreds of years
	Culverts / Bridges	Anthropogenic	Tens to hundreds of years
Blankets	*Sediment Bulges / Slugs	Debris Flow	Years to tens of years

Table 1. Effective timescales of barrier, buffer, and blanket features within the Tahoma Creek watershed. ‘Nature’ refers to the process, history, or forcing that gave rise to the given feature. Postulated effective timescales based on fieldwork evidence and Fryirs et al. (2007a). *Sediment bulges / slugs are noted as both barriers and blankets.

Chapter 3: Quantitative Estimations of Connectivity

In this chapter we lay out the methods of each of the quantitative approaches applied within this study. Section 3.1 outlines the methods applied to assess the spatial arrangement of process domains, the degree to which the landscape has or is adjusted to the contemporary processes below the modern glacier limits, and hillslope-channel coupling. Section 3.2 addresses methods of quantifying sediment connectivity at a variety of spatial resolutions and considering different controls (i.e. network structure, topography, etc.).

3.1 The Influence of Landscape History

Past glaciations are responsible for the spatial reorganization of geomorphic processes and valley morphology (Brardinoni and Hassan, 2007). This in turn dictates the channel slope, hillslope-channel coupling and subsequently the channel morphology, all of which influence sediment connectivity and disconnectivity. Process domains are delineated zones within the landscape in which a suite of processes play a significant role in the detachment, transport and deposition of sediment (Brardinoni and Hassan, 2007). It is therefore reasonable to assume that the organization of process domains, and perhaps more importantly process-form disequilibrium within the landscape affects sediment connectivity and disconnectivity. At Mount Rainier, any process-form disequilibrium is likely the combined result of the glacial, and thus paraglacial, or volcanic histories.

3.1.1 Process-Domain Delineation

3.1.1.1 Slope-Area Plots

We delineated the process domains along Tahoma Creek and its tributaries following the methods described by Brardinoni and Hassan (2006). The local slope and drainage area were calculated from a 10-meter DEM using ArcGIS software, and the Hydrology Toolbox. We then plotted the local slope vs. drainage area in log-log space and interpreted the topographic signatures in relation to those identified in other previously glaciated regions (Brardinoni and Hassan, 2006). In many but not all cases, kinks within the plots were interpreted as boundaries between domains.

3.1.2 Long-Profile Analysis

Process-form feedbacks indicate that, if in a ‘steady state’, the form of the landscape is controlled by the contemporary processes operating on it and vice-versa. Well-adjusted rivers tend to have a concave-up shape with a progressively decreasing slope in the downstream direction. The concavity of the profile therefore records long-term controls such as lithology (Hack, 1973), changing base level, or dominant processes (Montgomery and Foufoula-Georgiou, 1993).

In this study, we evaluate the long profile and its concavity by plotting the elevation vs. distance downstream of the Tahoma Glacier, measured from the 2008, 1-meter DEM. Further analyses include the calculation of the stream gradient index and plotting of valley cross-sections, both described in further detail in the paragraphs below.

3.1.2.1 Stream Gradient Index

The stream gradient index was calculated following Hack (1973) and begins at the South Tahoma Glacier terminus and runs until the confluence with the Nisqually River. The calculation follows Figure 9 below. The stream gradient index was calculated for each 500-meter reach along the 14-kilometer length of Tahoma Creek. The elevation measurements were sampled from a 10-meter DEM, chosen to smooth over channel bedform variations while preserving any potential convexities in the profile.

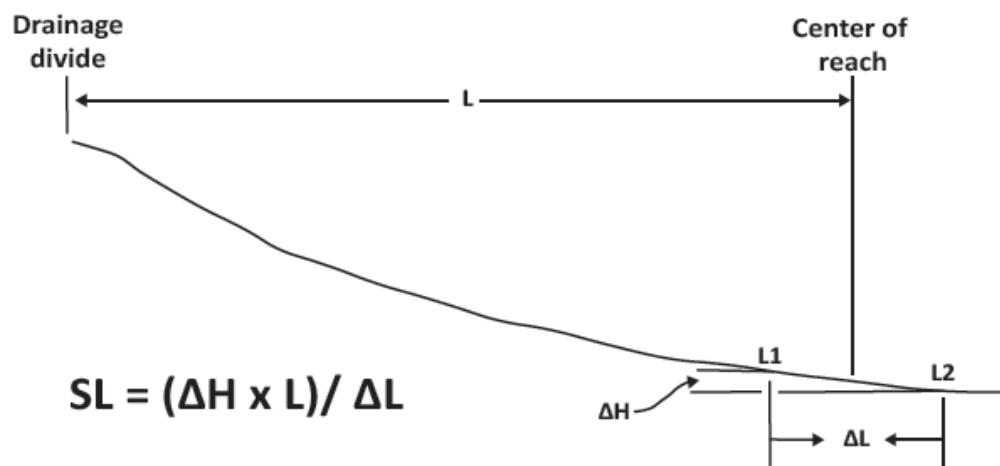


Figure 9. Methodological example of calculating the stream gradient index. Figure taken from Hack (1973).

3.1.2.2 Valley Cross-Sections

Valley cross-sections were created every two kilometers beginning at Tahoma Creek's confluence with the Nisqually River (RKM -0.5) and moving upstream to RKM 13.5, for a total of eight cross-sections. The cross-section elevations were sampled from the 2008 1-meter LiDAR with varying widths to include the entire valley bottom terminating on hillslopes at either end.

3.1.3 Whiting-Bradley Classification

In order to objectively estimate the degree of hillslope-channel coupling within the Tahoma Creek Watershed, we applied the classification system proposed by Whiting and Bradley (1993), hereafter referred to as the Whiting-Bradley classification. This is a simple two-part classification system that determines (i) the potential of the hillslopes to contribute sediment to the channel, and (ii) the potential of the channel to move this sediment downstream. This thesis focuses solely on the first component and does not consider downstream sediment transport using this method.

The strength of this method is its simplicity and empirical basis, only requiring measurements of the valley bottom and active channel width. It is assumed that debris flows derived from the hillslopes have a runout length of 25 meters (Ikeya, 1981), and therefore, if the valley width is less than 25 meters wider than the channel width, debris flows will almost certainly enter the channel. The logic then follows that a debris flow originating on a hillslope has a 50% chance of entering the channel if the valley bottom is less than 50 meters wider than the active channel, and so on.

The valley bottom and active channel widths were mapped in the field and can be seen in Figure 3. The river was subdivided into 50-meter segments, at which calculations of the channel width to valley width ratio were made and subsequently coded into four categories describing the probability that a debris flow would enter the channel, (i) AD – certainly; ~100%, (ii) MD – frequently; 50-100%, (iii) OD – occasionally; 10-50%, and (iv) SD – seldomly; <10% (Whiting and Bradley, 1993). Hassan et al. (2018) noted the methods insensitivity in distinguishing

between categories of only slightly different degrees of coupling (i.e. AD and MD) over century timescales due to the infrequent and episodic nature of hillslope sediment inputs. We therefore further lumped the categories into, coupled: AD-MD (100% - 50%) and decoupled: OD-SD (<50% - 0%).

Hillslope-channel coupling was assessed in the field based on observations of bank erosion, clast lithology and angularity, and degree of weathering. Colluvial sediment tends to be more angular and derived from the Ohanapecosh Formation which dominates the valley walls. Colluvial clasts often have weathering rinds and an oxidized matrix. Landforms that lie at the transition between colluvial and fluvial process domains (i.e. debris cones, fans, etc.) were also noted as well as their relative downslope extent in relation to the active channel and occurrence of incision when relevant.

3.2 Measures of Sediment Connectivity

3.2.1 Effective Catchment Area

As was discussed in chapter 2, sources of disconnectivity ensure that not all sediment transferred within the network reaches the outlet by preventing or limiting further downslope transfer. This phenomenon is often noted within the literature as the “sediment delivery problem” (Walling, 1983). The effective catchment area (ECA) method explicitly accounts for the spatial distribution of sediment delivery and lack thereof by delineating the area within a catchment that has the potential to directly contribute sediment to the specified outlet at a given scale (Fryirs et al., 2007b). Most applications of the method are based on the simple assumption that the slope gradient controls sediment delivery. The ECA provides a quick estimate of catchment-scale connectivity and disconnectivity, even if at a low-resolution. Lisenby et al. (2017) note that applied at the catchment-scale, the ECA is best approximated using coarse-scaled inputs and suggest a DEM resolution of 25 meters. They found that higher resolution DEMs (i.e. 1-meter) created erroneous disconnections when applying a slope threshold to intermediate-sized catchments (~ 61 to 530 km²).

In this thesis, we apply the ECA method, following Fryirs et al. (2007a and 2007b), to six different scenarios in order to find the appropriate DEM resolution and slope threshold for quantifying connectivity (Lisenby et al., 2017; Heckmann et al., 2018). Three DEM resolutions were tested, 1-meter, 5-meter and 30-meter; while two different slope thresholds were tested, 2° (Fryirs et al., 2007a and 2007b), and 8° (Nicoll and Brierley, 2016).

3.2.2 Network Structural Connectivity

The network structural connectivity method (NSC), proposed by Cossart and Fressard in 2017, estimates the potential influence of the network on sediment transfer efficiency. The method leverages graph theory tools to calculate connectivity over a regularly spaced mesh of nodes and edges, where nodes represent landscape units and edges represent transfer pathways. The NSC index, calculated following equations [1], is simply the potential flow (F_i) divided by Shimbel's Index (Shi_i).

$$F_i = \frac{\sum_i F_{ijo}}{\sum F_{jo}} \quad [1]$$

$$Shi_i = \frac{\sum d_{ij}}{\sum d_{jk}} \quad [2]$$

$$NSC_i = \frac{F_i}{Shi_i} \quad [3]$$

The potential flow at a given node i , is a measure of the proportion of the total number of pathways that begin at any node j and reach the outlet o , while passing through i , to the total number of pathways from j to o (equation [1]). Shimbel's index for a given node i , is the sum of the length of all paths passing through i and connecting all other nodes j (considering directionality of the graph). This value is normalized by the length of all the paths in the network from j to k (equation [2]). Conceptually, the NSC index ranks the nodes in order of importance within the network, similar to the idea of geomorphic hotspots (Czuba and Foufoula-Georgiu, 2015).

The NSC was calculated for two different scenarios, (i) the contemporary network with disconnections and (ii) considering full connectivity except for nodes draining into lakes which act as long-term storage. The regularly spaced mesh of nodes was automatically created using the ‘*Fishnet Tool*’ with ArcGIS software, following which the edges were manually digitized based on fieldwork evidence of transfer pathways and a D-infinity flow direction algorithm (Tarbotan, 1997). Locations of disconnect resulted in breaks within the network (unconnected nodes), and in this case nodes are considered either fully connected or fully disconnected. A node spacing of 150 meters was chosen as a compromise between accurately representing the network structure, computational time, and visualization. The connected network was then exported as an adjacency matrix, and the remainder of the calculations were done using the iGraph package in the R software platform (Csardi and Nepusz, 2006; R Core Team, 2013). Additionally, the residual flow (RF) was calculated for each node by performing a linear regression between F_i and Shi (Fressard and Cossart, 2019). The RF is then simply the potential flow minus the predicted potential flow following equations [4] and [5] below.

$$F'_i = a \times Shi_i + b \tag{4}$$

$$RF_i = F_i - F'_i \tag{5}$$

The authors claim that the RF provides a more stable and robust measure of the under- and over-representation of sediment volume in each node than does the NSC index. Residual flow values at or near 0 indicate the potential flow of a given node is described by its location within the network; whereas positive and negative values indicate more or less sediment is passing through a given node than is described by its location, respectively.

3.2.3 Index of Connectivity

In 2008, Borselli et al. defined an index of connectivity (IC) as a way to quantify the degree of catchment hydrological connectivity. This method is applied to a DEM and measures the influence of morphology on connectivity based on simple calculations (refer to equations [6] below). This method was later modified to model sediment pathways dealing with debris flows

and channelized sediment transport and aimed at better exploitation of high-resolution DEMs (Cavalli et al., 2013). Three main changes were made to the index of connectivity:

1. The application of the D-infinity flow direction algorithm (Tarbotan, 1997), instead of the original single flow direction algorithm, resulting in a more realistic proportioning of the flow.
2. The addition of an upper limit (1m/m) on calculated slopes to limit the bias introduced by high IC values on steep slopes.
3. The weighting factor is calculated from measured roughness in the DEM instead of requiring manual determination.

Later, in 2018, Crema and Cavalli introduced open-sourced software (SedInConnect) for calculating the index of connectivity. This application allows for the calculation of the weighting raster following Cavalli et al., 2013, or normalized based on flow-direction following Trevisani and Cavalli, 2016. Additionally, a sinks feature was introduced to account for disconnections in the sediment cascade introduced by lakes, ponds, dams, etc. This feature removes the area upstream of sinks and the analysis is performed on the remaining area (Crema and Cavalli, 2018). The index of connectivity method (Cavalli et al., 2013) is represented in the following equations,

$$IC = \log_{10} \left(\frac{D_{up}}{D_{dn}} \right) \quad [6]$$

$$D_{up} = \bar{W} \bar{S} \sqrt{A} \quad [7]$$

$$D_{dn} = \sum_i \frac{d_i}{W_i S_i} \quad [8]$$

where W is a weight factor that accounts for topographic roughness impeding flow, S is the slope, A is the drainage area, and d_i is the length of the flow path along the i^{th} cell according to the steepest downslope direction. This index provides an estimate of the potential sediment

connectivity and does not represent actual measurements of sediment movement. It is worth noting that the individual calculated IC values are relative. The IC method has since been applied in several studies (Micheletti et al., 2016; Foerster et al., 2014), but with little comparison to other quantitative methods. One interesting application of this method, the joint index of connectivity (IC_j) calculates the weighting raster as a hybrid considering the influence of vegetation (Ortiz-Rodriguez et al., 2017). The IC_j uses the C-factor of USLE-RUSLE models in vegetated areas of the catchment (Borselli et al., 2008), and roughness index (RI) values calculated directly from the DEM in areas lacking vegetation (Cavalli et al., 2013; Trevisani and Cavalli, 2016).

In this study, we applied the index of connectivity method to the Tahoma Creek watershed following two different scenarios, (i) considering flow-direction roughness when calculating W (Trevisani and Cavalli, 2016), and (ii) calculating a joint weight factor following Ortiz-Rodriguez et al., 2017. Both scenarios calculated the index of connectivity with respect to the river considering sinks.

3.2.4 Spatially Distributed Sediment Delivery Ratio

In contrast to most indices of sediment connectivity, including the IC as described above, the spatially distributed sediment delivery ratio method is based on actual measurements of sediment transfer and therefore is a measure of functional rather than structural connectivity. The method is applied to an area of interest with no upslope sediment inputs to avoid misrepresenting the relative delivery ratios. The method requires two overlapping high-resolution DEMs that are first subtracted to create a DEM of difference (DoD). The DoD is then combined with the multiple flow-direction (MFD) routing algorithm to calculate the sediment yield (source to sink accumulation of DoD values, or accDoD), total erosion (source to sink accumulation of erosion, or accErosion), and subsequently the sediment delivery ratio (Heckmann et al., 2018; Freeman, 1991).

$$SDR = \frac{\textit{Sediment Yield}}{\textit{Erosion}}$$

This method builds on previous work by Pelletier et al. (2014) who accumulated raster values along flow paths to calculate the sediment yield for each raster cell.

The result is a map with individual raster cells containing a calculated SDR value ranging between 1 (all eroded sediment is exported), and 0 (all eroded sediment is redeposited). The requirement of having a zero-flux boundary for the study area is one major limitation of this method and restricts its application to discrete hillslopes. Three areas of interest (AOIs) were identified, two of which are along the lateral moraines within the proglacial zone, and a third between RKM 9 and 10 on river right. AOIs 1 and 2 have clear upslope boundaries along the lateral moraine crests and lack any significant vegetation, while AOI 3 reaches the watershed boundary but is forested. The DoDs were created for the periods 2008 – 2002, and 2012 – 2008 after ensuring that the datasets were properly co-referenced (see appendix A.2: Co-referencing). A threshold of 0.3 was applied based on conservative uncertainty estimates (see appendix A.2: Uncertainty Estimates). The 2002 and 2008 DEMs were used to calculate the flow pathways for the 2008-2002 and 2012-2008 periods, respectively. ArcGIS, SAGA, and R software was used to perform the above calculations (ESRI, 2011; Conrad et al., 2015; R Core Team, 2013). For more details concerning the SD SDR method, the reader is referred to Heckmann and Vericat, 2018.

While the sediment delivery ratio approach has been criticized for making inferences based on monitoring a single point in the catchment (Bracken et al., 2015), the spatially distributed sediment delivery ratio method utilizes real measurements at the scale of individual raster cells and is thus better equipped to assess spatial patterns of sediment delivery.

Chapter 4: Results

We argue throughout this thesis that connectivity is essentially a measure of the efficiency of sediment transfer as a result of process-form feedbacks. Landscape history sets the topography and boundary conditions over which process-form feedbacks operate. The topographic signature therefore likely controls, to some degree, sediment connectivity. Magnitude-frequency relationships that result from the local climate (i.e. precipitation, temperature), sediment characteristics, vegetation, and topography also play a role in controlling sediment transfer pathways and efficiencies. Additionally, at the catchment-scale, the network structure and spatial arrangement of landscape components (i.e. process domains) is thought to influence sediment connectivity. We also argue that the prevalence and location of sources of disconnectivity (i.e. terraces, lakes, etc.) will largely affect sediment transfer pathways and sediment connectivity. In considering the above controls of connectivity, this chapter is composed of two parts, (i) exploring the influence of landscape history, and (ii) applying semi-quantitative measures of sediment connectivity. Here we describe the results of a variety of methods, each with their own assumptions, and each focusing on a supposed control of sediment connectivity to evaluate their performance in replicating spatial patterns of connectivity.

4.1 The Influence of Landscape History

Previous studies have noted the influence of past glaciations in reorganizing process domains and controlling hillslope-channel coupling. Hassan et al. (2018) note,

“The spatial distribution of coupled and decoupled reaches (...) reflects the spatial arrangement of relict erosional glacial macro-forms...”

Non-glaciated basins often have simple patterns of hillslope-channel coupling in which the uplands are coupled and decoupling becomes more prominent in the downstream direction. In contrast, glaciated basins may alternate between coupled and decoupled reaches as a result of stepped longitudinal profiles (Hassan et al., 2018), and repeated process domain and channel type sequences (Brardinoni and Hassan, 2007).

4.1.1 Process-Domain Delineation

Slope-area plots are an effective tool in delineating process domains (Montgomery and Foufoula-Georgiou, 1993), and when relevant, understanding the effects of past glaciations (Brardinoni and Hassan, 2006 and 2007). However, complications arise when attempting to follow these same methods in a currently glaciated basin with a wide, cobble-boulder dominated valley train. Figure 10 presents the resulting slope-area plot. Notice that drainage areas below $\sim 1.4 \text{ km}^2$ are not represented as a result of excluding the glaciated portions of the catchment. Additionally, large breaks in the data correspond to major tributaries entering the mainstem and instantaneously increasing the drainage area. The resulting plot is anticlimactic, showing no indication (i.e. kinks or bends) of domain transitions. Additional measurements to fill in the gaps may provide interesting insight into the system but are out of the scope of this thesis. However, slope-area plots were also created for several fluvial and colluvial tributary channels (Figure 30). Only channels originating in glacial cirques showed a classic glacial signature with repeated process domains (Figure 30d).

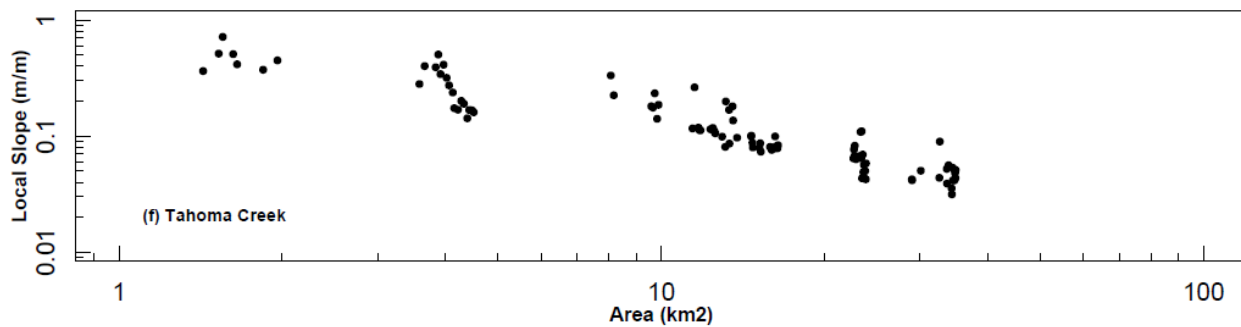


Figure 10. Slope-Area plot of Tahoma Creek.

4.1.2 Long-Profile Analysis

Longitudinal profiles were created for the years 2002, 2008, and 2012 (Figure 11). The profiles have a concave-up shape as is common for fluvially dominated channels. The 2002 profile does have two convexities from about 0 - 600m, and 1200 - 2300m below the glacier (Figure 11b). As seen by the elevation differences in Figure 11, significant erosion, on the order of 40-meters, occurred between 2002 and 2008 likely during the November 2006 flood event. Little net change occurred between 2008 and 2012.

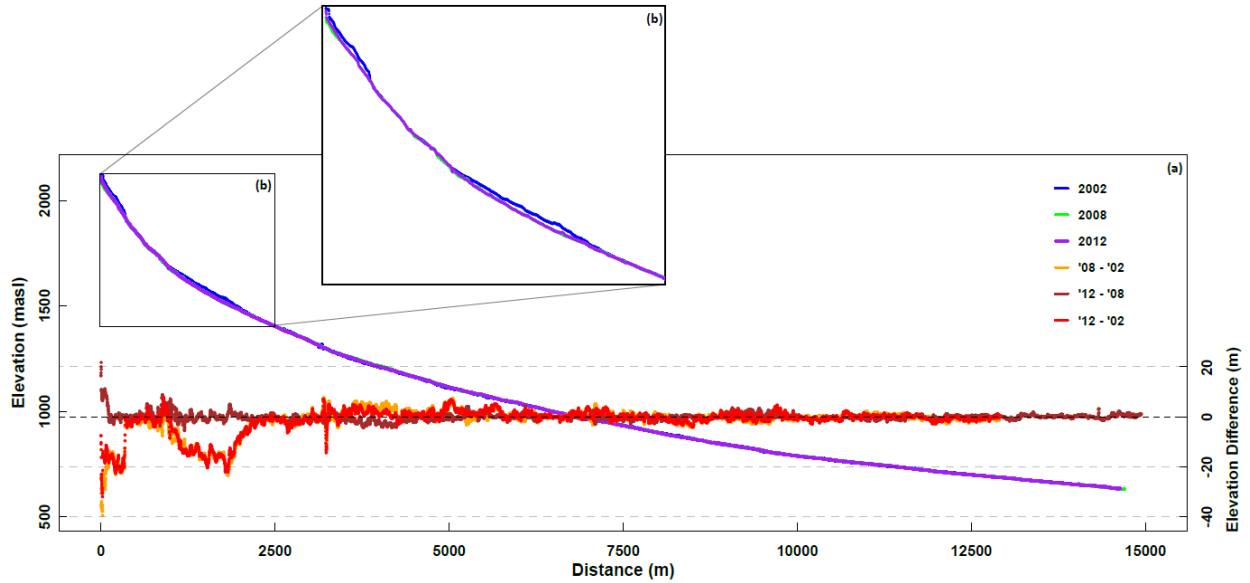


Figure 11. Longitudinal profiles and profiles of difference along Tahoma Creek. Profiles are from 2002, 2008, and 2012.

Additionally, Figure 12 shows the 2008 Tahoma Creek longitudinal profile with general notations of processes acting within the channel noted below, as well as the mean slope within each domain. It should be noted that fluvial transport does significant work along the entire length of the profile during large flood events. Debris flows originating from outburst floods at the glacier terminus erode a significant amount of material between RKM 13.2 and 10 (14000 – 10400m, Figure 12). Between RKM 10 and 8.5 (10400 – 7900m) debris flows do not result in significant net change. Debris flow deposition then occurs between RKM 8.5 and 3.5 (7900 – 3500m) depending on magnitude of flow. Below RKM 3.5 (< 3500m) is dominated by fluvial processes and is beyond the extent of coarse debris flow deposits, although the hyper-concentrated phase of these events continues past the catchment outlet.

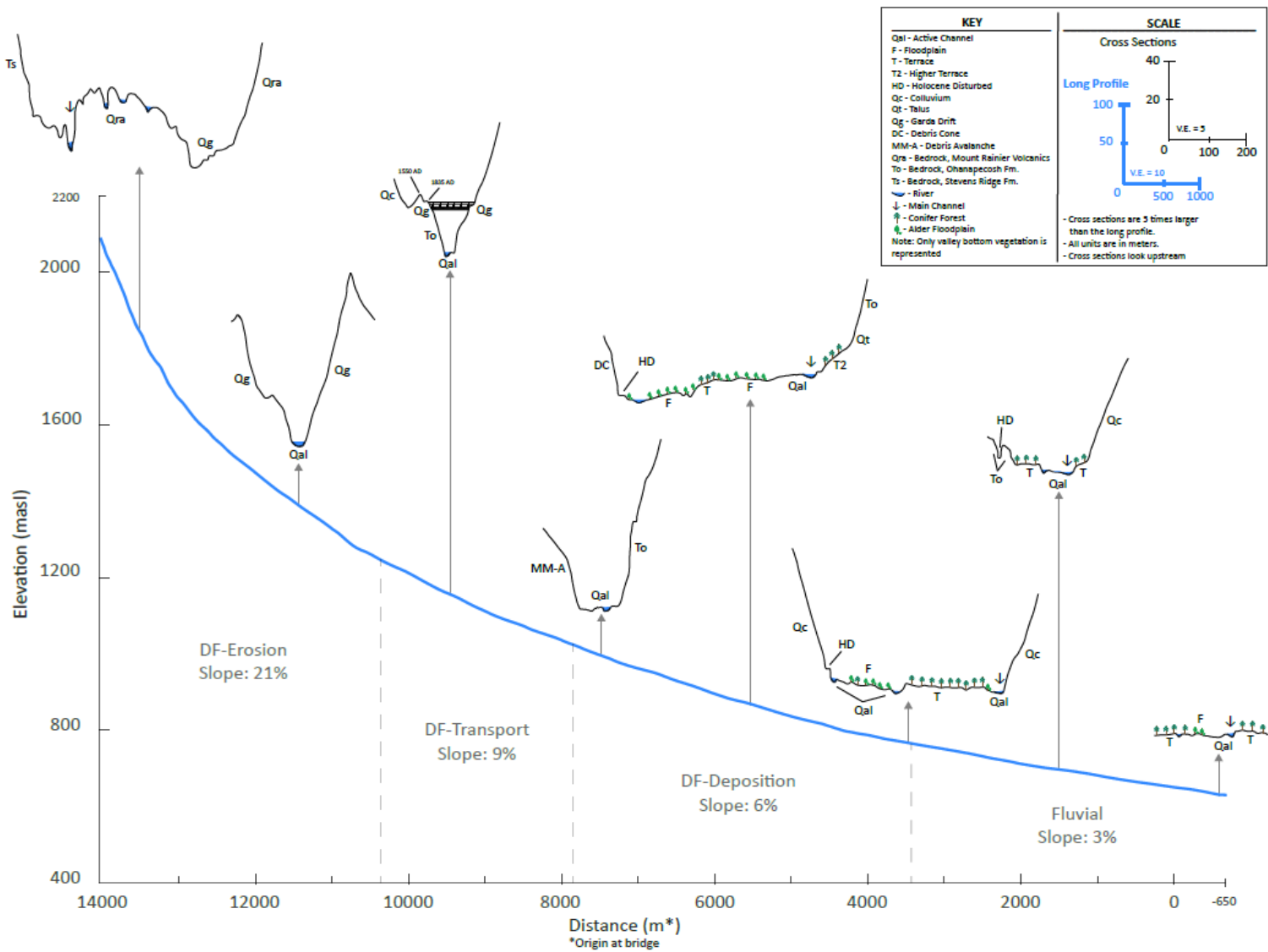


Figure 12. Tahoma Creek long profile and cross-sections. All elevations were sampled from the 2008 LiDAR dataset.

4.1.2.1 Stream Gradient Index

The stream gradient index (SL) suggests that the 2008 Tahoma Creek profile does not substantially differ at any point along its length from a logarithmic profile (Figure 13). The anomalously low SL value at the head of the stream is likely due to error introduced as a function of the $L/\Delta L$ ratio. The error introduced likely becomes insignificant by the second or third SL bin. Even excluding the first couple of bins, the SL values within the debris flow erosional zone particularly between about 1000 – 3000 meters below the glacier terminus are the lowest along the profile. The highest SL index values occur with the debris flow depositional zone with a value of 459.

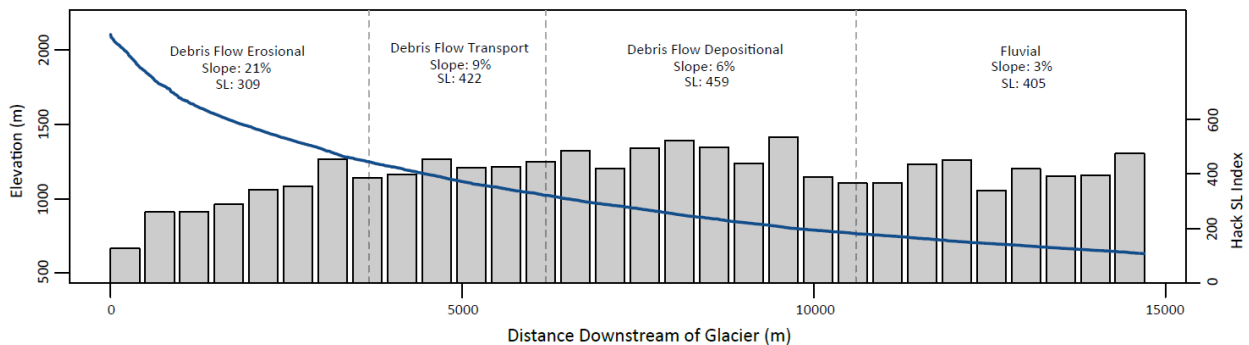


Figure 13. Stream gradient index for Tahoma Creek calculated following methods proposed by Hack (1973).

4.1.2.2 Valley Cross-Sections

The valley cross-sections, measured every 2 kilometers along Tahoma Creek, illustrate the contemporary boundary conditions and valley morphometrics (Figure 12). At RKM 13.5, the upstream most cross-section, four major channels spill over volcanic bedrock with a thin veneer of glacial till. Here the channel has not yet entered the valley bottom and is not laterally confined. The next three cross-sections, between RKM 11.5 and 7.5 show a mostly single-threaded channel incised up to 40-meters into glacial till within a laterally confined valley bottom no more than 100-meters wide. The remaining four valley cross-sections, between RKM 5.5 and -0.5, illustrate an entirely different valley setting. Here the valley is up to 600-meters wide, and lined with terraces densely vegetated with Douglas Fir, Western Hemlock and Western Red Cedar, as well as floodplains vegetated with Red Alder.

4.1.3 Whiting-Bradley Classification

Panel (a) of Figure 14 displays the hillslope inputs based on fieldwork evidence. Tahoma Creek exits the South Tahoma glacier as multiple meltwater channels approximately 13 kilometers above the Tahoma Creek bridge where it cascades over several bedrock ridges before coalescing into a single channel. The position of these meltwater streams changes regularly, causing a surge of water to go over loose, unconsolidated till and occasionally triggering debris flows (i.e. August 2015, August 2019).

Between RKM 12-10, Tahoma Creek is confined to a narrow canyon carved into Neoglacial tills and lahars. Regular gullying, slumping, and surface wash supply abundant volumes of sediment to the channel resulting in coupling of the lateral moraines. Bank erosion is sporadic for the next ~ 3 km of channel, with increased occurrence at the snout of landslide deposits. Landslide deposits are correlated to relative valley bottom narrowing and increased bank erosion.

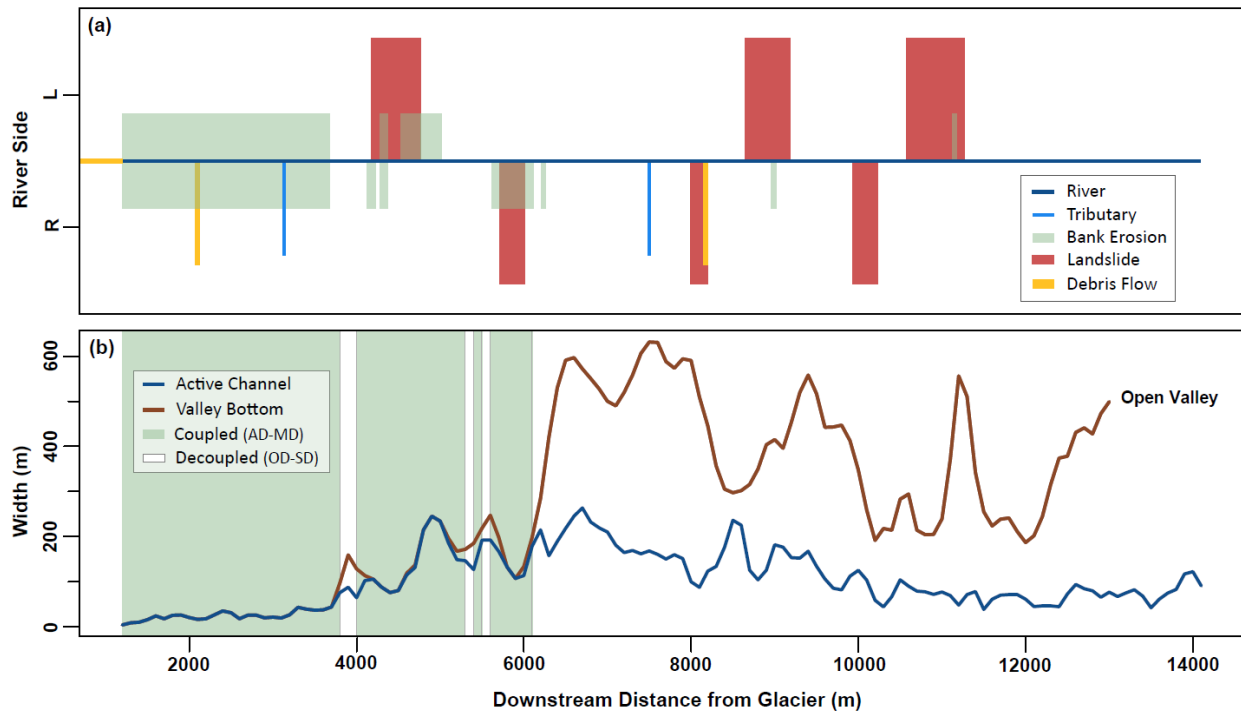


Figure 14. Degree of hillslope-channel coupling along Tahoma Creek. (a) Hillslope inputs based on fieldwork. (b) Valley bottom width, active channel width, and probability of hillslope-channel coupling following methods proposed by Whiting and Bradley (1993).

Downstream bank erosion is limited, occurring in discrete locations where the contemporary channel is pinned to the valley wall.

The majority of debris flows events originate at the South Tahoma glacier terminus as subglacial outburst floods that subsequently bulk into debris flows. Historical records, while incomplete, indicate that 33 or more such events have occurred since 1967 (Richardson, 1968; Crandell, 1971; Walder and Driedger, 1994; Beason et al., 2019). The outburst floods are likely the result of changes in subglacial drainage patterns (Walder and Driedger, 1995) often occurring on hot/dry days (Beason et al., 2019). A well-documented debris flow occurred in 1988 as the result of a liquified glacial till flowslide entering the channel approximately 2 km below the contemporary glacier terminus (Figure 14a). Additionally, approximately 8 km below the glacier, three debris flows originating from Dry Creek (2003, 2015, and 2016) entered the mainstem. It is likely that many other unrecorded debris flow events have occurred throughout the last century. Many small debris cones between RKM 2-6 attest to paraglacial debris flow activity in other locations within the watershed, although events are likely to go unrecorded in these remote locations. Over a millennial timescale, 5 large landslides have reached the mainstem channel. These large events occurred post Fraser Glaciation likely during a time of increased instability as a result of hillslope debuitressing.

The classification system proposed by Whiting and Bradley (1993) provides an estimate of the degree of hillslope-channel coupling. The longitudinal pattern of coupling within the Tahoma Creek watershed is similar to non-glaciated basins. The upper ~ 6 km of channel are laterally confined and narrow, resulting in coupled hillslopes (AD-MD); while the downstream ~ 8 km of channel are laterally unconfined or bounded on either side by continuous floodplain and terrace landforms, resulting in decoupled hillslopes (OD-SD) (Figure 14b). The transition between coupled and decoupled conditions occurs at the upstream boundary of debris flow deposition and valley widening (see Figure 12 and Figure 14b).

4.2 Measures of Sediment Connectivity

4.2.1 Effective Catchment Area

The effective catchment area represents the area within a catchment that has the potential to contribute sediment to the outlet. The ECA values vary widely as a result of DEM resolution (Figure 15). When applying a 2-degree slope threshold, percent contributing areas ranged from ~7% to ~75% at a DEM resolution of 1-meter and 30-meter, respectively. Similarly, applying an 8-degree threshold resulted in percent contributing values of ~0.4% and ~37.8% at a DEM resolution of 1- and 30-meters, respectively. The 5-meter DEM paired with an 8-degree slope threshold provided the most reasonable comparison to fieldwork ECA estimates in terms of both

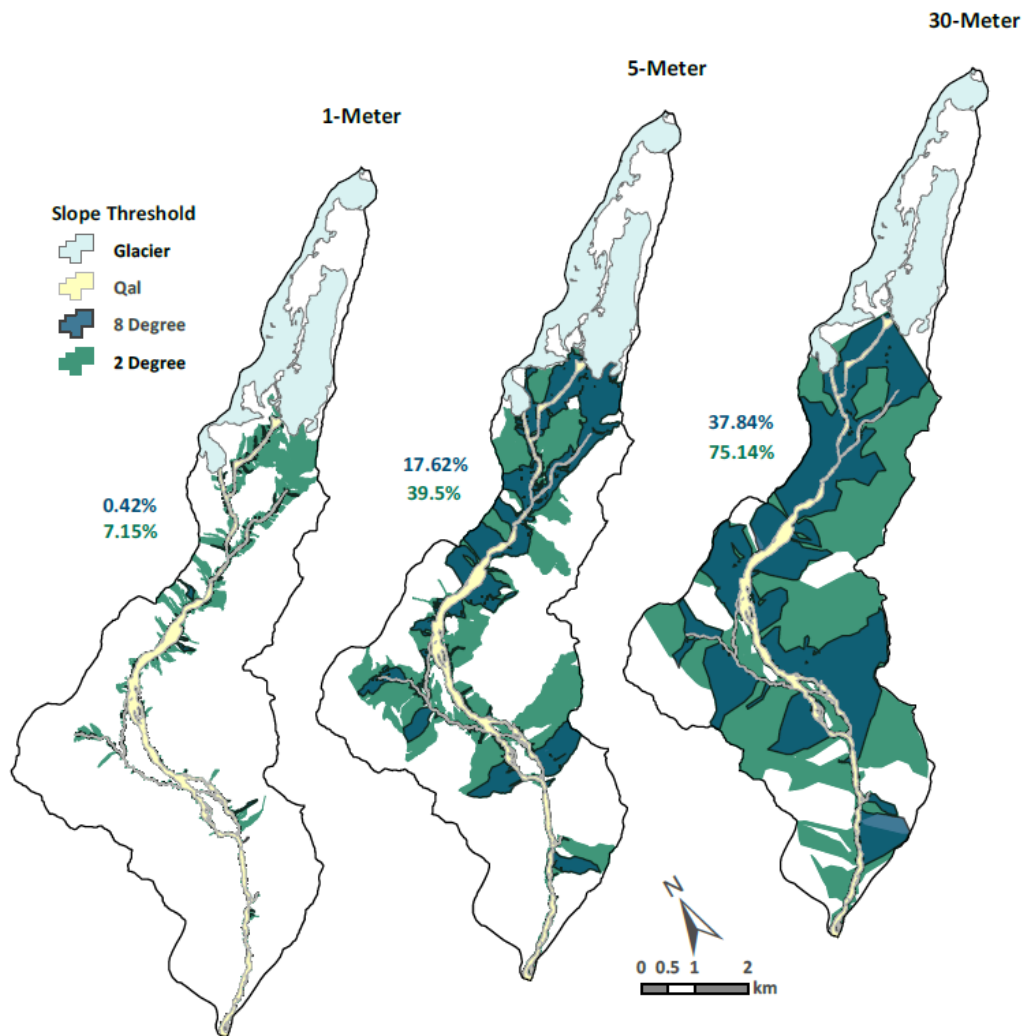


Figure 15. Effective catchment area calculated using a variety of DEM resolutions and slope thresholds.

specific areas contributing sediment and the total percent contributing area. The 1-meter DEM resulted in erroneous disconnections arising at the cell-level, affectively disconnecting all upstream cells. These small disconnections may limit transfer that would occur during annual magnitude events but are likely easily overcome during higher magnitude events (i.e. decadal, centennial). Conversely the 30-meter DEM smoothed over ‘real’ disconnections (i.e. small lakes, small moraine crests, etc.) and systematically overestimated the ECA at both slope thresholds.

4.2.2 Network Structural Connectivity

4.2.2.1 Contemporary Network

The NSC and RF methods highlight potential hotspots of geomorphic change. The results of these methods can be visualized in Figure 16, where the Shimbel’s, potential flow, NSC, and RF indices are mapped within the catchment. The inverse of Shimbel’s index indicates the accessibility of a given node (Figure 16a). Source nodes that are close to the catchment outlet result in higher accessibility values as a result of shorter path lengths. These nodes contribute to maximizing the compactness of the network. High accessibility values should correspond to shorter transit times (assuming a single transport process) and a decreased probability of entering intermediate storage. These nodes therefore should have higher values of connectivity based on the network structure alone.

Figure 16b illustrates the potential flow at each node within the network. In this case, considering only uninterrupted convergent flow, the potential flow classically increases in a downstream direction. Potential flow increases rapidly at confluences (junction nodes) highlighting their influence on the network. The NSC index considers both the potential flow and eccentricity of a given node (Equation [3]) and therefore relates to the potential degree of coupling between the sources and the outlet, given the current network structure. Figure 16c displays the NSC values of each node within the network. High NSC values correspond to nodes with relatively high potential flow, but also high accessibility. The top 1% NSC values lie along a major tributary, Fish Creek, near its confluence with the mainstem. The map also shows moderately high values along the mainstem between RKM’s 5 and 10.

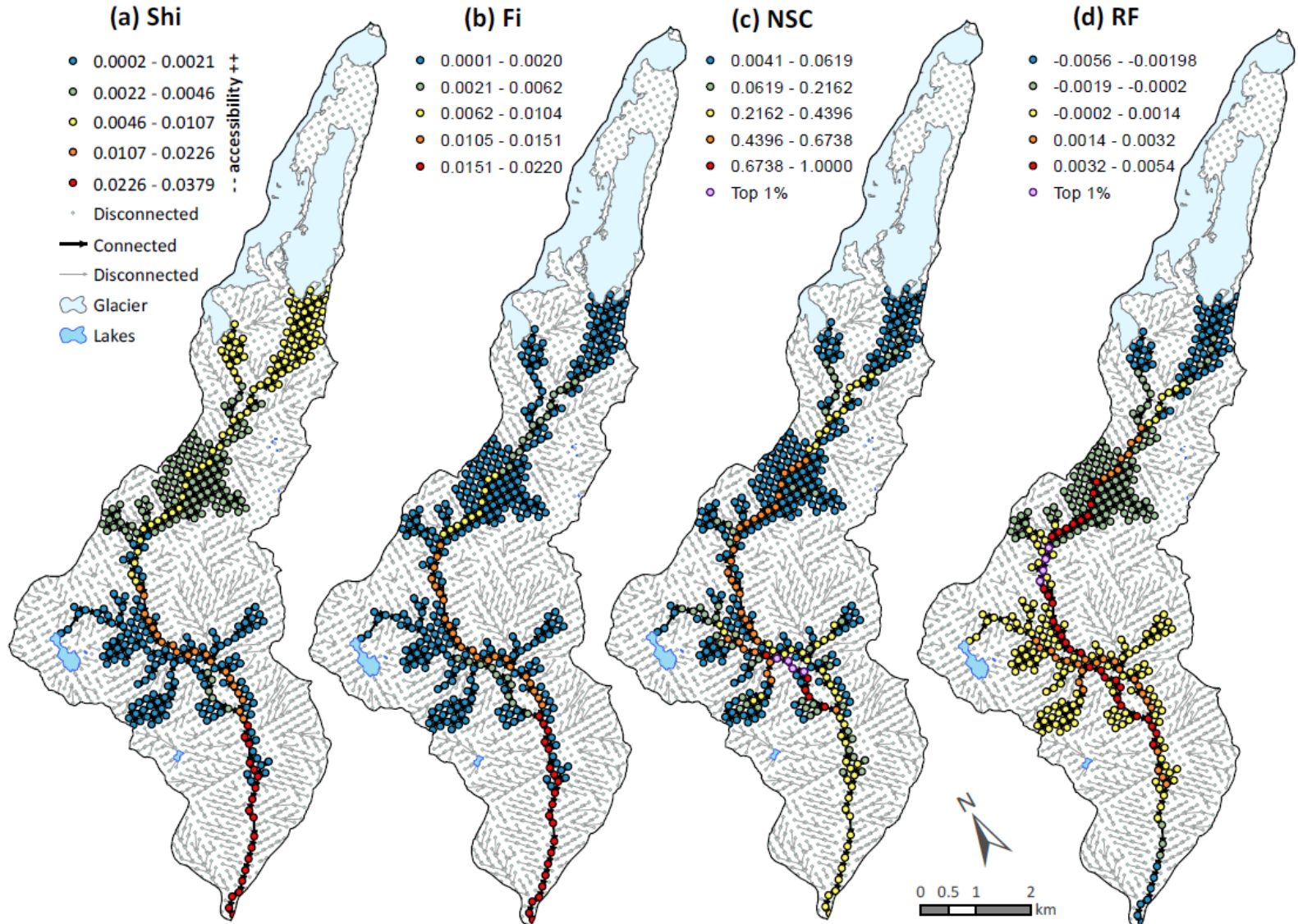


Figure 16. Accessibility, potential flow, NSC, and RF indices of the contemporary network at Tahoma Creek.

Fressard and Cossart (2019) noticed that the potential flow through a given node tends to increase linearly as the eccentricity of that node increases. The residual flow method (Equations [4] and [5]) provides a measure of the under- or over-prediction of potential flow given a nodes location within the network. Figure 16d displays a map of the RF index results, while Figure 17 displays the linear regression between F_i and Sh_i . The top 1% RF values lie along the mainstem between RKMs 7-7.5, with high values between RKMs 9.5 and 3. Below RKM 3, RF values rapidly decline, eventually becoming negative as a result of high eccentricity.

The linear regression between F_i and Sh_i has an R^2 value of 0.86 a slope of 0.76 and y-intercept of -0.0014. Figure 6 shows an initial increase in F_i with low Sh_i values that corresponds to nodes along Fish Creek, a major tributary. The increasing flow results in moderate to high RF values and an over-prediction of sediment given the location within the network. Following this initial increase, F_i values fall back to zero as a result of eccentric source nodes, mainly in the proglacial zone. Sh_i values greater than about 0.007 correspond to nodes along the mainstem and display a non-linear trend as a result of valley width (measured ridge to ridge) narrowing and decoupled hillslopes.

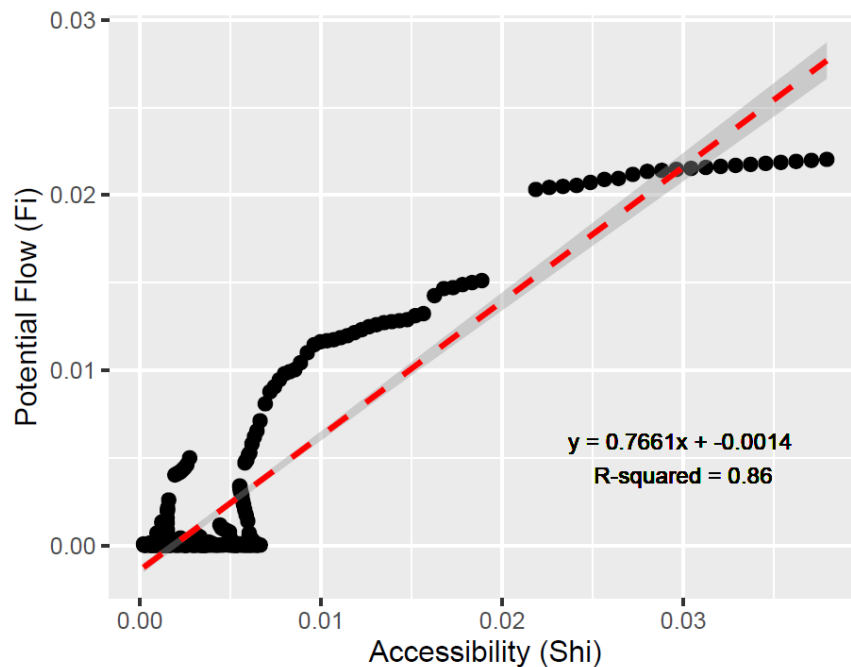


Figure 17. Residual flow regression plot of the contemporary network.

4.2.2.2 Near Complete Connectivity

We also applied the NSC method to a second scenario considering full connectivity except for nodes draining into lakes which act as long-term storage. In considering a nearly completely connected network, the top 1% NSC values shifted towards the outlet as a result of highly accessible source nodes (Figure 18a). All nodes within the top 1% lie on the western hillslope near the mainstem.

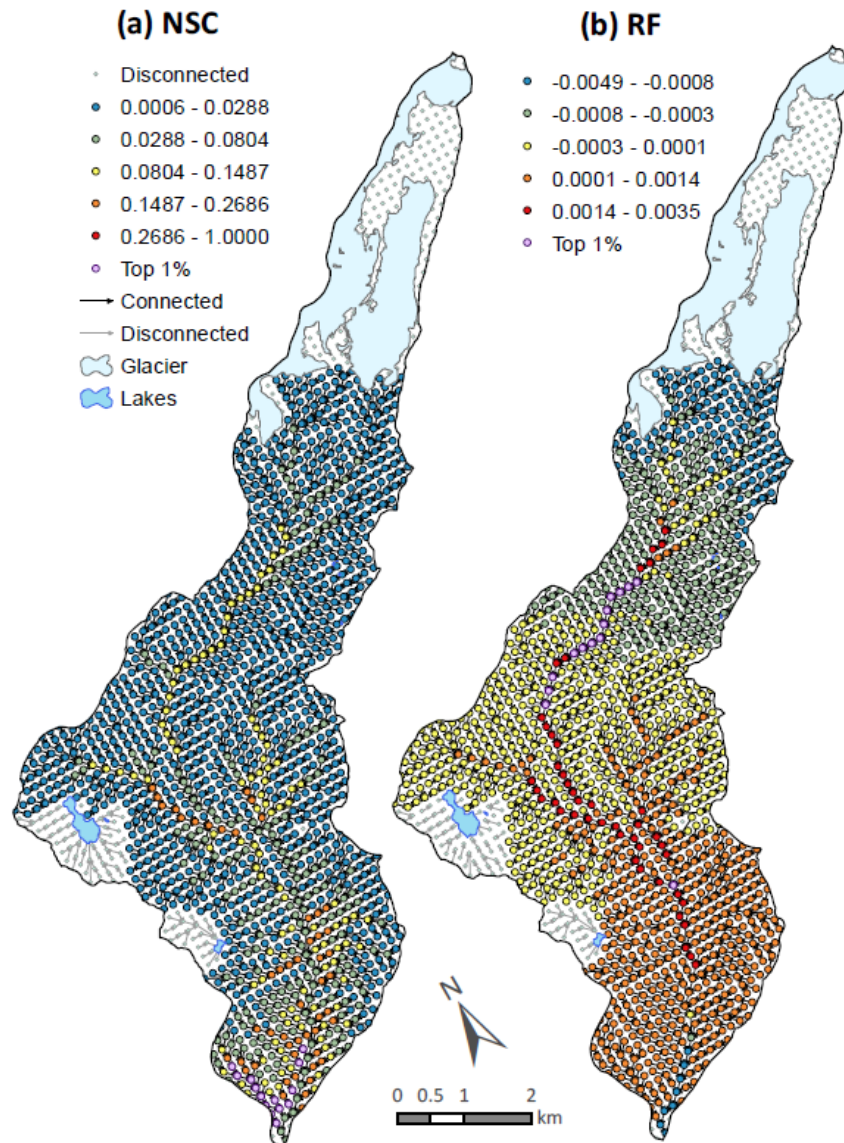


Figure 18. NSC and RF indices of Tahoma Creek assuming near complete connectivity.

In the case of near complete connectivity, the residual flow index indicates high connectivity along the mainstem between RKM 10 and 2.5, and along Fish Creek near its confluence with Tahoma Creek (Figure 18b). The top 1% RF values are concentrated between RKM 9.5 and 6.5. These values overlap with those of the contemporary network suggesting consistency in predicting hotspots within the network. An additional hotspot was identified near RKM 3 at a major confluence.

The linear regression between F_i and Sh_i can be seen in Figure 19. The linear regression has an R^2 value of 0.94, a slope of 0.7503 and y-intercept of -0.0004. In comparing the residual flow regression plots between the two different scenarios, very little changed. The general pattern of over- and under- predicting remained the same, except near the origin of Figure 19. The initial spike in F_i at low Sh_i from scenario 1, previously associated with Fish Creek, now overlaps with values from the mainstem.

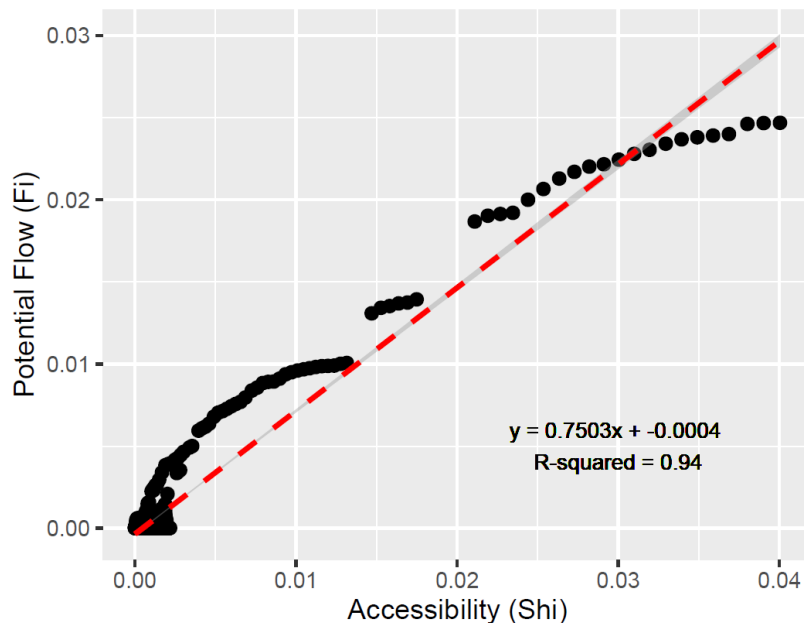


Figure 19. Residual flow regression plot of the nearly completely connected network.

4.2.3 Index of Connectivity

4.2.3.1 Standard Index of Connectivity

The IC method provides an estimate of sediment connectivity based on the topographic characteristics of the area, and in this case where we used the river as the target, is highly dependent on the lateral position of the river within the valley bottom. Within the Tahoma Creek watershed IC values are generally high near the termini of the Tahoma and South Tahoma glaciers, within the entrenched canyon between RKM 12 and 10.5, and along Emerald Ridge (river right between RKM 10.5 and 9) (Figure 20). Downstream of RKM 9, IC values tend to be high on hillslopes where the river is immediately adjacent to the corresponding valley wall, and additionally within the Mount Wow complex (river right between RKM 6 and 4.5) as a result of steep slopes.

In considering the contemporary lakes within the catchment as millennial-scale sediment sinks, the upstream contributing areas are affectively completely disconnected with respect to downstream areas. This results in large areas being excluded from the IC calculation. The glacier cirques containing Lake George and Lake Allen as well as the parkland containing Mirror Lakes are subsequently considered disconnected. One major limitation of this method is the inability to accurately capture all flow paths from the variety of sediment transfer processes active within the watershed. Within the Tahoma Creek watershed this is most obvious near the catchment outlet. Below RKM 2 the D-infinity flow routing algorithm applied within the IC method does not route flow towards the contemporary river as a result of a convex valley bottom debris fan. For this reason, the hillslopes are considered completely disconnected with respect to the river. While this disconnection is the result of flow-routing alone, we note that these hillslopes are generally disconnected as a result of buffering from the continuous paired terraces. While less dramatically obvious everywhere else, small inaccuracies in flow routing are an inherent limitation of this method.

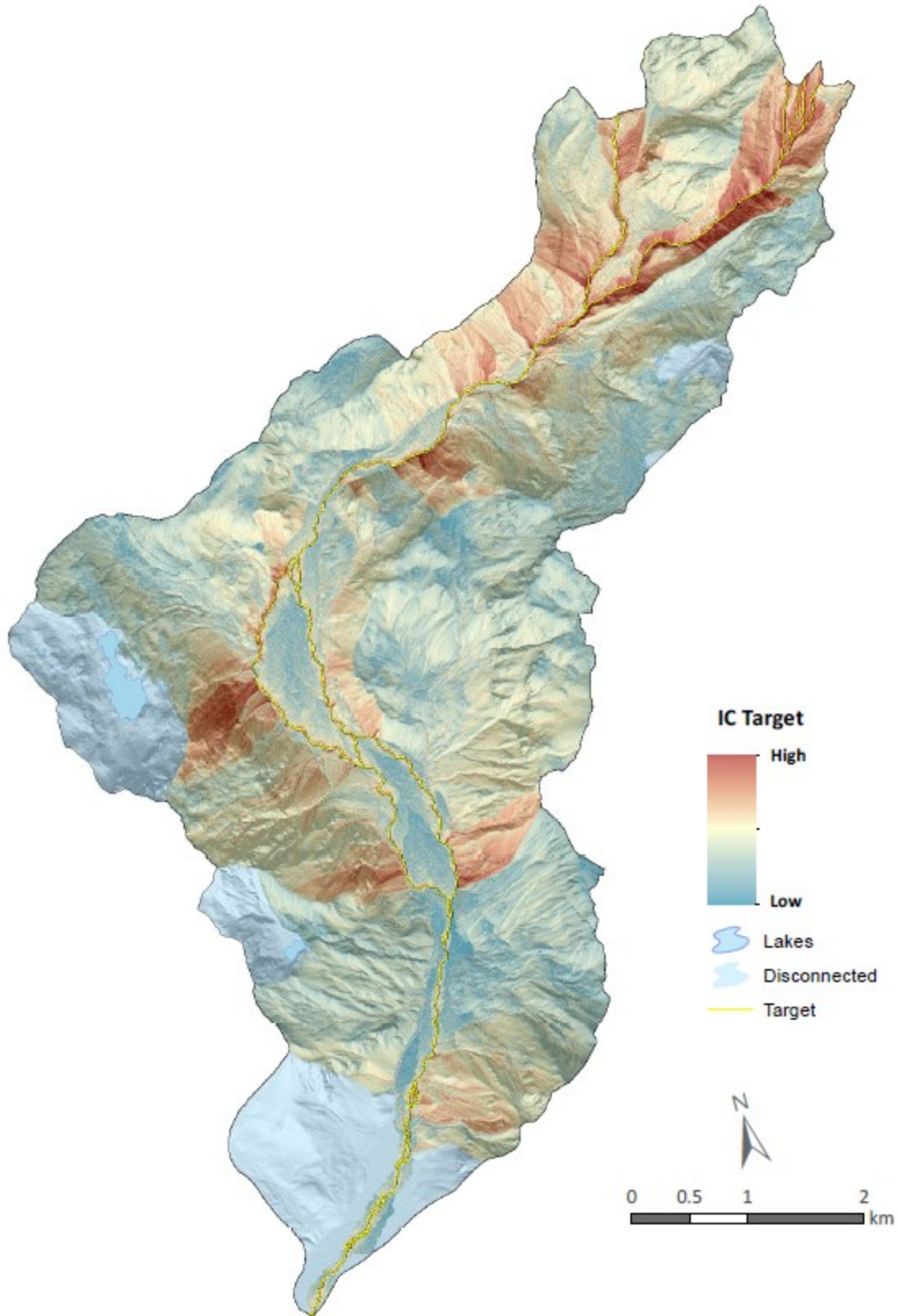


Figure 20. Index of connectivity (IC) map of Tahoma Creek with the river as the target. The weighting raster was calculated following Cavalli et al. (2013) and normalized considering flow-direction roughness (Trevisani and Cavalli, 2016)

4.2.3.2 Joint Index of Connectivity

Another limitation of the IC method proposed by Cavalli et al. (2013) is the lack of modeling the influence that vegetation plays on sediment connectivity. Vegetation increases surface roughness and infiltration, stabilizes sediment, and generates disconnections within the sediment cascade thereby reducing sediment connectivity (Ortiz-Rodriguez et al., 2017). In this study we applied the Joint Index of Connectivity which modifies the weight factor within the IC to account for vegetation effects (Borselli et al., 2008; Ortiz-Rodriguez et al., 2017). In unvegetated areas the RI based weight factor proposed by Cavalli et al. (2013) was used. Vegetated areas were subdivided into two different categories based on fieldwork, (i) mixed forest assigned weight factor values of 0.001, and (ii) discontinuous forest and riparian vegetation assigned weight factor values of 0.006.

The results of the IC_j can be seen in Figure 21. The main differences between the standard IC application and the IC_j are increased connectivity values within the proglacial zone, active channel, and within the Mount Wow complex as a result of a lack of vegetation in these areas (refer to Figure 20 and Figure 21). Accounting for vegetation affects improves the calculation of connectivity with respect to fieldwork estimates.

4.2.3.3 Weight Factor Values

It is important to consider the distribution and range of weight factor values used for calculating the IC because these values will determine the range of IC values possible. Weight factor values for the two different scenarios can be seen in Figure 22. In general, W values calculated using the flow-direction roughness measured from the DEM range from 0.001 to 1, with most values lying between about 0.3 and 0.8. In contrast, when applying C-factor values used in USLE-RUSLE models to vegetated areas, close to 75,000 raster cells have values of either 0.001 (mixed forest) or 0.006 (riparian/discontinuous forest), while the remaining unvegetated areas still have the same distribution of values as the W1 raster. This provides a clear distinction between vegetated and unvegetated areas and dramatically decreases the relative connectivity where vegetation is present.

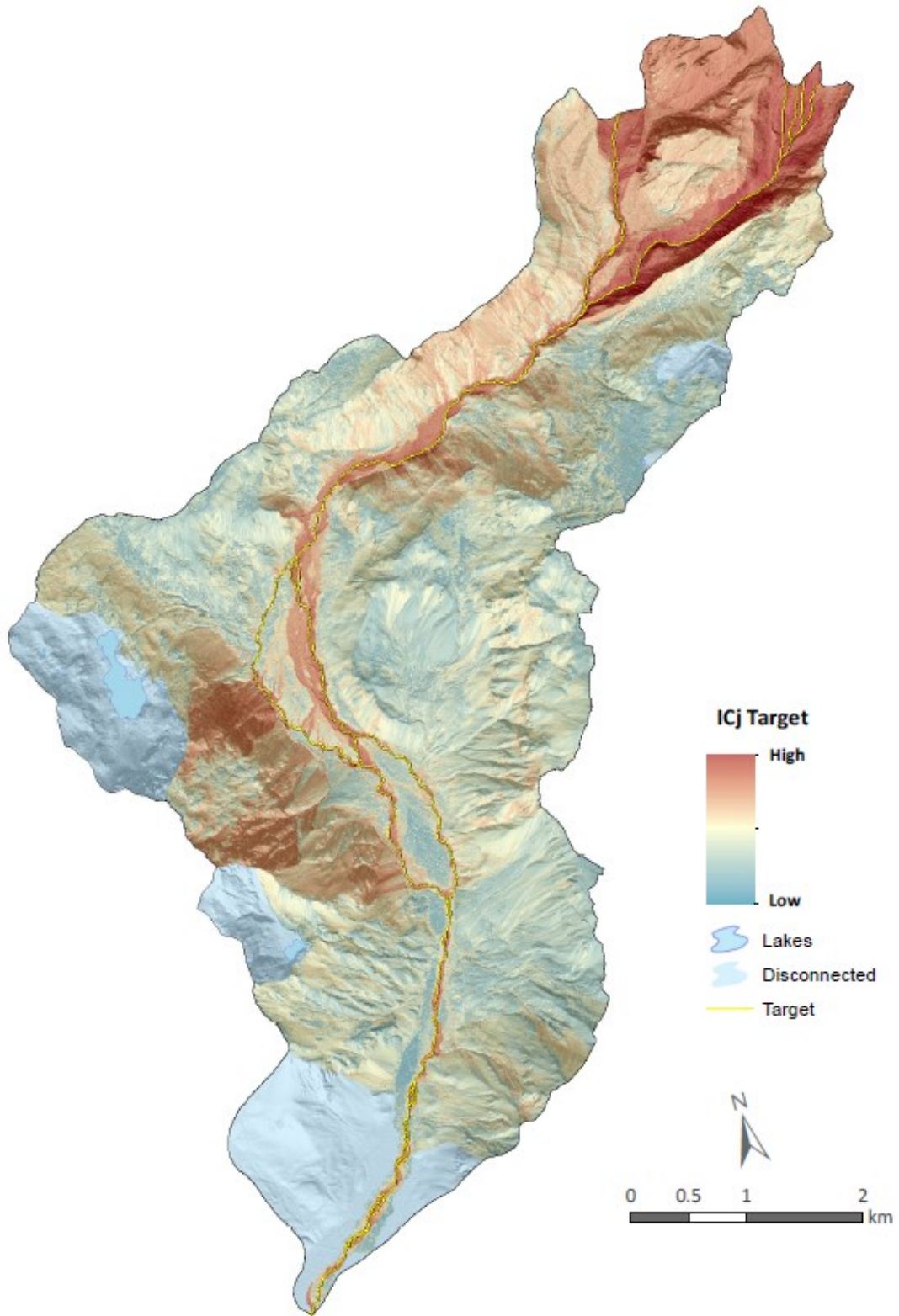


Figure 21. Joint Index of Connectivity (IC_j) map of Tahoma Creek with the river as the target. The weighting raster was calculated following Ortiz-Rodriguez et al., 2017.

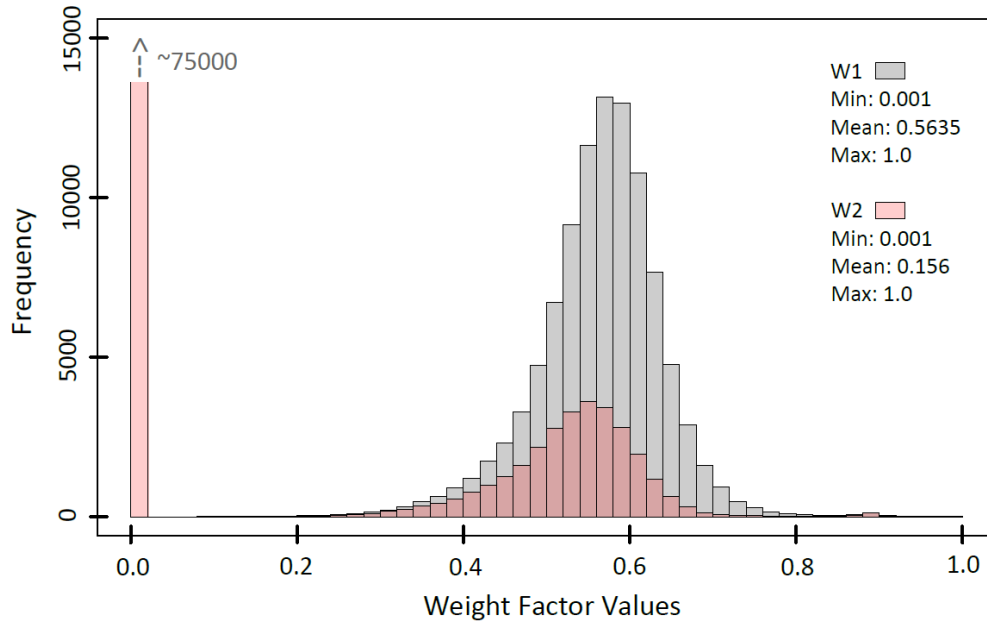


Figure 22. Distribution of weight factor values considering the two different scenarios. W1: weight factor calculated based on DEM flow-direction roughness alone, and W2: joint weight factor including C-factor values appropriate for vegetated areas.

4.2.4 Spatially Distributed Sediment Delivery Ratio

4.2.4.1 AOIs 1 and 2 (2002 – 2008)

The spatially distributed sediment delivery ratio method produces a map of the estimated functional connectivity of the chosen area at the scale of individual raster cells. Maps of the net change and SDR for AOIs 1 and 2 for the period 2008 – 2002 can be seen in Figure 23. Net degradation occurred throughout much of the defined area (up to 38 meters) while aggradation (up to 5 meters) was isolated to lower gradient areas (Figure 23, panel a).

During the 2002 to 2008 period, a majority of the sediment eroded within the AOI was exported from the same area. Summing up erosion and deposition separately results in values of -642,000 m³ and 18,000 m³ for AOI 1 and -408,000 m³ and 900 m³ for AOI 2, respectively. The morphological budgets for AOIs 1 and 2 are -624,000 m³ and -407,000 m³, respectively. These values result in specific sediment yields (SSYs) of 3.45 m over the six-year period (0.58 m yr⁻¹) for AOI 1 and 3.22 m (0.54 m yr⁻¹) for AOI 2. Vertical datum uncertainty, which scales linearly

with area, is conservatively estimated as 0.025m (Appendix A.2:) resulting in values of 4600 m³ for AOI 1 and 3200 m³ for AOI2.

The same general pattern can be seen in the SDR map (Figure 23, panel b). Areas of net aggradation correspond to low delivery ratios, while much of the area has SDR values at or near 1. The mean SDR values of AOIs 1 and 2 were 0.90 and 0.98, respectively.

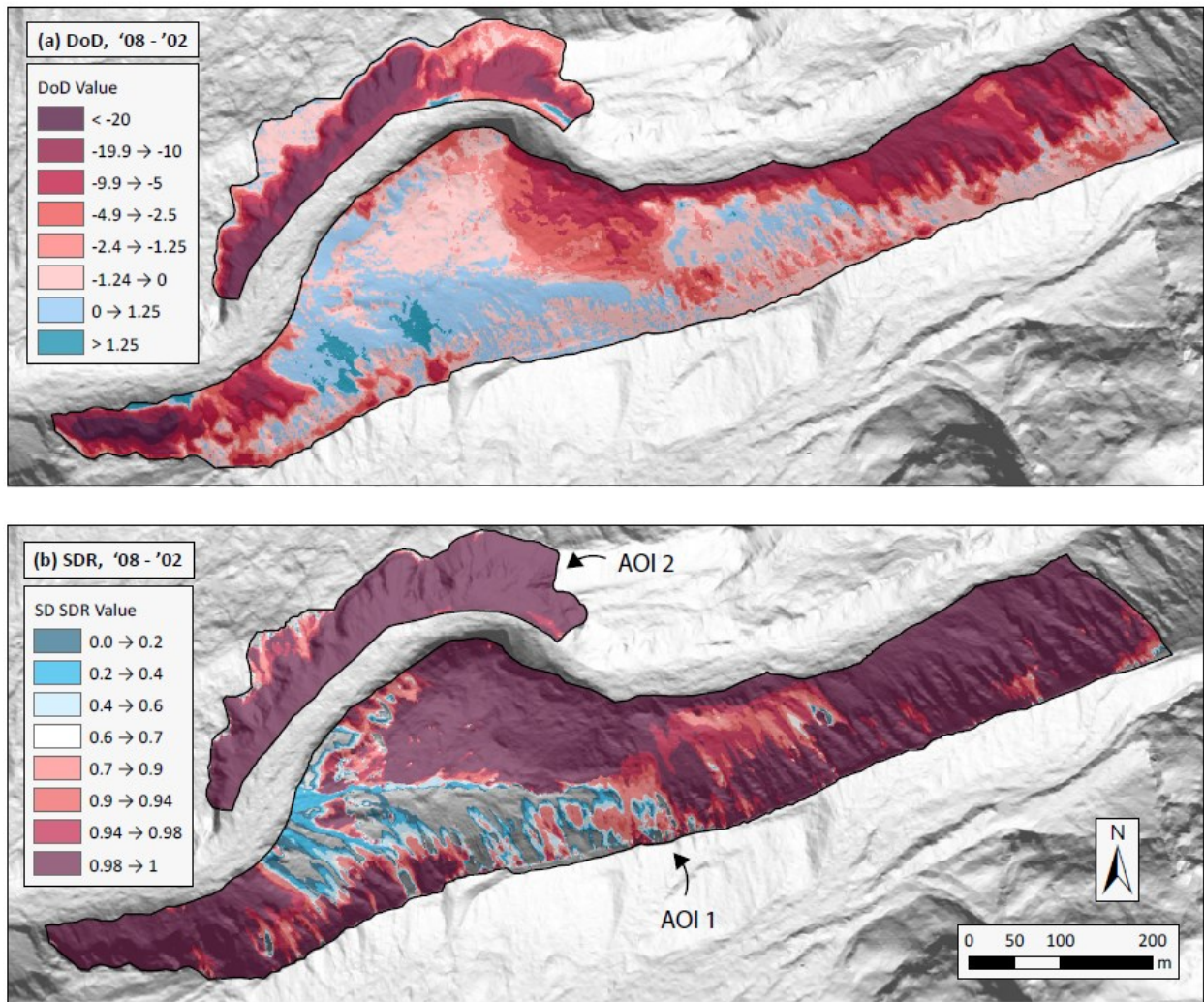


Figure 23. DoD and SDR maps of AOIs 1 and 2 for the period 2008 – 2002.

4.2.4.2 AOIs 1 and 2 (2008 – 2012)

During the 2008 to 2012 period much of the sediment eroded from near the crest of the moraine was redeposited downslope within the AOI (Figure 24, panel a). This manifests as low delivery ratios at the base of the slopes (Figure 24, panel b). During this period, locations experienced up to 16 meters of erosion while up to 6 meters of deposition occurred downslope. The morphological budgets of AOIs 1 and 2 amount to $-90,000 \text{ m}^3$ and $-14,800 \text{ m}^3$, respectively. These values correspond to SSYs of 0.50 m over the four-year period (0.13 m yr^{-1}) for AOI 1, and 0.12 m (0.03 m yr^{-1}) for AOI 2. Summing gross erosion and deposition separately results in $-134,000 \text{ m}^3$ and $43,000 \text{ m}^3$ for AOI 1, and $-36,000 \text{ m}^3$ and $22,000 \text{ m}^3$ for AOI 2, respectively.

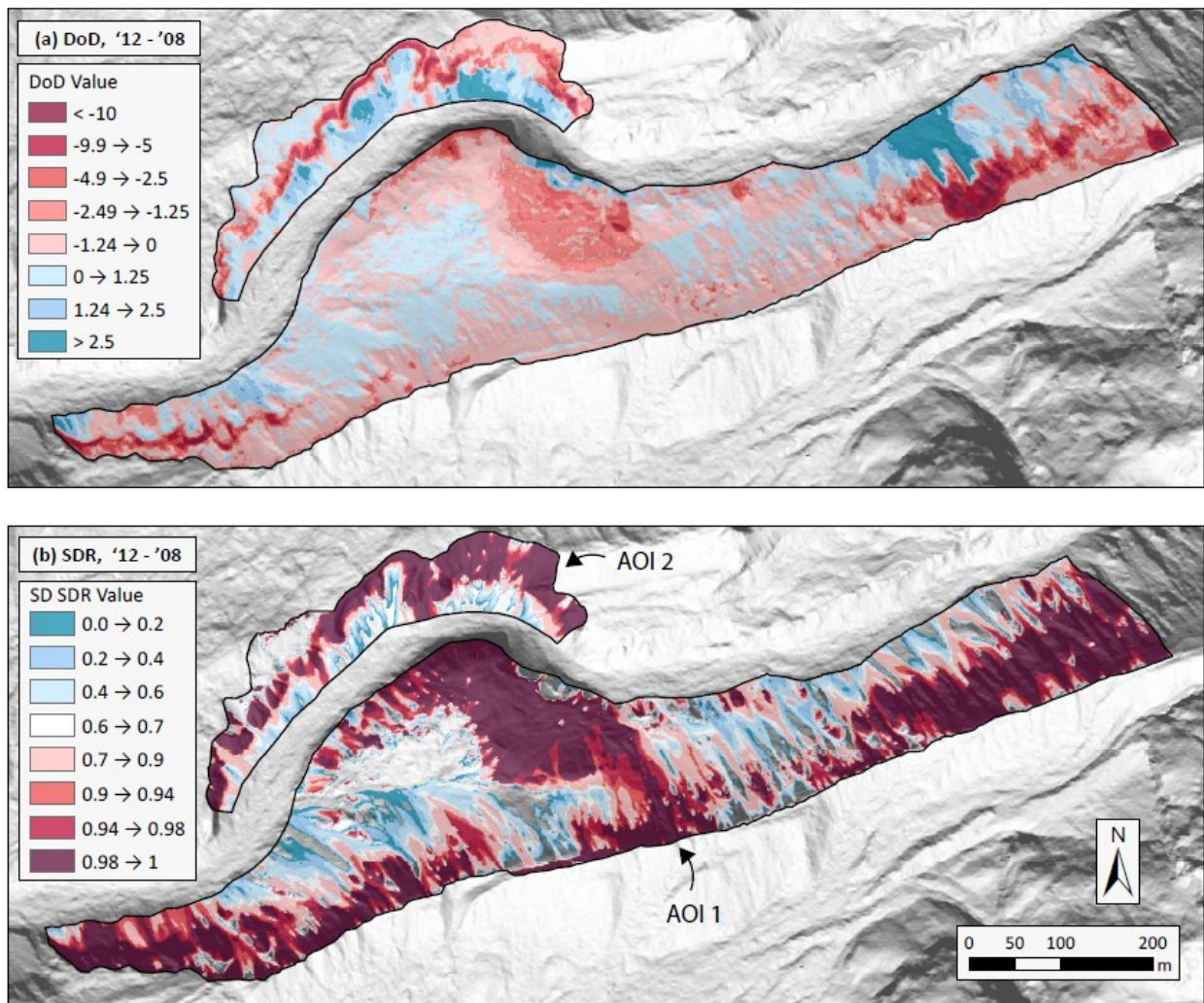


Figure 24. DoD and SDR maps of AOIs 1 and 2 for the period 2012 – 2008.

The mean delivery ratios for AOIs 1 and 2 were 0.81 and 0.82, respectively. These values are slightly less than corresponding values from 2002 – 2008 owing to increased deposition at the base of gullies.

4.2.4.3 AOI 3 (2002 – 2008)

DoD values at AOI3, which lies along Emerald Ridge (river right between RKM 9 and 10), range between -31 and 22 meters (Figure 25, panel a). The positive DoD values are generally

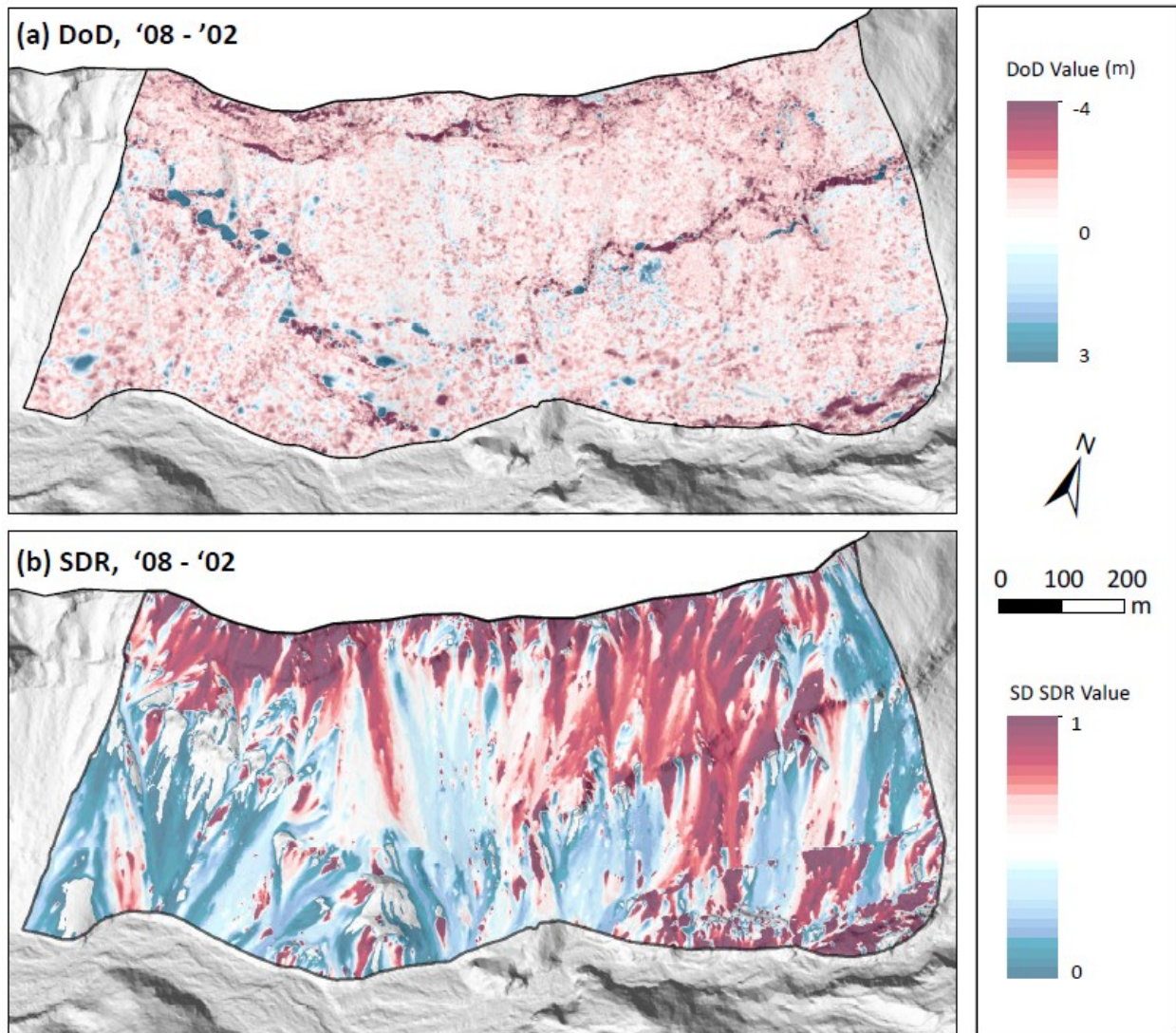


Figure 25. DoD and SDR maps of AOI 3 for the period 2008 – 2002.

concentrated just upslope of many of the small bedrock knobs while erosion is highest at the downslope end of the same. Sediment transport in this area is likely the result of rockfall, diffusive processes, and minor gullyng. The morphological budget of the total AOI equals -289,000 m³ ±18,000 m³ (see appendix A.2: Uncertainty Estimates). This value equates to an SSY of roughly 40.5 mm for the six-year period (6.75 mm yr⁻¹). Summing up erosion and deposition separately results in values of -364,000 m³ and 75,000 m³, respectively. SDR values generally decrease in the downslope direction and are often at a minimum near the bedrock knobs where deposition was concentrated. The mean SDR value for the entire AOI is 0.86 indicating that much of the sediment eroded is exported.

4.2.4.4 Areas Removed

Areas where the delivery ratio would be negative (apparent deposition within contributing area is higher than apparent erosion from the same area) have been removed. Heckmann and Vericat (2018) note 4% of the raster cells in their study were affected by this issue while 4.1% to 20.4% of the cells in this study were affected depending on the AOI and period of interest (Table 1).

AOI #	Period	% Removed
1	08 - 02	10.7
1	12 - 08	16.5
2	08 - 02	4.1
2	12 - 08	20.4
3	08 - 02	6.9

Table 2. Percent of area removed when calculating the SD SDR.

Negative delivery ratios are likely the result of one or more of the following scenarios,

1. The inability of the flow-routing algorithm to predict all possible flow pathways.
 - a. Non-fluvial processes are significant.
 - b. Pathways changed significantly during the inter-survey period while flow pathways were calculated for one single year.
2. The density of the deposited material is less than that of the original landform.
3. The AOI does not satisfy the zero-flux boundary condition requirement.

Chapter 5: Discussion

5.1 Qualitative Assessment

We set out to explore whether disconnectivity or connectivity control the spatial variability of sediment transfer within the Tahoma Creek watershed at Mount Rainier, WA. We address this question below by discussing the spatial patterns of sediment transfers and subsequently sediment connectivity, as well as sources of disconnectivity and their upslope affected areas.

5.1.1 Field Observations: Patterns and Degree of Connectivity

5.1.1.1 Hillslope-Channel Coupling

Hillslope-channel coupling is mainly facilitated by bank erosion (i.e. fluvial erosion by the mainstem, and gullying/slumping), and mass wasting processes (i.e. debris flows, rockfall, landsliding, etc.) that reach the valley floor. Bank erosion is common in the uppermost ~ 6 km of channel, with increased occurrence along the base of the lateral moraine and at the snout of landslide deposits. The majority of debris flows directly enter the mainstem near or at the glacier terminus, further coupling the glacial and proglacial zone to the fluvial network.

Bank erosion is limited in the lowermost 7 km of channel, occurring only in discrete locations where the contemporary channel is pinned to the valley wall. Mass wasting processes couple the east face of Mount Wow to the valley floor. Debris flows frequently torrent Dry Creek before fanning out into the active channel. Mass wasting rockfall events transport boulders and rock fragments to the valley floor, although much of the debris is too coarse to be transported by the fluvial system. The lowermost 7 km of channel is nearly completely disconnected from the adjacent hillslopes as a result of the paired terraces and floodplains at its margins.

5.1.1.2 Effective Catchment Area

The effective catchment area is highly dependent on the temporal scale of interest, increasing in area as the length of time increases. This study is primarily concerned with coarse sediment transfers over a human-timescale. At this scale, the ECA is approximately only 15% of the total watershed and is generally restricted to the proglacial zone and valley floor (within the limits of the contemporary floodplain). The proglacial zone delineated by the prominent lateral moraines

makes up a significant proportion of the ECA. Over longer timescales mass wasting and channel migration significantly increases the proportion of hillslopes contributing sediment.

Not all connected areas contribute equal volumes of sediment. This is because sediment transfer is a function of connectivity (efficiency of transfer), magnitude of the event, and sediment availability. The proglacial zone supplies approximately 74% of the total volume of eroded sediment within the catchment; likely because it is steeper, consists of unconsolidated sediment, and is not vegetated. This suggests that contributing areas below RKM 10 supply relatively little coarse sediment at the human-timescale.

5.1.1.3 Efficient Sediment Pathways

We defined sediment connectivity as the efficiency of sediment transfer within and between process domains. We then created a conceptual sediment budget defining the sediment pathways and specified their relative importance. The relative importance is based on fieldwork conducted by the author and limited volumetric measurements gleaned from the literature and two DoDs spanning a ten-year period. It should be noted that the “relative importance” shown in Figure 4 is also not a direct assessment of connectivity, rather it is the result of the degree of connectivity and sediment availability. It would then be a mistake to directly compare volumetric sediment transfers to connectivity indices. Instead we created an unbalanced sediment budget that provides relative transfer efficiencies for the process domains within the DoD coverage.

The most significant coarse sediment pathway at the human-timescale within Tahoma Creek watershed begins within the proglacial zone, where contemporary glacial and Neoglacial deposits (i.e. moraines dating to the LIA) are eroded by hillslope processes, debris flows, and floods and are eventually exported from the system via fluvial transport. Between 2002-2008, a period encompassing a large-magnitude flood, ~95% of the material eroded from contributing proglacial hillslopes/banks reached the fluvial network. During the same period, ~45% of material supplied to the fluvial network was transported out of the watershed. Keep in mind that these values come from a small proportion (~8%) of the total catchment and excludes areas outside the ECA. Between 2008-2012 only ~65% of the material mobilized from adjacent

proglacial hillslopes/banks reached the fluvial network while a meager ~20% of the coarse material supplied to the fluvial network was exported out of the system. These results highlight two things, (i) sediment transfer efficiencies (sediment connectivity) vary over time and with different magnitude events, and (ii) even the most significant catchment scale sediment pathways are inefficient at transferring sediment over an annual-decadal scale.

The only other sediment transfer efficiency estimate within the watershed is from a mass wasting rockfall event in 2014. During this event approximately 50% of the total material mobilized reached the valley floor, much of which was then too coarse to be transported by the fluvial network. Lower magnitude rockfall events throughout the watershed likely are even less efficient at transferring material to the fluvial network.

5.1.1.4 Event Magnitude Controls Connectivity

The previous section highlighted the difference in transfer efficiencies between a period encompassing an exceptionally large (approx. 100-year flood) flood event and a period with relatively average events. Anderson and Pitlick (2014) associate the increased volume of sediment mobilized to the 3-day event in 2006. It is then reasonable to associate a portion of the increased connectivity to the high-magnitude event. Essentially, the high-magnitude event resulted in an increased volume of sediment mobilized (connectivity + sediment availability), and a much higher sediment delivery ratio (connectivity). The high-magnitude event contributed to an increase of roughly 25% in sediment transfer efficiency throughout the fluvial network. During the large flood, flood waters filled much of the valley floor, causing restructuring of the channel network, and temporarily connecting many (still relatively few) of the hillslopes. Event sequencing likely also plays a role in the degree of sediment connectivity. Redeposition at the base of the lateral moraine greatly reduced the delivery ratio of hillslope sediments to the fluvial network between 2008-2012. Comparing the patterns of erosion between 2002-2008 to the patterns of redeposition during 2008-2012 reflects the refilling of intermediate stores (colluvial apron) that were emptied during the large 2006 flood. It is entirely possible that once the colluvial apron reaches a critical slope (~30°), upslope sediment input would be balanced by sediment output, a condition of connectivity regardless of the magnitude of the event.

As previously mentioned in the ECA section above, the large 2006 event also greatly increased the contributing area by temporarily increasing the hillslope-channel coupling (primarily through bank erosion) downstream of the proglacial zone.

5.1.2 Field Observations: Patterns and Degree of Disconnectivity

Sources of sediment disconnectivity are bio-geomorphometric characteristics of the landscape or landforms that reduce the efficiency of sediment transfer. Sources of disconnectivity are relatively easy to map in the field or using remote sensing techniques and are more tangible than connectivity. Sources of disconnectivity are abundant within the Tahoma Creek watershed. Here they are further categorized into buffers, barriers, and blankets following Fryirs et al. (2007a).

5.1.2.1 Buffers

The primary buffering landforms within the watershed are the lateral and end moraines, lakes, parklands, terraces, floodplains, debris fans and cones, and debris flow levees. These landforms lie at or near the valley bottom margin (see Figure 3) and often mark the transition between the hillslope and fluvial process domains. Low-gradient slopes, vegetation, and network structure are characteristics of the landscape that introduce disconnectivity. Additionally, anthropogenic structures such as roads and culverts cause disconnectivity along the valley margin. Buffers contribute to disconnectivity both within and between process domains. In this watershed, lakes and vegetation increase disconnectivity within the hillslope and colluvial process domains, while the remainder of buffering landforms/characteristics primarily cause disconnectivity at the boundary between the colluvial and fluvial process domains. Buffers are extremely effective sources of disconnectivity within the Tahoma Creek watershed, resulting in approximately 85% of the catchment being disconnected from the outlet, and the lower 8 km of channel completely decoupled from the hillslopes.

5.1.2.2 Barriers

Barriers to sediment transport within Tahoma Creek include in-stream LWD and natural dams, grain size vs. competence effects, valley constrictions, sediment slugs, culverts, and bridges. Barriers cause disconnectivity within the fluvial process domain by reducing the efficiency of

downstream sediment transport. As noted by Fryirs et al. (2007a), barriers such as LWD and natural dams often disrupt downstream transport through their effect on the local channel gradient/base level. By creating backwater areas of reduced gradient, barriers cause localized deposition upstream. Areas of localized deposition attest to the importance of in-stream LWD, log jams, and dead-standing trees in causing disconnectivity. Additionally, the largest zone of deposition within the valley bottom (RKMs 3.5 - 7) corresponds to river competence deficiency relative to the bouldery debris deposited by debris flows. This zone, and presumably barriers acting upon it, including grain size – competency, reduced the SDR between 40-50% based on DoD estimates. Throughout the entire fluvial network, barriers prevented between 55-80% of sediment mobilized from reaching the outlet.

5.1.2.3 Blankets

Sediment slugs prevent the vertical reworking of sediment within the active channel by smothering other landforms and through coarsening. These features generally result from debris flow deposition or hillslope inputs that overwhelm the system causing localized deposition. Because debris flows and mass wasting processes have a wide grain size distribution that is often too coarse to be transported by the fluvial network except during extreme floods, sediment slugs may remain in the channel for some time. It is difficult to measure the effects of blankets on sediment transfer efficiencies, but the depositional zone between RKMs 3.5 – 7 has certainly been affected by them.

5.1.2.4 Inefficient Sediment Pathways

In general, coarse sediment pathways beginning with bedrock sources are relatively inefficient over human-timescales. As seen in Figure 4, mass wasting processes (i.e. rockfall, landslides, lahars, etc.) are largely responsible for connecting bedrock sources to the fluvial network. Mass wasting processes are episodic and occur over long (centennial +) timescales thereby limiting their effect over human-timescales. Additionally, upland and valley margin sediment reservoirs are largely disconnected from the fluvial network as a result of spatially limited and infrequent bank erosion. The Tahoma Creek watershed is a highly fragmented system.

5.1.2.5 Spatial Patterns

Vegetation is the most spatially extensive source of disconnectivity, covering much of the watershed (Figure 26 and Table 3). It reduces the efficiency of sediment transfer by stabilizing sediment accumulations, increasing surface roughness, and reducing surface wash through increased infiltration. It is currently unclear how to quantify the effect of vegetation in creating disconnectivity.

Within the Tahoma Creek watershed, lakes fully disconnect upslope contributing areas from the downstream network. Lakes occur within the deglaciated cirques and parkland within upland areas and are a direct result of past glaciations. They disconnect approximately 2.14 km² or ~7% of the total area below the limit of contemporary glaciers.

Most sources of disconnectivity are concentrated along the valley margin or valley floor, often occurring at the boundary between process domains (Figure 7 and Figure 26). Valley margin landforms, such as debris fans and cones, mark the downslope location at which the gradient is no longer sufficiently steep to support runoff of colluvial processes. Yet these landforms are often well above the stage height of even the largest floods and rely on episodic bank erosion to access stored sediment. Valley floor landforms such as terraces and floodplains are extensive in the lower 8 km of channel resulting in near complete disconnectivity within the lower watershed. Terraces and floodplains disconnect approximately 34% and 23% of the watershed below glacial limits, respectively (Table 3).

One of the most intriguing results of mapping the spatial coverage of disconnectivity elements (Figure 26) is the general agreement with field-based estimations of inactive/active areas within the watershed, and with inefficiency/efficiency estimates. Areas that appear unaffected in Figure 26 (white) correspond to areas connected to the outlet and that actively contribute sediment. On the other hand, areas that are affected by one or more disconnectivity elements tend to be inactive and are not connected to the outlet. Disconnectivity elements are relatively easy to map in the field and using remote sensing techniques, and when paired with general flow routing to map upstream affected areas provides accurate and spatially resolved disconnectivity and

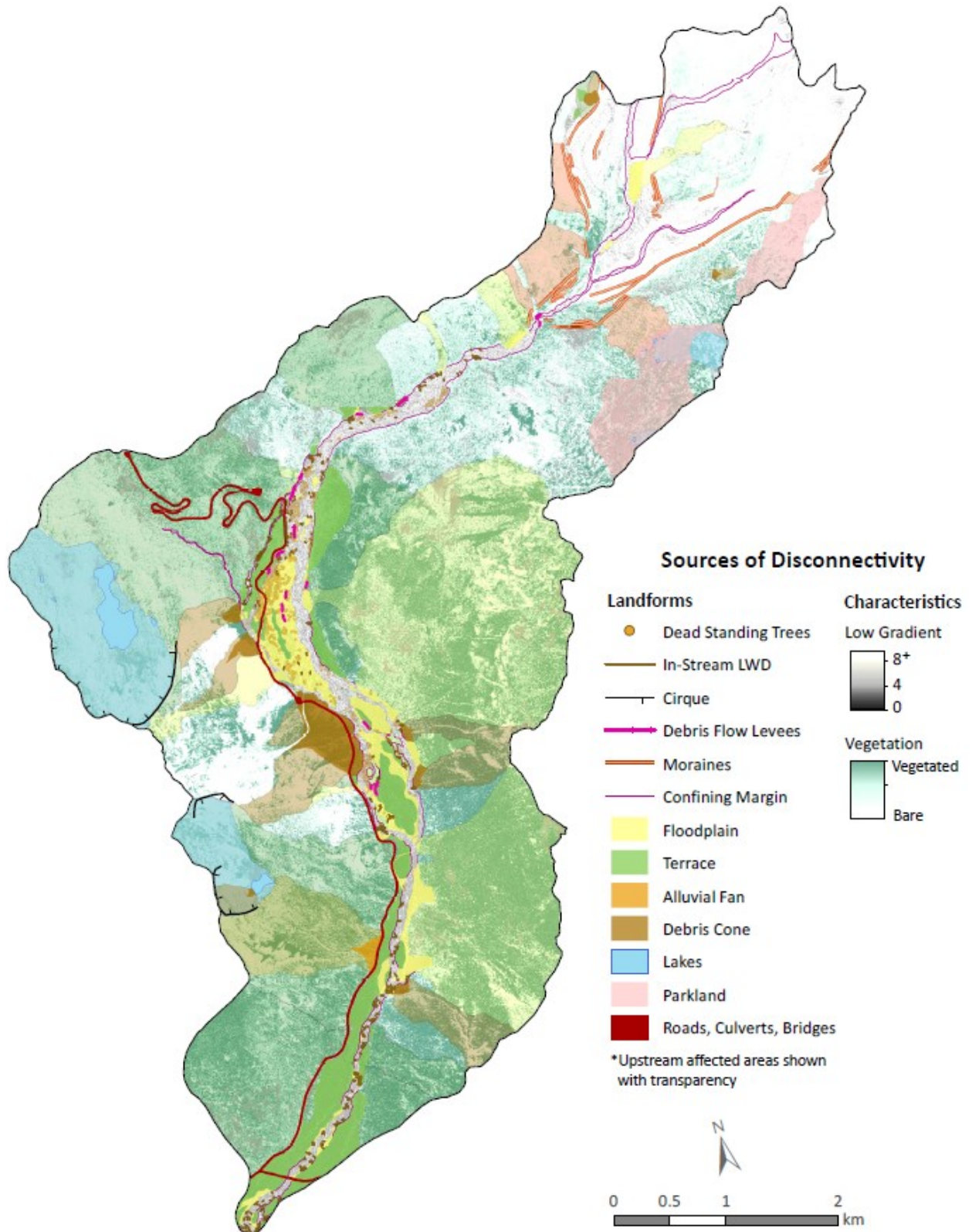


Figure 26. Map of disconnection elements and their upstream affected areas based on flow routing. The upstream affected areas are based on D8 flow routing and are displayed in the same colour as their associated landform with transparency added.

subsequently connectivity estimates. The spatial distribution of disconnectivity elements seems to control the spatial patterns of sediment transfers. Additionally, simple statistics, such as those shown in Table 3, aid in evaluating the importance of various sources of disconnectivity within the study area. Here, vegetation, terraces, and floodplains affect the largest proportion of the landscape, while lakes are more permanent sinks. An additional column populated with values for the trapping efficiency of each landform would be particularly useful. This information can then be compared to the postulated effective timescales (Table 1) of each disconnectivity element as will be discussed in the following paragraph.

Landform/ Characteristic	Coverage Area (km ²)	Upstream Affected Area (km ²)	Percent Total Area Affected
Terraces	1.39	9.7	34%
Floodplains	0.86	6.82	23%
Lakes	0.17	1.97	7%
Debris Cones	0.36	1.45	6%
Alluvial Fans	0.04	0.8	3%
Moraine Crests	NA	0.7	2%
Parkland	1.05	NA	3%
Vegetated*	~18.7	NA	57%
Slope < 8°	3.64	NA	11%
Slope < 4°	1.43	NA	4%
Slope < 2°	0.5	NA	2%
Total Area Below Glacier Limits	32.9	*based on manually verified NDVI value	

Table 3. Estimated spatial coverage values of selected sources of disconnectivity and their upstream affected areas.

5.1.2.6 Effective Timescales

The postulated effective timescales of individual landforms can be seen in Table 1. Buffers, which create lateral disconnectivity, are typically long term (hundreds to thousands of years) and are the result of landscape history and macroforms. During past glaciations, glaciers carved a wide valley bottom which was subsequently filled with paraglacial and laharc sediment. This sediment forms the contemporary valley bottom and valley transition landforms that contribute to long term disconnectivity. Floodplains are buffers that operate over much shorter timescales

(typically ~100 years by definition). During large flood events these buffers are breached, and upslope areas may be temporarily reconnected. As much as 23% of the watershed was temporarily reconnected during the three days encompassing the large 2006 flood event, although sediment availability in these areas is relatively low. The ability of other buffers to moderate sediment fluxes was likely reduced as a result of increased bank erosion.

Longitudinal disconnectivity is controlled by barriers, which typically evolve over human-timescales. They are generally the result of vegetation and the local morphology. The Tahoma Creek channel profile has adjusted relatively quickly (decadal-scale adjustments) following rapid glacier retreat. Anthropogenic structures such as bridges and culverts can be permanent until removed, although large events (i.e. 2006 flood) have destroyed them in the past. Grain size effects may be longer term, with debris flow deposition between RKM 8.5-4.5. The largest boulders are likely only mobilized during extreme floods, if at all. Valley constrictions are one exception to this trend. They are often the result of the landscape history and can persist for thousands of years.

Vertical connectivity, which is controlled by blankets, is the shortest-term form of connectivity. Depositional and erosional sequences occur within single events, and unless progressive deposition occurs, sediment is reworked readily within the active channel and floodplain.

5.2 Quantitative Connectivity Assessment

5.2.1 Landscape History and Hillslope-Channel Coupling

The importance of landscape history in controlling the spatial patterns of hillslope-channel coupling and process domains has been noted within the literature (Hassan et al., 2018; Brardinoni and Hassan, 2006 and 2007). Previous studies also note the importance of landscape history and morphological characteristics in controlling coarse sediment connectivity (Cavalli et al., 2013).

5.2.1.1 Landscape History

Numerous glaciations of varying intensity continuously shaped and reshaped the Tahoma Creek watershed. Today, remnant glaciers are restricted to the volcanic cone of Mount Rainier and are misfit to many of the macroforms. Parklands and cirques attest to glaciations that reached the uplands and breached valley divides. The contemporary channel carves and braids through massive glaciofluvial and paraglacial deposits in the wide valley floor.

The Tahoma Creek profile seems well-adjusted to fluvial processes, with very few deviations from a classic concave channel form (Figure 11). This is confirmed by applying the stream-gradient index proposed by Hack (1973) (Figure 13), and additionally by applying the slope-area method of delineating process domains (Figure 10). The slope-area plot of Tahoma Creek does not convincingly have any kinks or abrupt changes in slope that would suggest a transition between process domains. These methods were applied to elevation measurements from the 2008 DEM and therefore post-date the large 2006 flood event. Figure 11 highlights two convexities that existed within the profile in 2002 that were subsequently eroded before 2008. These channel adjustments likely occurred during the 2006 flood event and suggests that the profile rapidly adjusts as a result of large events. Walder and Driedger (1994a) note similar adjustments to the channel profile during large events. During the debris flows and floods of 1967, Tahoma Creek incised between 5-7 meters into bedrock just upstream of RKM 10, beginning the formation of a bedrock gorge. In 1992, Tahoma Creek further incised 15-20 meters in depth and width for a distance of 30-40 meters. Upstream near the glacier front, the river incised up to 40 meters into the glaciofluvial sediment. Additionally, the tributary stream draining the Tahoma Glacier has a planar profile and is approximately 40 meters higher than Tahoma Creek followed by a knickpoint at the confluence. Tahoma Creek has the necessary tools and energy to rapidly (decadal scale) adjust its profile, erasing the in-channel topographic signature of debris flows and past glaciations.

The stream-gradient values in Figure 13 peak within the zone of debris flow deposition, and may reflect slight adjustments to the channel gradient (steepening) in order to be able to transport the large volumes of coarse material supplied to this reach. The stream-gradient values may also be

an artifact of the scale over which the method was applied. We would expect greater variation with a finer resolution.

5.2.1.2 Hillslope - Channel Coupling

General patterns of hillslope-channel coupling often track with changing process domains (Brardinoni and Hassan, 2006). The influence of past glaciations is preserved in the topographic signature of tributaries draining cirques. These tributaries likely follow simple coupling-decoupling patterns, with colluvial channels coupled, and fluvial channels decoupled from the adjacent hillslopes. Coupling patterns along the mainstem cannot be explained in this same manner because it appears to be adjusted to fluvial processes along its entire length. Instead, we applied the method proposed by Whiting and Bradley (1993). This method estimates coupling in the upper 6 km of the channel and decoupling in the lower 8 km. One of the biggest simplifications of this method is that the lateral position of the channel within the valley floor is not taken into account.

5.2.2 Measures of Sediment Connectivity

5.2.2.1 ECA

Approximately only 15% of the catchment contributes sediment to the outlet based on field estimates and analysis of historical aerial imagery. The ECA was also delineated using GIS methods and applying several different slope thresholds and DEM resolutions. In comparing field-based estimations to GIS modeling results, a 5-meter DEM paired with an 8° slope threshold best performed. The 5-meter resolution DEM likely represents the best compromise between low-resolution DEMs that smooth over ‘real’ disconnections in the landscape, and high-resolution DEMs that contain many cell-level erroneous disconnections. The performance of a given DEM resolution likely varies in relation to catchment size. Lisenby et al. (2017) note that a 25-meter DEM best performed when applied to intermediate-sized (~ 61 to 530 km²) catchments.

The 5-meter DEM paired with an 8° slope threshold performed rather well both in terms of the specific locations and the total overall area that contributes sediment to the outlet. Discrepancies mainly occur in areas that are vegetated (Figure 26), which greatly reduces sediment transfer, but

are not accounted for using this method. Alternatively, ECA estimates based on incorrectly chosen slope thresholds or DEM resolutions greatly over- or underestimate (ranging from 0.5% - 75%) the total contributing area, highlighting the necessity of ground truthing in the field. In adopting the definition of coupling by Brunnsden and Thornes (1979) which views the linkage between two landscape compartments in end member terms, coupled or decoupled, the following can be said; the ECA method provides simplified estimates of sediment connectivity by analyzing assemblages of coupled landforms in relation to the outlet. The ECA only highlights the components that are coupled together in a continuous chain and reach the outlet, and when one link is decoupled, all upstream links are considered decoupled as well. While this information is useful, more detailed measures of connectivity assess the degree of coupling (i.e. efficiencies expressed between 0% - 100%) between the many components rather than viewing end-member values only.

Figure 27b presents an overlay of the ECA and hillslope-channel coupling. While it is true that a higher proportion of the hillslopes are included in the ECA where considered coupled, many exceptions exist. The main disagreement between the two methods seems to lie in the importance of the lateral positioning of the channel within the valley floor. The Whiting – Bradley method does not take it into account, while the ECA does. This is most apparent between RKM 3 - 4.5, where Tahoma Creek is pinned against the valley wall on either side of a large vegetated island. The island does not prevent hillslope sediments from entering the channel and so it should not be taken into account when calculating the valley bottom width. A simple adjustment could be made to the Whiting – Bradley method where coupling is calculated for river left and river right separately and only include the distance of the channel from the valley margin. Comparisons between the ECA and IC methods will be presented in the IC section of the discussion below.

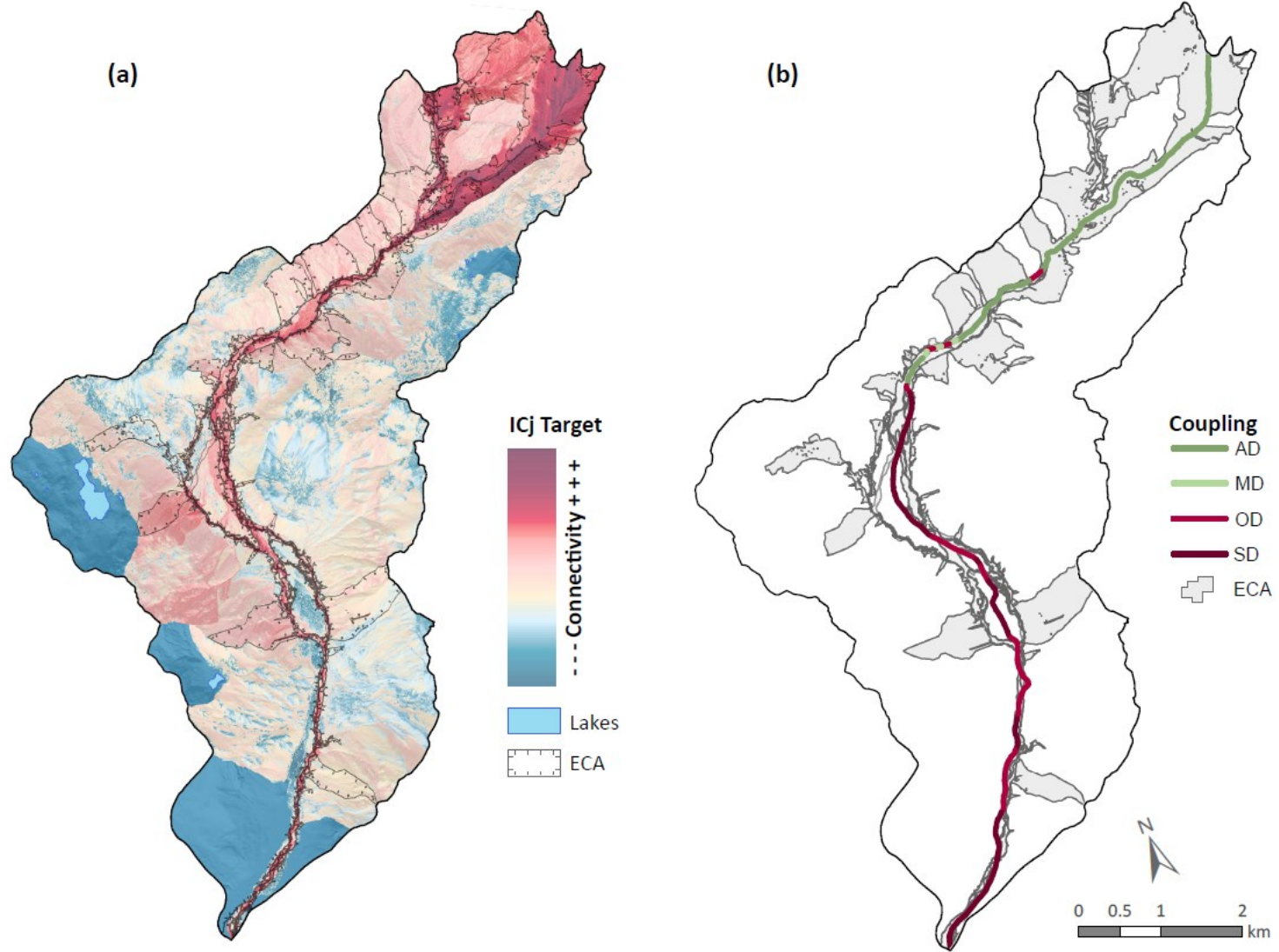


Figure 27. Overlay map of connectivity indices. (a) provides a comparison between IC and ECA results. (b) provides a comparison of hillslope-channel coupling and ECA results.

5.2.2.2 NSC and RF Indices

The network structural connectivity index assesses the role of network structure on sediment connectivity by abstracting the system as a digraph composed of nodes (i.e. sources, sinks) and edges (i.e. flow pathways) and applying graph theory tools (Cossart and Fressard, 2017). More specifically, the NSC index considers (i) the centrality of each node, emphasizing pathways in which the sources are near the outlet, and (ii) the potential flow of sediment through each node, emphasizing junction and other connector nodes. Cossart and Fressard (2017) note that nodes with high NSC values correspond to hotspots of geomorphic change or zones of sediment persistence where aggradation is likely to occur. These locations are likely to have a relatively higher impact on the sediment cascade than nodes with lower NSC values.

The Tahoma Creek watershed is narrow and elongate predominantly following the path of a single ice flow, resulting in a herringbone style network structure. Low-order channels directly enter the mainstem along its entire length resulting in a mainstem dominant pattern of connectivity (Walley et al., 2018). The Tahoma Creek digraph is highly fragmented with only 21% of nodes connected to the outlet (Figure 16). Fragmentation of the network is primarily due to buffers, barriers, and blankets. The NSC applied to this rather simple looking system identified a geomorphic hotspot along Fish Creek, near its confluence with the mainstem (~ RKM 5). This location is dynamic and has experienced aggradation and recent tree-kill. Air photo interpretation suggests that the recent and rapid geomorphic change in this area is more a result of the period of increased debris flow activity and flooding noted by Walder and Driedger (1994a and 1994b) that directly entered the mainstem, than a result of the network structure. For the scenario of near complete connectivity, the NSC index erroneously identified nodes near the outlet as hotspots of geomorphic change solely based on proximity.

The residual flow index, while closely related to the NSC, is a more robust method for identifying nodes that deviate from the simple linear relation between centrality and potential flow (Figure 17 and Figure 19). This is best illustrated in the results from the case assuming near complete connectivity (Figure 18). Interestingly, the RF method identifies a zone of sediment

persistence in virtually the same location between the two scenarios (Figure 16 and Figure 18). As stated before, while this location has also experienced progressive aggradation and rapid geomorphic change, it is difficult to attribute these changes to the network structure as opposed to process-specific controls. Within this zone, the valley floor becomes unconfined (see Figure 12) and the slope decreases to approximately 6° , causing debris flow deposition and subsequent channel migration (Benda and Cundy, 1990).

The NSC and RF indices seem to be the farthest removed methods of estimating connectivity from field observations, although they ‘happily’ identified areas of sediment persistence and intense geomorphic change. The method would likely be more applicable to systems with more complex network structures, and if edge weights based on transfer efficiencies measured in the field were used.

5.2.2.3 IC and IC_j

In this study, we calculated the IC using the open-source tool SedInConnect created by Crema and Cavalli (2018) by applying two different formulations of the weighting factor, (i) DEM-based measurement of surface roughness normalized by flow direction, and (ii) a joint weighting factor that includes the effect of vegetation following Ortiz-Rodriguez et al. (2017). This method results in cell-level estimations of structural connectivity based on topography, and in the case of IC_j also includes the effects of vegetation.

In comparing the results of the IC method to field observations general agreement exists for the broad spatial patterns of connectivity, but upon closer inspection many oddities are found. For example, it estimates lower connectivity values for the active floodplain than many of the adjacent hillslopes. Relying on DEM-based surface roughness and slope alone cannot accurately capture the dynamics and relative connectivity of valley trains. In this case the bouldery channel has high surface roughness and a low slope, resulting in low connectivity estimates (Figure 20). Additionally, the use of a pit-filled DEM for the flow routing inaccurately reconnects ‘real’ sinks in the landscape. This is best seen just north of the valley floor between RKM 10-10.5. Here, lateral moraines disrupt the sediment cascade by causing localized deposition of hillslope

sediment on the distal slope of the moraines. This is one of many examples in which sediment pathways are more fragmented and discontinuous than the flows transporting the sediment. The IC_j method further incorporates the influence of vegetation, and in so doing better captures the spatial pattern of connectivity (Figure 21). The main improvement is the increased values of relative connectivity within the active channel, proglacial zone, and dry creek rock fall area, and decreased values for hillslope locations that are densely forested. The predictive power of vegetation in this watershed likely stems from two sources, (i) vegetation is an important source of disconnectivity, and (ii) temperate rainforests revegetate quickly following disturbance and so the lack of vegetation often indicates appreciable recent geomorphic change and high connectivity. Although, since the floodplain is vegetated, it is still inaccurately represented as having low relative connectivity.

Figure 27a presents an overlay of the IC_j and ECA results. Generally, locations outlined by the ECA method align with higher values of IC_j . Discrepancies occur just south of Round Pass and river left near RKM 3 where the ECA overlies low IC_j values. Additionally, relatively high IC_j values at the base of Mount Wow were not identified by the ECA method. Many of these discrepancies are the result of considering vegetation in the IC_j method and not in the ECA method. This can be seen by visually comparing Figure 20 and Figure 27a. The IC , and IC_j methods also somewhat contradict with the Whiting-Bradley method, showing that the lateral position of the river within the valley bottom is important when considering hillslope-channel coupling (Figure 27).

5.2.2.4 SD SDR

The spatially distributed sediment delivery ratio method provides a quantitative measure of the functional connectivity. The method leverages DoD values and flow-routing to calculate the delivery ratio at each cell. It is an intriguing method because it is based on actual measures of the efficiency of sediment transfer (functional connectivity) as opposed to the potential efficiency (structural connectivity).

Many limitations are inherent within this method including the requirement of having a zero-flux upslope boundary. This limited the application of the SD SDR method to three small AOIs within the watershed, the first two within the proglacial zone, and the second a hillslope section near RKM 10. At this spatial scale, the SD SDR method measures connectivity within a single process domain, highlighting the variability at small spatial scales. The method requires two, high-resolution DEMs that are accurately co-referenced. Even small co-referencing errors are propagated along flow paths and can become significant. If the inter-survey period is too long or encompasses significant geomorphic change the flow pathways may be altered and result in unrealistic delivery ratios ($SDR < 0$ in a location with a zero-flux upslope boundary). On the other hand, if too little change occurs it is likely to be below the level of detection.

Between 2008 - 2002, all three AOIs exported much of the mobilized sediment, and as a result had relatively high SDR values (0.86 – 0.98). Much of the eroded material derived from the colluvial apron at the base of the lateral moraine (Figure 23). The colluvial apron is an intermediate storage site that is progressively filled during low-magnitude events through gullying, surface wash, and slumping, and subsequently released during large floods and debris flows. This process is highlighted in Figure 24, with the refilling of sediment stores previously emptied (Figure 23). This resulted in lower SDR values for AOIs 1 and 2, at 0.81 and 0.82, respectively. These values would likely be even lower if not for the much higher proportion of cells with supposed negative delivery ratios during this period (Table 2). Intense morphological change (up to 40m) including increased deposition likely greatly modified the flow pathways during the inter-survey period causing the spurious results. SDR values, while appearing to show clear downslope trends in Figure 23 and Figure 24, do not appear correlated to drainage area (Figure 31). Figure 31c is one exception to this rule, where the SDR increases in the downstream direction.

Chapter 6: Conclusions

In recognition of the need for generalized definitions of connectivity and disconnectivity (Wohl, 2018), and the lack thereof in the present literature, we suggest defining disconnectivity as the dominant but inefficient state of the system in transferring matter and/or energy within and between system components. Connectivity is then a special case within disconnectivity in which the efficient transfer of matter and/or energy occurs within the spatiotemporal scale of interest. Catchment scale sediment connectivity would then be the efficient transfer of sediment and/or energy within and between process domains within the spatiotemporal scale of interest.

Following the above definitions, we conducted a case study within the Tahoma Creek Watershed of Mount Rainier National Park, WA, in which we present fieldwork and historical data in the framework of a geomorphic map and conceptual sediment budget, map all sources of disconnectivity within the watershed, and perform a DEM analysis over a ten-year period. These analyses are then compared to methods of measuring the influence of landscape history and hillslope-channel coupling, followed by several semi-quantitative indices of connectivity. The three static indices applied (ECA, NSC, IC) each represent a broad category of connectivity indices (ECA-based, object/network-based, and raster-based, respectively) and the diverse applications of connectivity as a concept (Heckmann et al., 2018). Additionally, an index measuring functional connectivity (SD SDR) was applied.

Very few studies exist that provide comparisons between measures of connectivity, Nicoll and Brierley (2016) is one example, and to our knowledge, no studies compare indices from all three categories (both structural and functional) in relation to qualitative and quantitative field estimates. We recognize that each method approaches the quantification of connectivity in a different manner using a variety of proxy variables making comparisons difficult. For this reason, we compare between the spatial patterns of connectivity rather than absolute values. Our methods allowed us to address two main questions,

1. Does disconnectivity or connectivity control the spatial variability of sediment transfer within the Tahoma Creek watershed at Mount Rainier, WA?

2. How well do current methods of quantifying sediment connectivity describe the observed spatial patterns of sediment transfer.

6.1 Main Conclusions

The main findings of this study regarding the two research questions posed are:

1. The spatial distribution of sources of disconnectivity and their upslope affected areas explains the spatial patterns of sediment transfers and assumed transfer efficiencies within the watershed. Even locations with intense morphodynamics, such as Mount Rainier, are predominantly disconnected (spatially) at the human-timescale. This supports our definition of disconnectivity as the dominant but inefficient state of the landscape.
2. The methods of quantifying sediment connectivity all performed rather well within their own stated limitations and inherent resolution, although discrepancies exist. The main sources of error result from inaccurately modeling runoff pathways (predominantly within the wide valley floor) and overlooking the effects of vegetation.

The IC method provided the most detailed assessment of structural connectivity, and generally aligned with field-based estimations when accounting for vegetation. The ECA, while the simplest method, provided reasonable results given that DEM resolution and slope thresholds are chosen based on fieldwork. The NSC method is the most removed from fieldwork estimations of connectivity but correctly identified zones of sediment persistence.

6.2 General Conclusions

Since the LIA, the extent of glaciation within the watershed has declined from ~20% to ~11% today. Slope-Area plots clearly show the influence of yet older glaciations within the confines of relict cirques, while the mainstem channel appears to be fully adjusted to contemporary fluvial processes. These adjustments occurred rapidly (~20 to 30 years after ice retreat) as a result of outburst floods and debris flows, while the adjacent tributary draining the Tahoma Glacier has not yet adjusted its profile. Hillslope-channel coupling estimates based on the method proposed by Whiting and Bradley (1983) generally match fieldwork evidence; where the uppermost 6 km of channel are coupled to the hillslopes, and the lowermost 7 km are decoupled.

The effective catchment area reflects this same general pattern, with approximately only 15% of the watershed supplying sediment to the outlet. The ECA mainly encompasses the proglacial zone, contemporary floodplain, and active channel with limited contributions from hillslopes. DEM-based ECA delineations using a 5-meter resolution DEM and applying an eight-degree slope threshold produced a quick first-order estimate of sediment connectivity that roughly matched fieldwork evidence. The main discrepancies between GIS-modeled ECA estimates and field-based estimates are likely a result of vegetation. GIS-modeled ECA estimates applying previously published DEM resolutions and slope thresholds were inaccurate.

The index of connectivity method was also applied using 1-meter LiDAR, and best performed when calculating a joint weighting factor that accounted for both topographic roughness and the effect of vegetation. Vegetation plays an important role in decreasing the efficiency of sediment transfer within the watershed and provides a lot of predictive power in distinguishing between areas dominated by connectivity and disconnectivity. Major limitations arise from the incorrect weighting of vegetation and surface roughness within the weight factor.

The network structural connectivity and subsequent residual flow methods are the most removed from field observations, although the method identified hotspots within the system that correspond to areas of deposition (sediment-choked areas). The applicability of the method is reduced by the simplicity of the Tahoma Creek digraph which is fragmented by numerous sources of disconnectivity. The method could be improved upon and better grounded in physical observations if edge weights corresponding to transfer efficiencies were used.

Finally, the application of the SD SDR method was limited to small hillslope areas due to data limitations. The results suggested higher functional connectivity values during a period encompassing a large flood event in addition to a volumetric increase in sediment transfer. The intense morphodynamics and subsequent rearrangement of transfer pathways during the inter-survey period resulted in increased uncertainty and a higher proportion of unrealistic SDR values.

Sources of disconnectivity are easily mapped in the field or using remote sensing techniques and explain the spatial patterns in sediment dynamics and the assumed transfer efficiencies. In this study we added several sources of disconnectivity, mainly glacial in origin, to the seminal work by Fryirs et al. (2007a), and suggest greater focus be placed on the issue within geomorphology. Most applications of connectivity indices are mainly conceptual and rely on minimal ground-truthing. Here we mapped both connectivity and disconnectivity by identifying common sediment transfer pathways and sources of disconnectivity in the field, respectively.

Future sediment disconnectivity and connectivity research could greatly benefit from being more grounded in physical observations and measurements and placing more emphasis on disconnectivity. We suggest the integration of sources of disconnectivity within connectivity indices or the creation of an index of disconnectivity. The use of trapping efficiencies in spatially explicit models may present an avenue for future research. Graph theory might provide the necessary mathematical framework for such an application.

References

- Anderson, S. (2013). Sediment fluxes in a changing climate: Tahoma Creek over daily to centennial time-scales (Unpublished Master's Thesis). University of Colorado at Boulder, Boulder, Colorado.
- Anderson, S., & Pitlick, J. (2014). Using repeat lidar to estimate sediment transport in a steep stream. *Journal of Geophysical Research: Earth Surface*, 621–643. <https://doi.org/10.1002/2013JF002933>.
- Beason, S. (2017). Change in Glacial Extent at Mount Rainier National Park from 1896 to 2015. Natural Resource Report NPS/MORA/NRR-2017/1472, 98. <http://www.morageology.com/pubs/12.pdf>
- Beason, S. R., Legg, N. T., Kenyon, T. R., Jost, R. P., & Kennard, P. M. (2019). Forecasting and seismic detection of debris flows in pro-glacial rivers at Mount Rainier National Park, Washington, USA. 7th International Conference on Debris-Flow Hazards Mitigation.
- Beason, S.R. (2020). Mount Rainier Geology and Weather (morageology.com): Known Mount Rainier Geologic Events [Online]. <http://www.morageology.com/geoEvent.php>.
- Benda, L. E., & Cundy, T. W. (1990). Predicting deposition of debris flows in mountain channels. *Canadian Geotechnical Journal*, 27(4), 409–417. <https://doi.org/10.1139/t90-057>
- Benda, L., Andras, K., Miller, D., & Bigelow, P. (2004). Confluence effects in rivers: Interactions of basin scale, network geometry, and disturbance regimes. *Water Resources Research*, 40, 1–15. <https://doi.org/10.1029/2003WR002583>
- Bennett, G. (2004). Integrating Biodiversity Conservation and Sustainable Use: Lessons Learned from Ecological Networks. IUCN, Gland, Switzerland, and Cambridge, UK. vi + 55 pp.
- Borselli, L., Cassi, P., & Torri, D. (2008). Prolegomena to sediment and flow connectivity in the landscape: A GIS and field numerical assessment. *Catena*, 75(3), 268–277. <https://doi.org/10.1016/j.catena.2008.07.006>
- Bracken, L. J., & Croke, J. (2007). The Concept of Hydrological Connectivity and its Contribution to Understanding Runoff-Dominated Geomorphic Systems. *Hydrological Processes*, 21, 1749–1763. <https://doi.org/10.1002/hyp.6313>
- Bracken, L. J., Wainwright, J., Ali, G. A., Tetzlaff, D., Smith, M. W., Reaney, S. M., & Roy, A. G. (2013). Concepts of hydrological connectivity: Research approaches, Pathways and future agendas. *Earth-Science Reviews*, 119, 17–34. <https://doi.org/10.1016/j.earscirev.2013.02.001>

- Bracken, L. J., Turnbull, L., Wainwright, J., & Bogaart, P. (2015). Sediment connectivity: A framework for understanding sediment transfer at multiple scales. *Earth Surface Processes and Landforms*, 40(2), 177–188. <https://doi.org/10.1002/esp.3635>
- Brardinoni, F., & Hassan, M. A. (2006). Glacial erosion, evolution of river long profiles, and the organization of process domains in mountain drainage basins of coastal British Columbia. *Journal of Geophysical Research*, 111(F1), F01013. <https://doi.org/10.1029/2005JF000358>
- Brardinoni, F., & Hassan, M. A. (2007). Glacially induced organization of channel-reach morphology in mountain streams. *Journal of Geophysical Research: Earth Surface*. <https://doi.org/10.1029/2006JF000741>
- Brierley, G., Fryirs, K. A., & Jain, V. (2006). Landscape connectivity: The geographic basis of geomorphic applications. *Area*, 38(2), 165–174. <https://doi.org/10.1111/j.1475-4762.2006.00671.x>
- Brunsdon, D., & Thornes, J. (1979). Landscape Sensitivity and Change. *Transactions of the Institute of British Geographers*, 4(4), 463-484. doi:10.2307/622210
- Cantreul, V., Bièlders, C., Calsamiglia, A., & Degré, A. (2018). How pixel size affects a sediment connectivity index in central Belgium. *Earth Surface Processes and Landforms*, 43(4), 884–893. <https://doi.org/10.1002/esp.4295>
- Carrivick, J. L., & Heckmann, T. (2017). Short-term geomorphological evolution of proglacial systems. *Geomorphology*, 287, 3–28. <https://doi.org/10.1016/j.geomorph.2017.01.037>
- Cavalli, M., Trevisani, S., Comiti, F., & Marchi, L. (2013). Geomorphometric assessment of spatial sediment connectivity in small Alpine catchments. *Geomorphology*, 188, 31–41. <https://doi.org/10.1016/j.geomorph.2012.05.007>
- Chorley, R. J., & Kennedy, B. A. (1971). *Physical geography: a systems approach*. Prentice Hall.
- Church, M., & Ryder, J. M. (1972). Paraglacial Sedimentation: A Consideration of Fluvial Processes Conditioned by Glaciation. *Geological Society of America Bulletin*, 83, 3059–3072.
- Church, M., & Slaymaker, O. (1989). Disequilibrium of Holocene sediment yield in glaciated British Columbia. *Nature*, 337(6206), 452–454. <https://doi.org/10.1038/337452a0>
- Church, M. (2010). The trajectory of geomorphology. *Progress in Physical Geography*, 34(3), 265–286. <https://doi.org/10.1177/0309133310363992>

- Conrad, O., Bechtel, B., Bock, M., Dietrich, H., Fischer, E., Gerlitz, L., Wehberg, J., Wichmann, V., and Böhner, J. (2015): System for Automated Geoscientific Analyses (SAGA) v. 2.1.4, *Geosci. Model Dev.*, 8, 1991-2007, doi:10.5194/gmd-8-1991-2015
- Copeland, E. A. (2009). Recent Periglacial Debris Flows from Mount Rainier, Washington (Unpublished Master's Thesis). Oregon State University, Corvallis, Oregon.
- Cossart, É. (2008). Landform connectivity and waves of negative feedbacks during the paraglacial period, a case study: the Tabuc subcatchment since the end of the Little Ice Age (massif des Écrins, France). *Géomorphologie: Relief, Processus, Environnement*, 4, 249–260. <https://doi.org/10.4000/geomorphologie.7430>
- Cossart, É., & Fressard, M. (2017). Assessment of structural sediment connectivity within catchments: insights from graph theory. *Earth Surf. Dynam*, 5, 253–268. <https://doi.org/10.5194/esurf-5-253-2017>
- Cowie, N. M., Moore, R. D., & Hassan, M. A. (2014). Effects of glacial retreat on proglacial streams and riparian zones in the Coast and North Cascade Mountains. *Earth Surface Processes and Landforms*. <https://doi.org/10.1002/esp.3453>
- Csardi G, Nepusz T. (2006). The igraph software package for complex network research, *InterJournal, Complex Systems* 1695. <http://igraph.org>
- Crandell, D. R. (1971). Postglacial lahars from Mount Rainier Volcano, Washington. U. S. Geological Survey Professional Paper, 667, 80.
- Crandell, D. R., & Miller, R. D. (1974). Quaternary stratigraphy and extent of glaciation in the Mount Rainier region, Washington. U. S. Geological Survey Professional Paper, 59.
- Crema, S., & Cavalli, M. (2018). SedInConnect: a stand-alone, free and open source tool for the assessment of sediment connectivity. *Computers and Geosciences*, 111(September 2017), 39–45. <https://doi.org/10.1016/j.cageo.2017.10.009>
- Croke, J., Fryirs, K., & Thompson, C. (2013). Channel-floodplain connectivity during an extreme flood event: Implications for sediment erosion, deposition, and delivery. *Earth Surface Processes and Landforms*, 38(12), 1444–1456. <https://doi.org/10.1002/esp.3430>
- Curry, A. M., Sands, T. B., & Porter, P. R. (2009). Geotechnical controls on a steep lateral moraine undergoing paraglacial slope adjustment. *Geological Society, London, Special Publications*, 320(1), 181–197. <https://doi.org/10.1144/SP320.12>
- Czuba, J. A., & Fofoula-Georgiou, E. (2015). Dynamic connectivity in a fluvial network for identifying hotspots of geomorphic change. *Water Resources Research*, 51(3), 1401–1421. <https://doi.org/10.1002/2014WR016139>

- Delaney, I., Bauder, A., Huss, M., & Weidmann, Y. (2018). Proglacial erosion rates and processes in a glacierized catchment in the Swiss Alps. *Earth Surface Processes and Landforms*, 43(4), 765–778. <https://doi.org/10.1002/esp.4239>
- Dell’Agnese, A., Brardinoni, F., Toro, M., Mao, L., Engel, M., & Comiti, F. (2015). Bedload transport in a formerly glaciated mountain catchment constrained by particle tracking. *Earth Surface Dynamics*, 3(4), 527–542. <https://doi.org/10.5194/esurf-3-527-2015>
- Delong, S. B., Prentice, C. S., Hilley, G. E., & Ebert, Y. (2012). Multitemporal ALSM change detection, sediment delivery, and process mapping at an active earthflow. *Earth Surface Processes and Landforms*, 37(3), 262–272. <https://doi.org/10.1002/esp.2234>
- Dietrich, W. E., Dunne, T., Humphrey, N. F., & Reid, L. M. (1982). Construction of Sediment Budgets for Drainage Basins. In F. J. Swanson, R. J. Janda, Thomas Dunne, & D. N. Swanson (Eds.), *Sediment budgets and routing in forested drainage basins* (pp. 5–23). Pacific Northwest Forest and Range Experiment Station, General Technical Report PNW-141.
- ESRI 2011. *ArcGIS Desktop: Release 10*. Redlands, CA: Environmental Systems Research Institute.
- Fiske, R. S., Hopson, C. A., & Waters, A. C. (1963). *Geology of Mount Rainier National Park, Washington*. Geological Survey Professional Paper, 444.
- Foerster, S., Wilczok, C., Brosinsky, A., & Segl, K. (2014). Assessment of sediment connectivity from vegetation cover and topography using remotely sensed data in a dryland catchment in the Spanish Pyrenees. *Journal of Soils and Sediments*, 14(12), 1982–2000. <https://doi.org/10.1007/s11368-014-0992-3>
- Fressard, M., & Cossart, É. (2019). A graph theory tool for assessing structural sediment connectivity: Development and application in the Mercurey vineyards (France). *Science of the Total Environment*, 651, 2566–2584. <https://doi.org/10.1016/j.scitotenv.2018.10.158>
- Fryirs, K. A., Brierley, G. J., Preston, N. J., & Kasai, M. (2007). Buffers, barriers and blankets: The (dis)connectivity of catchment-scale sediment cascades. *Catena*, 70(1), 49–67. <https://doi.org/10.1016/j.catena.2006.07.007>
- Fryirs, K. A., Brierley, G. J., Preston, N. J., & Spencer, J. (2007). Catchment-scale (dis)connectivity in sediment flux in the upper Hunter catchment, New South Wales, Australia. *Geomorphology*, 84(3–4), 297–316. <https://doi.org/10.1016/j.geomorph.2006.01.044>

- Fryirs, K. A. (2013). (Dis)Connectivity in catchment sediment cascades: A fresh look at the sediment delivery problem. *Earth Surface Processes and Landforms*, 38(1), 30–46. <https://doi.org/10.1002/esp.3242>
- Geilhausen, M., Morche, D., Otto, J.-C., & Schrott, L. (2013). Sediment discharge from the proglacial zone of a retreating Alpine glacier. *Zeitschrift Fur Geomorphologie*, 57, 29–53. <https://pd.zhaw.ch/publikation/upload/205383.pdf>
- Graham, J. 2005. Mount Rainier National Park Geologic Resource Evaluation Report. Natural Resource Report NPS/NRPC/GRD/NRR—2005/007. National Park Service, Denver, Colorado.
- Gran, K. B., & Czuba, J. A. (2017). Sediment pulse evolution and the role of network structure. *Geomorphology*, 277, 17–30. <https://doi.org/10.1016/j.geomorph.2015.12.015>
- Grant, G. E., O'Connor, J., & Safran, E. (2017). Excursions in fluvial (dis)continuity. *Geomorphology*, 277, 145–153. <https://doi.org/10.1016/j.geomorph.2016.08.033>
- Hack, J. T. (1973). Stream-profile analysis and stream-gradient index. *Journal of Research of the U.S. Geological Survey*, 1(4), 421–429.
- Harvey, A. M. (2001). Coupling between hillslopes and channels in upland fluvial systems: implications for landscape sensitivity, illustrated from the Howgill Fells, northwest England. *CATENA*, 42, 225–250. [https://doi.org/10.1016/S0341-8162\(00\)00139-9](https://doi.org/10.1016/S0341-8162(00)00139-9)
- Harvey, A. M. (2002). Effective timescales of coupling within fluvial systems. *Geomorphology*, 44(3–4), 175–201. [https://doi.org/10.1016/S0169-555X\(01\)00174-X](https://doi.org/10.1016/S0169-555X(01)00174-X)
- Hassan, M. A., Bird, S., Reid, D., Ferrer-Boix, C., Hogan, D., Brardinoni, F., & Chartrand, S. (2018). Variable hillslope-channel coupling and channel characteristics of forested mountain streams in glaciated landscapes. *Earth Surface Processes and Landforms*, 16. <https://doi.org/10.1002/esp.4527>
- Heckmann, T., & Schwanghart, W. (2013). Geomorphic coupling and sediment connectivity in an alpine catchment - Exploring sediment cascades using graph theory. *Geomorphology*, 182, 89–103. <https://doi.org/10.1016/j.geomorph.2012.10.033>
- Heckmann, T., Mccoll, S., & Morche, D. (2016). Retreating ice: Research in pro-glacial areas matters. *Earth Surface Processes and Landforms*, 41, 271–276. <https://doi.org/10.1002/esp.3858>
- Heckmann, T., Cavalli, M., Cerdan, O., Foerster, S., Javaux, M., Lode, E., Smetanová, A., Vericat, D., & Brardinoni, F. (2018). Indices of sediment connectivity: opportunities, challenges and limitations. *Earth-Science Reviews*, 187(December 2017), 77–108. <https://doi.org/10.1016/j.earscirev.2018.08.004>

- Heckmann, T., & Vericat, D. (2018). Computing spatially distributed sediment delivery ratios: inferring functional sediment connectivity from repeat high-resolution digital elevation models. *Earth Surface Processes and Landforms*, 43(7), 1547–1554.
<https://doi.org/10.1002/esp.4334>
- Heine, J. T. (1998). Extent, timing, and climatic implications of glacier advances Mount Rainier, Washington, U.S.A., at the pleistocene/holocene transition. *Quaternary Science Reviews*, 17(12), 1139–1148. [https://doi.org/10.1016/S0277-3791\(97\)00077-2](https://doi.org/10.1016/S0277-3791(97)00077-2)
- Hilger, L. (2017). Quantification and regionalization of geomorphic processes using spatial models and high-resolution topographic data: A sediment budget of the Upper Kauner Valley (Unpublished Doctoral Dissertation). Katholische Universitat, Germany.
- Hoffmann, T. (2015). Sediment residence time and connectivity in non-equilibrium and transient geomorphic systems. *Earth-Science Reviews*, 150, 609–627.
<https://doi.org/10.1016/j.earscirev.2015.07.008>
- Hooke, J. M. (2003). Coarse sediment connectivity in river channel systems: A conceptual framework and methodology. *Geomorphology*, 56(1–2), 79–94.
[https://doi.org/10.1016/S0169-555X\(03\)00047-3](https://doi.org/10.1016/S0169-555X(03)00047-3)
- Horton, R.E. 1945: Erosional development of streams and their drainage basins: hydrophysical approach to quantitative morphology. *Geological Society of America Bulletin* 56, 275–370.
- Ikeya, H. (1981): A method of designation for area in danger of debris flow, Erosion and Sediment Transport in Pacific Rim Steeplands. I.A.H.S. publ. No.132, pp. 576-578.
- Jordan, P., & Slaymaker, O. (1991). Holocene Sediment Production in Lillooet River Basin, British Columbia: A Sediment Budget Approach. *Géographie Physique et Quaternaire*, 45(1), 45. <https://doi.org/10.7202/032844ar>
- Lane, S. N., Bakker, M., Gabbud, C., Micheletti, N., & Saugy, J.-N. (2017). Sediment export, transient landscape response and catchment-scale connectivity following rapid climate warming and Alpine glacier recession. 210–227.
<https://doi.org/10.1016/j.geomorph.2016.02.015>
- Leenman, A., & Tunnicliffe, J. (2020). Tributary-junction fans as buffers in the sediment cascade: a multi-decadal study. *Earth Surface Processes and Landforms*, 45(2), 265–279.
<https://doi.org/10.1002/esp.4717>
- Legg, N. T., Meigs, A. J., Grant, G. E., & Kennard, P. (2014). Debris flow initiation in proglacial gullies on Mount Rainier, Washington. *Geomorphology*, 226, 249–260.
<https://doi.org/10.1016/j.geomorph.2014.08.003>

- Lisenby, P. E., & Fryirs, K. A. (2017). 'Out with the Old?' Why coarse spatial datasets are still useful for catchment-scale investigations of sediment (dis)connectivity. *Earth Surface Processes and Landforms*, 42(10), 1588–1596. <https://doi.org/10.1002/esp.4131>
- Micheletti, N., & Lane, S. N. (2016). Water yield and sediment export in small, partially glaciated Alpine watersheds in a warming climate. *Water Resources Research*, 52(51), 5974–5997. <https://doi.org/10.1002/2016WR018977>.Received
- Montgomery, D. R., & Foufoula-Georgiou, E. (1993). Channel Network Source Representation Using Digital Elevation Models. *Water Resources Research*, 29(12), 3925–3934.
- Morche, D., Schuchardt, A., Dubberke, K., & Baewert, H. (2015). Channel morphodynamics on a small proglacial braid plain (Fagge River, Gepatschferner, Austria). *Proceedings of the International Association of Hydrological Sciences*, 367, 109–116. <https://doi.org/10.5194/piahs-367-109-2015>
- Nicholas, A. P., Ashworth, P. J., Kirkby, M. J., Macklin, M. G., & Murray, T. (1995). Sediment slugs: Large-scale fluctuations in fluvial sediment transport rates and storage volumes. *Progress in Physical Geography*, 19(4), 500–519. <https://doi.org/10.1177/030913339501900404>
- Nicoll, T., & Brierley, G. (2016). Within-catchment variability in landscape connectivity measures in the Garang catchment, upper Yellow River. *Geomorphology*, 277, 197–209. <https://doi.org/10.1016/j.geomorph.2016.03.014>
- Ortiz-Rodríguez, A. J., Borselli, L., & Sarocchi, D. (2017). Flow connectivity in active volcanic areas: Use of index of connectivity in the assessment of lateral flow contribution to main streams. *Catena*, 157(October), 90–111. <https://doi.org/10.1016/j.catena.2017.05.009>
- Pelletier, J. D., & Orem, C. A. (2014). How do sediment yields from post-wildfire debris-laden flows depend on terrain slope, soil burn severity class, and drainage basin area? Insights from airborne-LiDAR change detection. *Earth Surface Processes and Landforms*, 39, 1822–1832. <https://doi.org/10.1002/esp.3570>
- Poepl, R. E., & Parsons, A. J. (2018). The geomorphic cell: a basis for studying connectivity. *Earth Surface Processes and Landforms*, 43(5), 1155–1159. <https://doi.org/10.1002/esp.4300>
- R Core Team (2013). R: A language and environment for statistical computing. R Foundation for Statistical Computing, Vienna, Austria. URL <http://www.R-project.org/>
- Richardson, D. (1968). Glacier Outburst Floods in the Pacific Northwest. U. S. Geological Survey Professional Paper, 600-D, D79–D86.

- Riedel, J., and S. Dorsch. 2016. Geomorphology of Mount Rainier: Landform mapping at Mount Rainier National Park, Washington. Natural Resource Report NPS/MORA/NRR—2016/1234. National Park Service, Fort Collins, Colorado.
- Scott, K. M., J. W. Vallance, P. T. Pringle, Sedimentology, behavior, and hazards of debris flows at Mount Rainier, Washington, U.S. Geol. Surv. Prof. Pap., 1547, 56, 1995.
- Schumm, S. A., & Lichty, R. W. (1965). Time, Space, and Causality in Geomorphology. *American Journal of Science*, 263, 110–119.
- Schumm, S. A. (1979). Geomorphic thresholds: the concept and its applications. *Transactions of the Institute of British Geographers*, 485–515.
- Sigafoos, R. S., & Hendricks, E. L. (1972). Recent Activity of Glaciers of Mount Rainier, Washington.
- Slaymaker, O., Souch, C., Menounos, B., & Filippelli, G. (2003). Advances in Holocene mountain geomorphology inspired by sediment budget methodology. *Geomorphology*, 55(1–4), 305–316. [https://doi.org/10.1016/S0169-555X\(03\)00146-6](https://doi.org/10.1016/S0169-555X(03)00146-6)
- Slaymaker, O. (2004). Mass balances of sediments, solutes and nutrients: The need for greater integration. *Journal of Coastal Research, SPEC. ISS. 43*, 109–123.
- Slaymaker, O., Clague, J. J., Gilbert, R., Friele, P. A. Jordan, P., Menounos, B., Schiefer, E. (2017). Lillooet-Harrison Drainage Basin: Variable Landscapes Within the Coast Mountains. In O. Slaymaker (Ed.), *Landscapes and Landforms of Western Canada* (pp. 303-320). Springer Nature.
- Slaymaker, O., & Embleton-Hamann, C. (2018). Advances in global mountain geomorphology. *Geomorphology*, 308, 230–264. <https://doi.org/10.1016/j.geomorph.2018.02.016>
- Staines, K. E. H., Carrivick, J. L., Tweed, F. S., Evans, A. J., Russell, A. J., Jóhannesson, T., & Roberts, M. (2015). A multi-dimensional analysis of pro-glacial landscape change at Sólheimajökull, Southern Iceland. *Earth Surface Processes and Landforms*, 40(6), 809–822. <https://doi.org/10.1002/esp.3662>
- Strahler, A.N. 1950: Equilibrium theory of erosional slopes approached by frequency distribution analysis. *American Journal of Science* 248, 673–96, 800–14.
- Strahler, A.N. 1952: Dynamic basis of geomorphology. *Geological Society of America Bulletin* 63, 923–37.
- Tarboton, D. G. (1997). A new method for the determination of flow directions and upslope area in grid digital elevation models. *Water Resources Research*, 33(2), 309–319.

- Thomas, M. A. and P. Kennard. 2015. Topographic and hydrologic insight for the Westside Road problem: Mount Rainier National Park. Natural Resource Report NPS/MORA/NRR—2015/1057. National Park Service, Fort Collins, Colorado.
- Trevisani, S., & Cavalli, M. (2016). Topography-based flow-directional roughness: Potential and challenges. *Earth Surface Dynamics*, 4(2), 343–358. <https://doi.org/10.5194/esurf-4-343-2016>
- Walder, J. S., & Driedger, C. L. (1994). Rapid Geomorphic Change Caused by Glacial Outburst Floods and Debris Flows along Tahoma Creek, Mount Rainier, Washington, U.S.A. *Arctic and Alpine Research*, 26(4), 319–327.
- Walder, J. S., & Driedger, C. L. (1994). Geomorphic Change Caused by Outburst Floods and Debris Flows at Mount Rainier, Washington, with Emphasis on Tahoma Creek Valley. *Water-Resources Investigations Report*, 93–4093.
- Walder, J. S., & Driedger, C. L. (1995). Frequent outburst floods from South Tahoma Glacier, Mount Rainier, USA: relation to debris flows, meteorological origin, and implications for subglacial hydrology. *Journal of Glaciology*, 41(137), 1–10. <https://doi.org/10.1017/S0022143000017718>
- Walker, M. 2005: Quaternary dating methods. Chichester: Wiley, 286 pp.
- Walley, Y., Tunnicliffe, J., & Brierley, G. (2018). The influence of network structure upon sediment routing in two disturbed catchments, East Cape, New Zealand. *Geomorphology*, 307, 38–49.
- Walling, D. E., & Collins, A. L. (2008). The catchment sediment budget as a management tool. *Environmental Science and Policy*, 11(2), 136–143. <https://doi.org/10.1016/j.envsci.2007.10.004>
- Whiting, P. J., & Bradley, J. B. (1993). A Process-Based Classification System for Headwater Streams. *Earth Surface Processes and Landforms*, 18, 603–612.
- Wohl, E. E. (2017). Connectivity in rivers. *Progress in Physical Geography*, 41(3), 345–362. <https://doi.org/10.1177/0309133317714972>
- Wohl, E. E., Brierley, G., Cadol, D., Coulthard, T. J., Covino, T., Fryirs, K. A., Grant, G., Hilton, R. G., Lane, S. N., Magilligan, F. J., Meitzen, K. M., Passalacqua, P., Poepl, R. E., Rathburn, S. L., & Sklar, L. S. (2018). Connectivity as an emergent property of geomorphic systems. *Earth Surface Processes and Landforms*. <https://doi.org/10.1002/esp.4434>
- Wolman, M. G., & Miller, J. P. (1960). Magnitude and Frequency of Forces in Geomorphic Processes. *The Journal of Geology*, 68(1), 54–74. <http://www.jstor.com/stable/30058255>

Appendices

Appendix 1: DEM Co-referencing and Uncertainty

A.1: Co-referencing

In performing the DEM analysis, including co-referencing, and calculating uncertainty, we followed methods by Anderson and Pitlick (2014) who used the same datasets for similar purposes. The general steps we took for co-referencing are:

1. Project all DEMs to the same horizontal (NAD_1983_UTM_Zone_10N) and vertical datums (NAVD_1988).
2. Convert to orthometric elevations using GEOID03
3. Snap and resample the 2002 and 2012 datasets to the 2008 grid. Since we only needed relative values, we chose 2008 as the baseline.
4. Create DoDs by subtracting DEMs from later years from the previous year (i.e. 2008 – 2002). This ensures that deposition is represented by positive values.
5. Identify geomorphically stable locations covered by all datasets. In our case, the Westside road was chosen.
6. Perform a terrain-matching technique by graphing apparent change as a function of aspect. If systematic errors exist, they will show up as a sinusoid in the graph, with the peak and troughs indicating the direction of offset (Figure 28).
7. Adjust for horizontal offsets based on the previous step. In our case we identified offsets on the order of ~ 9 cm.
8. Adjust for vertical offsets by comparing elevations along the Westside road (Figure 29). In our case we found vertical offsets on the order of ~ 4 cm.

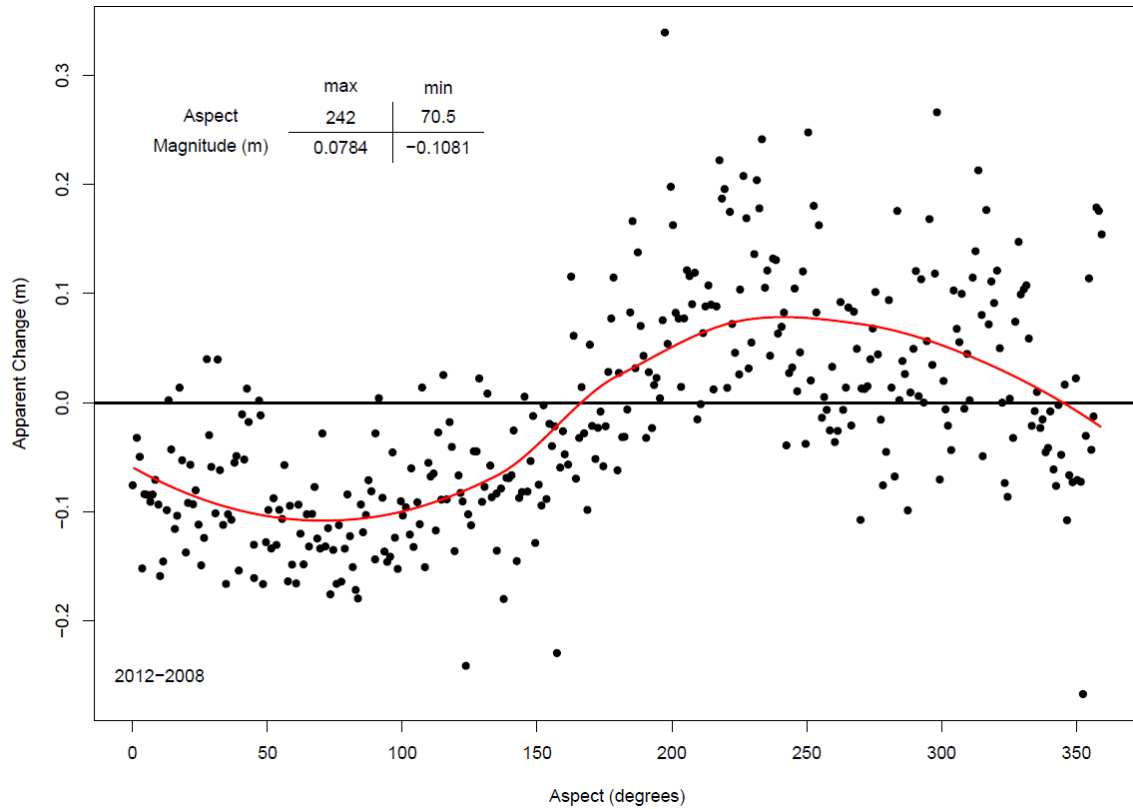


Figure 28. Graph of apparent change by aspect when performing a terrain-matching technique.

A.2: Uncertainty Estimates

Spatially Variable Uncertainty

The spatially variable uncertainty (σ_{sv}), was estimated by calculating the standard deviation of unresolved errors between the 2002 and 2012 road surfaces. In our case, σ_{sv} was roughly 0.08 for both time periods, and it was conservatively increased to 0.3 m, consistent with values from Anderson and Pitlick (2014). Note that areas with greater topographic complexity may fall outside of this estimate. The equation for calculating the spatially variable uncertainty of a given area is,

$$\sigma_{sv}\sqrt{n}$$

where n is the area of interest in m^2 . In most cases, where the area of interest is large, the uncertainty contribution from spatially variable errors is negligible and is not included within the calculations. Of course, this is only true if the errors are assumed to be normally distributed.

Vertical Datum Uncertainty

The vertical datum uncertainty (σ_{vd}), was estimated by calculating the mean elevation differences between the 2002 and 2012 road surfaces. In our case, σ_{vd} was approximately 0.017, which we conservatively increased to 0.025 m consistent with Anderson and Pitlick (2014).

Unless otherwise specified, all uncertainty estimates were calculated using the vertical datum uncertain alone and applying the value of 0.025 m to the equation,

$$\sigma_{vd}n$$

where n is the area of interest in m².

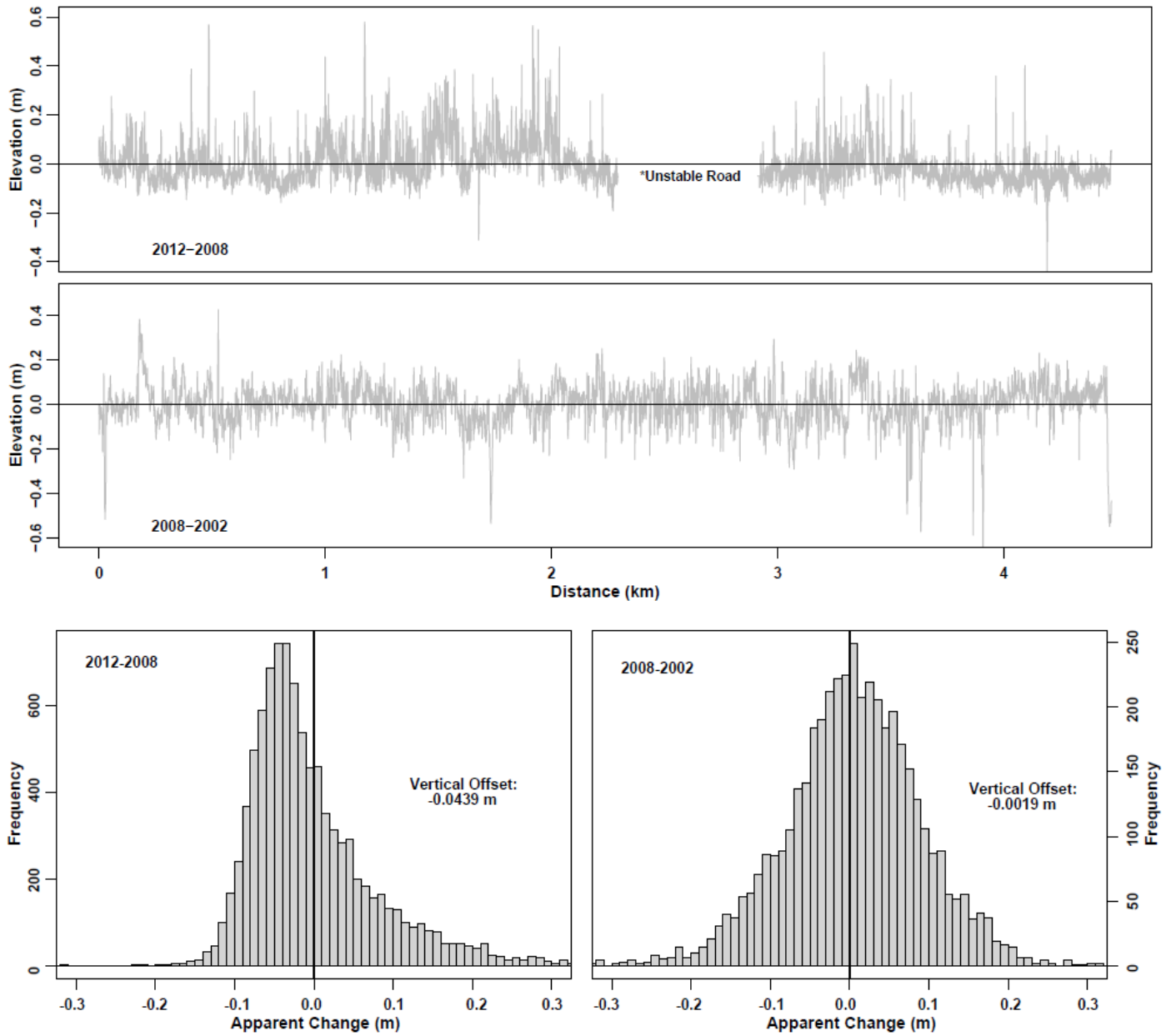


Figure 29. Long profiles and histograms of apparent change along the Westside Road.

Appendix 2: Quantitative Methods

A.3: Slope-Area Plots

Slope-area plots were created for several fluvial and colluvial tributary channels within the Tahoma Creek watershed to better understand the topographic signature of past/current glaciations (Figure 30). Panels (a), (c), and (e) of Figure 30 show only an inconclusive potential transition from hillslope to valley step domains. Panel (b), the only named tributary, displays a weak hillslope, valley-step, and fluvial signature. The here named ‘George Creek’ in panel (d), shows the only clear glacial signature, with multiple kinks as the channel passes from a cirque to the valley floor. ‘George Creek’ originates on the hillslope above a prominent cirque containing Lake George in the Western portion of the catchment.

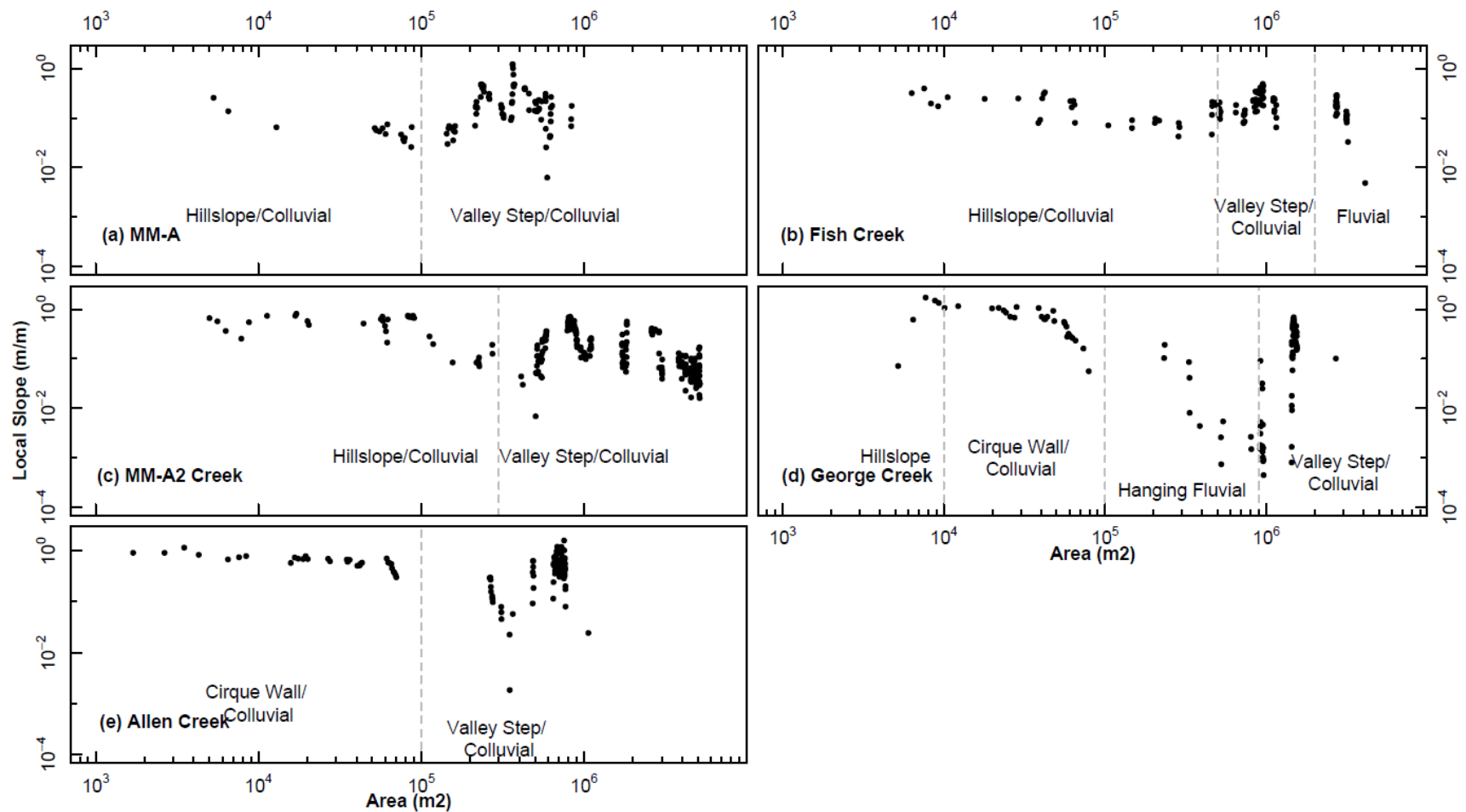


Figure 30. Slope – Area plots of selected tributary channels in the Tahoma Creek Watershed. Potential process domains are noted, and transitions delineated.

A.4: SDR – Area Plot

SDR-area plots were created for each area of interest and period combination to evaluate any potential trends between the two variables. Delivery ratios are likely to decrease with longer transfer pathways as a result of temporary deposition along route. We therefore expected to find a positive correlation between drainage area and delivery ratio. Panels a, b, d, and e of Figure 31 show no correlation between the drainage area and delivery ratio, while panel c seems to display an increasing delivery ratio with increasing area. This is likely the result of the evacuation of material from the talus apron (resulting in $SDR \approx 1$) along the base of the lateral moraine (high drainage area) during the 2002-2008 period.

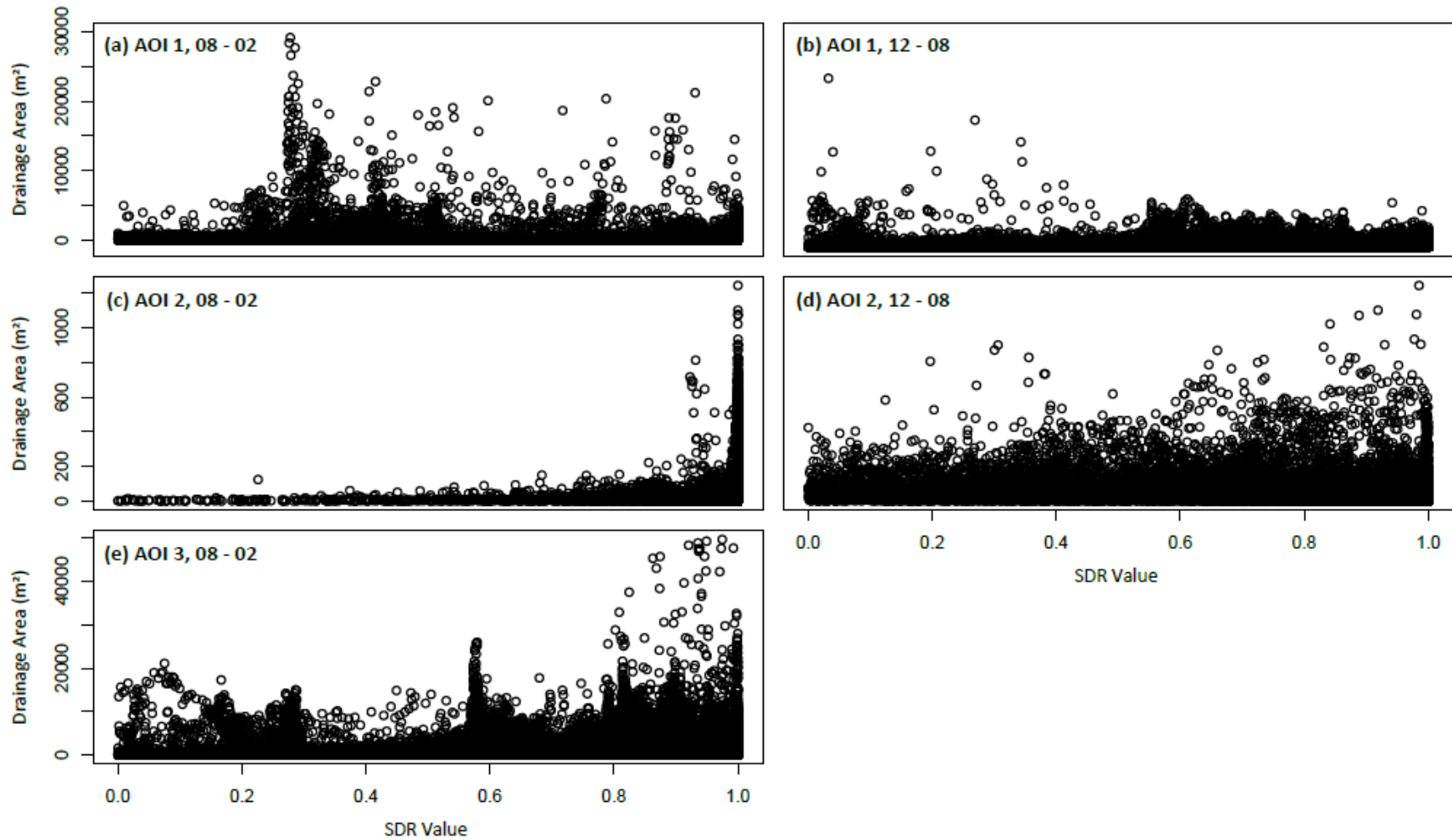


Figure 31. SDR – Area plots based on the SD SDR method. The period of interest is organized from left to right, while the area of interest is organized from top to bottom.